



NTNU – Trondheim
Norwegian University of
Science and Technology

Numerical Analysis of the Dynamic Behaviour of Railway Catenary Systems in Accordance with Norwegian Conditions

Petter Røe Nåvik

Civil and Environmental Engineering

Submission date: June 2013

Supervisor: Anders Rönquist, KT

Norwegian University of Science and Technology
Department of Structural Engineering




Department of Structural Engineering

Faculty of Engineering Science and Technology

NTNU- Norwegian University of Science and Technology

ACCESSIBILITY

MASTER THESIS 2013

SUBJECT AREA: Structural dynamics	DATE: 10.06.13	NO. OF PAGES: 119
TITLE: Numerical Analysis of the Dynamic Behaviour of Railway Catenary Systems in Accordance with Norwegian Conditions Numerisk analyse av dynamisk oppførsel til kontaktledningsanlegg ved høy hastighet etter norske forhold		
BY: Petter Røe Nåvik		

SUMMARY:

The dynamic behaviour of the railway catenary system is of great importance as the speed of the train increases. The aim for this study was to make a numerical model of the catenary system in three dimensions to be able to investigate what should be done with existing catenary systems in Norway to increase the train speed. In Norway there is a high ratio of curves with small radius, thus it is very important to include three dimensions. Abaqus has been used to obtain the numerical model. Both static and dynamic analyses have been done on this model. The results from the analyses have been compared with measurements, and this has shown that the model is able to describe the dynamic behaviour of the catenary system with sufficient accuracy. In future work it is recommended to look especially into how the contact interaction between the contact wire and the pantograph is modelled.

RESPONSIBLE TEACHER: Associate Professor Anders Rönquist

SUPERVISOR(S): Associate Professor Anders Rönquist

CARRIED OUT AT: Department of Structural Engineering (Institutt for konstruksjonsteknikk)

Masteroppgave for Stud.techn. Petter Røe Nåvik, våren 2013

Numerisk analyse av dynamisk oppførsel til kontaktledningsanlegg ved høy hastighet etter norske forhold

Numerical Analysis of the Dynamic Behaviour of Railway Catenary Systems in Accordance with Norwegian Conditions

For strømforsyning til elektriske tog i Norge benyttes en kontaktledning som togenes strømvaktar glir mot. For at denne forsyningen skal være pålitelig og avbruddsfri i høye toghastigheter stilles det strenge statiske og dynamiske krav til kontaktledningsanleggets egenskaper som mekanisk konstruksjon. På grunn av topografiske forhold er norske jernbaner spesielt preget av mange og krappe kurver. Rundt 40 % av jernbanenettet består av kurveradier under 1100 m. I slike krappe kurver endres kreftene i anlegget i forhold til rettstrekning.

Oppgaven skal kartlegge hvordan det er mulig å etablere en numerisk modell i Abaqus for et komplett kontaktledningsanlegg etter norske forhold. Modellen skal kunne få frem de dynamiske effektene i hvert enkelspenn (mellom stolper) og for en komplett seksjon med midt anker, modellert i 3D. Det legges vekt på en riktig interaksjon mellom pantograf og kontaktledning, men viktige parametere må også verifiseres mot kjente- og målte verdier. Systemets konfigurasjon bør også vurderes mht. geometri av system, bruk av Y-line og antall hengtråder der viktige dynamiske egenskaper dokumenteres som egenfrekvenser og former i tillegg til systemets fleksibilitet. En viktig del av studiet er å evaluere systemet når sentrale parametere som oppløftkraft, spennkraft, temperatur varieres og mulig feedback i kontaktledningsanlegget studeres. Vurdere hvordan modell, analyse og resultat står i forhold til gjeldende regelverk.

Litteraturstudie og numerisk modellering, State-of-the-art:

- Kontaktledningsanleggets mekaniske funksjonalitet og dynamiske egenskaper.
- Pantografens mekaniske funksjonalitet og dynamiske egenskaper.
- Modell i Abaqus av enkelt spenn, rettstrekning.
- Modell i Abaqus av komplett seksjon, rettstrekning.
- Tidsplans løsninger (linjert eller ikke-linjert) med bevegelig last og kontakt, vurder friksjon
- Dynamiske egenskaper som frekvenser og moder etableres.
- Kontroller med håndberegninger
- Analyser ved samplede resultater for studie av frekvensinnhold og sammenligning med målte verdier fra liknende eksisterende konstruksjoner.
- Alternativ utforming og konsekvenser av resultat - typer tiltak som er / kan tenkes bli brukt.

Det vil være opp til kandidaten å selv vektlegge de enkelte delene i oppgaven der oppgaven utføres i henhold til retningslinjer for utførelse av hovedoppgaven ved Institutt for konstruksjonsteknikks gitt på instituttets hjemmesider.

Faglærer: Anders Rönnquist, NTNU

Besvarelsen skal leveres til Institutt for konstruksjonsteknikk innen 10. juni 2013



Abstract

The dynamic behaviour of the railway catenary system is of great importance as the speed of the train increases. The aim for this study was to make a numerical model of the catenary system in three dimensions to be able to investigate what should be done with existing catenary systems in Norway to increase the train speed. In Norway there is a high ratio of curves with small radius, thus it is very important to include three dimensions. Abaqus has been used to obtain the numerical model. Both static and dynamic analyses have been done on this model. The results from the analyses have been compared with measurements, and this has shown that the model is able to describe the dynamic behaviour of the catenary system with sufficient accuracy. In future work it is recommended to look especially into how the contact interaction between the contact wire and the pantograph is modelled.

Sammendrag

Den dynamiske oppførselen til kontaktledningssystemet på jernbanen er av stor betydning når hastigheten på togene øker. Målet for denne studien var å lage en numerisk modell av kontaktledningssystemet i tre dimensjoner. Dette ble gjort for å være i stand til å undersøke hva som må gjøres med det eksisterende kontaktledningssystemet i Norge for å kunne øke toghastigheten. I Norge er det en høy andel av kurver med liten radius, derfor er det svært viktig å inkludere tre dimensjoner. Abaqus har blitt brukt for å lage den numeriske modellen. Det har blitt kjørt både statiske og dynamiske analyser på modellen. Resultatene fra disse analysene har blitt sammenlignet med målinger, og dette har vist at modellen er i stand til å beskrive den dynamiske oppførselen til kontaktledningssystemet med tilstrekkelig nøyaktighet. I det fremtidige arbeidet anbefales det å se spesielt på hvordan kontakten mellom kontaktledningen og strømvaktakeren burde modelleres.

Acknowledgements

I wish to thank various people for their much appreciated contribution to my master thesis; first I would like to express my appreciation to Associate Professor Anders Rönquist for the opportunity to do this thesis, and for his willingness to guide me through it. Then I wish to acknowledge the help and information provided by Thor Egil Thoresen from The Norwegian National Rail Administration. I also wish to acknowledge the cooperation with Arnar Kári Hallgrímsson. I would like to thank Anders Jørstad for the help regarding the modal hammer measurements. My grateful thanks are given to Morten Juell for proof reading this work. I wish to extend my thanks to everyone at the office for all the help I have received, and the fun we have had together.

Finally, I wish to thank Rosie for proof reading this work, keeping me with company and giving me the motivation I have needed.

Table of Contents

Abstract	V
Sammendrag	VII
Acknowledgements	IX
Table of Contents	X
List of Figures	XIII
List of Tables.....	XVII
1 Introduction.....	1
1.1 The aim of the thesis.....	2
1.2 The layout of the thesis.....	2
2 Theory	3
2.1 The catenary system	3
2.1.1 Case study – catenary section “Wire 152” at Soknedal station.....	7
2.1.2 The contact wire	8
2.1.3 The messenger wire.....	9
2.1.4 The droppers.....	10
2.2 The cantilever	11
2.3 Pre-sag	12
2.4 Pre-tensioning and midpoint anchor.....	12
2.5 Summary of the properties of the wires in Table 54	14
2.6 The pantograph.....	15
2.7 The contact force	16
2.8 The Elasticity	19
2.9 The vertical displacement of the contact wire	19
2.10 Dynamic characteristics of typical overhead contact line designs	20
2.10.1 The natural frequencies of catenary systems.....	20
2.10.2 The wave propagation speed	20
2.10.3 The reflection coefficient	20
2.10.4 The Doppler factor	21
2.10.5 The amplification coefficient	21
2.10.6 The limiting speed.....	21
2.10.7 The non-uniformity	21
2.10.8 Damping	22

3	Numerical modelling	23
3.1	The geometry of the railroad	25
3.2	The catenary system	26
3.2.1	The contact wire	27
3.2.2	The Messenger wire	27
3.2.3	Droppers	27
3.3	The cantilever	28
3.3.1	Registration arms.....	28
3.3.2	Brackets	28
3.4	Pantograph	29
3.5	Damping of catenary systems.....	33
3.6	The pre-tensioning force.....	34
3.7	The contact force	35
3.8	The numerical steps of the analyses	37
3.8.1	The first step.....	37
3.8.2	The second step	37
3.8.3	Elasticity analyses	37
3.8.4	Frequency analyses	37
3.8.5	The dynamic analyses	38
4	Measuring methods	40
4.1	Geometry	40
4.2	Tension in the contact wire.....	41
4.3	Elasticity	41
4.4	Modal parameter identification	42
5	Results and discussion	45
5.1	Natural frequencies and modes.....	45
5.1.1	The numerical analyses	45
5.1.2	Results and discussion of the natural frequencies	46
5.2	Damping	53
5.2.1	Measurements.....	55
5.3	Elasticity	56
5.3.1	Numerical analyses	56
5.3.2	Measured values	56

5.3.3	Discussion of the elasticity.....	57
5.4	The tension force in the contact wire and the messenger wire.....	58
5.5	Wear.....	59
5.6	Pre-sag.....	60
5.7	Implicit dynamic analyses.....	61
5.7.2	The contact force.....	63
5.7.3	The uplift of the contact wire at support 1277.....	70
5.7.4	The displacement at mid span between support 1277 and 1278.....	76
5.7.5	The trajectory of the contact point between the pan head and the contact wire.....	80
6	Conclusion and future directions.....	84
	Bibliography.....	85
	Appendix.....	88
	Appendix A Wear of the contact wire[8].....	88
	Appendix B The pantograph model from Schunk Nordiska[17].....	89
	Appendix C-1 Overview of the properties of sections in the area of interest[8].....	90
	Appendix C-2 Table of poles for the section “Wire 152” from pole 1261 to 1288[8].....	92
	Appendix C-3 Geometrical design of the droppers in section “Wire 152” [8].....	94
	Appendix C-4 Geometrical design of the track[8].....	95
	Appendix D Matlab code for writing the input file for pre-scribed displacements and the .csv-file for the track geometry.....	96
	Appendix E-1 The cross sectional properties for the contact wire obtained from CrossX.....	100
	Appendix E-2 The cross sectional properties for the worn contact wire obtained from CrossX.....	101
	Appendix F Zip-file contents.....	102

List of Figures

Figure 1 The different parts of a simple catenary system[1].....	1
Figure 2 A pantograph.....	1
Figure 3 Model of a simple catenary system[5].....	3
Figure 4 A catenary system with stitch wires[6], the green line describes the catenary wire, the red line is describes the contact wire, the black wires describes the droppers and the blue wires describes the stitch wires.	3
Figure 5 The catenary system "System 20 A". The maximum span length is 75 metres, but the recommended length is 70 metres[6]. The figure is not in scale.....	4
Figure 6 The catenary system "System 20 B". The maximum span length is 75 metres, but the recommended length is 70 metres[6]. The figure is not in scale.....	4
Figure 7 The catenary system "System 20 C1". The maximum span length is 45 metres. [6] The figure is not in scale.	5
Figure 8 The catenary system "System 20 C2". The maximum span length is 30 metres. The system height is denoted SH[6]. The figure is not in scale.	5
Figure 9 The catenary system "System 25". The maximum span length is 30 metres[6]. The figure is not in scale.	6
Figure 10 Location of Wire 152 at Soknedal station. The location is shown by the "A" in the red marker. The figure is based on [9].	7
Figure 11 The geometry of the studied railway section seen from above. The black line marks the track. The figure is based on [10].	8
Figure 12 Zigzag of the catenary system	8
Figure 13 Cross section of the contact wire Ri 100 Cu[3]	9
Figure 14 The dropper's connection to the contact wire at "Wire 152". The connection to the messenger wire is approximately the same.	10
Figure 15 Description of a stranded type dropper[3]. In the studied section there are used dropper wires with massive cross sections.....	10
Figure 16 Description of a type of cantilever used in Norway[3].....	11
Figure 17 a) Pull-off support and b) push-off support on cantilevers[3]	11
Figure 18 Picture of the tensioning equipment used at "Wire 152"	13
Figure 19 The tensioning equipment used at "Wire 152"	13
Figure 20 Simplified description of the pantograph, model WBL88[12], showing the collector strips, the pan head the arm, the main frame and the drive.....	15
Figure 21 How the contact wire slides on top of the pantograph.....	16
Figure 22 Limits for the mean value of the contact force[18]	17
Figure 23 Largest standard deviation for the contact force[18]	18
Figure 24 Friction damping hanger and rubber damping hanger[30]	22
Figure 25 Numerical model of one catenary system span.	24
Figure 26 The obtained geometry for "Wire 152" in the numerical model in Abaqus; y-axis is scaled with a factor of five	25
Figure 27 The upper left model is a numerical model of the pantograph WBL 88, the model to the upper right is a simplified version of the same model. They are numerical models of the figure at the bottom. $M1$ and $M2$ is masses, $X1$ is the distance between the two collector strips, $K1$ is a spring constant, $C1$ and $C2$ is damping constants, $U1$ is a friction constant, $F1$ is a	

static uplift force and $Fa2$ is an aerodynamic uplift force, values for these parameters is displayed in Table 4.	29
Figure 28 The cross section of the pan head obtained from the Abaqus model.....	31
Figure 29 The mesh of the collector strip used in Abaqus.....	31
Figure 30 The positions where the force measurements on the pantograph are done are shown as $F1$, $F2$, $F3$ and $F4$. The figure is of the pantograph seen from above.[12]	32
Figure 31 The interaction properties of the contact between the pan head and the contact wire	35
Figure 32 The points where the force is applied in the elasticity analyses. The red dots are the position, the red arrows are the forces and the blue lines are the wires; the top one is the messenger wire, the bottom one is the contact wire and the vertical lines are the droppers....	37
Figure 33 Parts of the input file which is included in the main input files	39
Figure 34 The keyword which include the extra input file into the main input files	39
Figure 35 The method for measuring different geometrical values on the catenary system ...	40
Figure 36 Tension test at site with the device CableBull[48].	41
Figure 37 Dynamometer, Pesola PHS040[49]	42
Figure 38 Modal hammer, Brül and Kjær type 8208[51]	42
Figure 39 Accelerometer, Kistler type 8770A50[50].....	43
Figure 40 Signal conditioner/power supply, Kistler Type 5134[52].....	43
Figure 41 NI chassis type cDAQ-9174 with the NI dynamic mounted[53].....	43
Figure 42 The fastening of the accelerometer the contact wire. The accelerometer is the grey thing on the top of the dropper clamp. The white cable sends the measured information to the computer.....	44
Figure 43 The natural frequencies from 0 Hz to around 4 Hz of the whole section found in Analysis 15. This is the first 300 natural frequencies of the model.	46
Figure 44 The natural frequencies from 0 Hz to around 18 Hz of the whole section found in Analysis 26. This is the first 2000 natural frequencies of the model.	46
Figure 45 The natural frequencies from 0 Hz to around 18 Hz of the whole section found in Analysis 33. This is the first 2000 natural frequencies of the model.	47
Figure 46 The generalized mass ratio plotted against its natural frequency from Analysis 26. The ratio is computed as the generalized mass for each mode divided by the maximum value for the generalized mass. The cross section of the contact wire is unworn.	48
Figure 47 The generalized mass ratio plotted against its natural frequency from Analysis 33. The ratio is computed as the generalized mass for each mode divided by the maximum value for the generalized mass. The cross section of the contact wire is worn by 20%.	48
Figure 48 The natural frequencies between 0 Hz and approximately 4 Hz from Analysis 15.	49
Figure 49 The natural frequencies between 0 Hz and approximately 6 Hz from Analysis 26.	50
Figure 50 The natural frequencies between 0 Hz and approximately 6 Hz from Analysis 33.	50
Figure 51 Eigenmode 15 with frequency=0.87 Hz from Analysis 26. This displays half sine waves of the 60 metres long spans.	51
Figure 52 Eigenmode 95 with frequency=1.75 Hz from Analysis 26. This displays sine wave modes of the 60 metres long spans in the model.....	52
Figure 53 The eigenmode which has the highest generalized mass in Analysis 26. This is eigenmode 212 and the frequency is 3.23 Hz.	52

Figure 54 The effective damping ratios for each natural frequency in the whole model from Analysis 26.....	53
Figure 55 The effective damping ratios for each natural frequency in the whole model from Analysis 33.....	54
Figure 56 Interface of the modal parameter identification program with one of the measurements done at the site. In the figure one can see that there is found a natural frequency of 2.67 Hz and a corresponding damping ratio of 0.00891.....	55
Figure 57 Elasticity test in the middle of the span between pole 1877 and 1278 with the displacement shown and the red arrow illustrates the uplift force. The uplift force was 150 N. The y axis is scaled up with a factor of 20, and the deformation is scaled up by a factor of 5.	56
Figure 58 The elasticity results from Analysis 28, Analysis 34 and the measurements at site.	57
Figure 59 Tension forces in the numerical model without wear. The legend on the left shows which magnitude each colour describes.....	58
Figure 60 Pre-sag of some spans in the catenary section. There is included pre-sag found from measurements, analyses with and without a worn contact wire.....	60
Figure 61 The contact force along the section from Analysis 29, speed=70km/h and full cross section.....	63
Figure 62 The contact force along the section from Analysis 31, speed=90km/h and full cross section.....	64
Figure 63 The contact force along the section from Analysis 32, speed=130km/h and full cross section	64
Figure 64 The contact force along the section from Analysis 35, speed=200km/h and full cross section	65
Figure 65 The contact force along the section from Analysis 36, speed=90km/h and 20% worn cross section.....	65
Figure 66 The contact force along the section from Analysis 37, speed=130km/h and 20% worn cross section.....	66
Figure 67 Measurement of the contact force occurring along Wire 152 at 90 km/h. This is measured by The Norwegian National Rail Administration.[8]	66
Figure 68 The statistical analysis of the measurement of the contact force occurring at Wire 152 at 90 km/h. This is measured by The Norwegian National Rail Administration.[8]	67
Figure 69 The vertical displacement of the contact wire at support 1277 in Analysis 29, speed=70 km/h and full cross section	70
Figure 70 The vertical displacement of the contact wire at support 1277 in Analysis 31, speed=90 km/h and full cross section	71
Figure 71 The vertical displacement of the contact wire at support 1277 in Analysis 32, speed=130 km/h and full cross section	71
Figure 72 The vertical displacement of the contact wire at support 1277 in Analysis 35, speed=200 km/h and full cross section	72
Figure 73 The vertical displacement of the contact wire at support 1277 in Analysis 36, speed=90 km/h and 20% worn cross section	72
Figure 74 The vertical displacement of the contact wire at support 1277 in Analysis 37, speed=130 km/h and 20% worn cross section.....	73

Figure 75 The vertical displacement at mid span between support 1277 and 1278, Analysis 29 speed=70 km/h and the cross section is full	76
Figure 76 The vertical displacement at mid span between support 1277 and 1278, Analysis 31 speed=90 km/h and the cross section is full	77
Figure 77 The vertical displacement at mid span between support 1277 and 1278, Analysis 32 speed=130 km/h and the cross section is full	77
Figure 78 The vertical displacement at mid span between support 1277 and 1278, Analysis 35 speed=200 km/h and the cross section is full	78
Figure 79 The vertical displacement at mid span between support 1277 and 1278, Analysis 36. Speed=90 km/h and 20% worn cross section.....	78
Figure 80 The vertical displacement at mid span between support 1277 and 1278, Analysis 37. Speed=130 km/h and 20% worn cross section.....	79
Figure 81 The path of the pantograph in Analysis 29, speed=70 km/h and full cross section.	80
Figure 82 The path of the pantograph in Analysis 31, speed=90 km/h and full cross section.	81
Figure 83 The path of the pantograph in Analysis 32, speed=130 km/h and full cross section	81
Figure 84 The path of the pantograph in Analysis 35, speed=200 km/h and full cross section	82
Figure 85 The path of the pantograph in Analysis 36, speed=90 km/h and 20% worn cross section.....	82
Figure 86 The path of the pantograph in Analysis 37, speed=130 km/h and 20% worn cross section.....	83

List of Tables

Table 1 The components of Table 54[6]	14
Table 2 Contact force demands at different velocities	18
Table 3 Numerical values for the used pantograph (Appendix B).....	30
Table 4 Damping values used in the literature. α is the mass proportional damping coefficient, β is the stiffness proportional damping coefficient and ζ is the damping ratio.....	33
Table 5 Frequency areas with accumulation of modes in Analysis 33.	52
Table 6 Tension forces in the contact wire, both from measurements at site and from the numerical model.	58
Table 7 The measured wear of the contact wire in six different spans.	59
Table 8 Summary of important contact force values obtained from the numerical analyses. .	68

1 Introduction

The railway overhead wire system which is studied in this work consists of a contact wire, a messenger wire, droppers, registration arms and brackets as seen in Figure 1. The messenger wire carries the contact wire via the droppers, and makes it possible to obtain the desired geometry, stiffness and elasticity. The brackets carry the messenger wire, and are fastened to the poles. The main function of the registration arms, which are fastened to the contact wire, is to obtain the right horizontal geometry of the contact wire. The contact wire is the conductive part which transfers the electricity to the train through the pantograph.

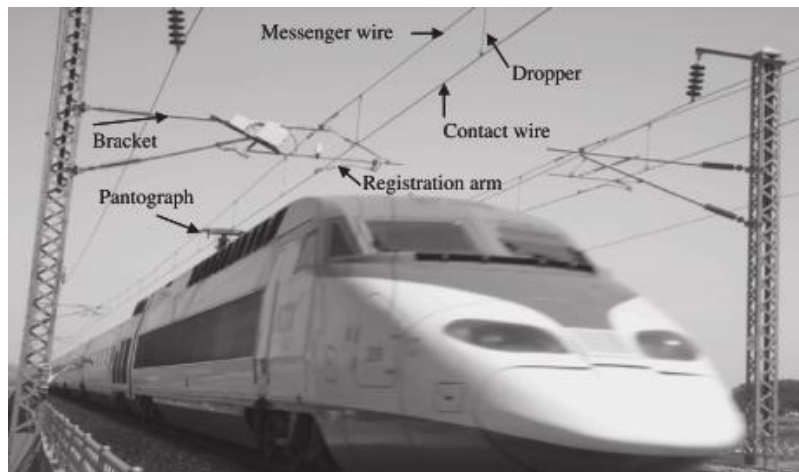


Figure 1 The different parts of a simple catenary system[1]

The pantograph, Figure 2, is the device on top of the train which transfers the electricity from the contact wire to the train. Two bow strips of coal at the top of the pantograph are the actual components which transfers the electricity. This transfer is crucial for the running of the train thus there has to be contact between the pantograph and the contact wire. Simeon and Arnold [2] describes this contact as the most critical part in the transmission of the electricity to the trains of today. The contact is mainly ensured by introducing an upwards pressure in the pantograph.



Figure 2 A pantograph

The contact force between the pantograph and the contact wire varies as the train moves and this introduces the importance of dynamic analyses to ensure contact in every situation. Contact may be lost due to large oscillations[2]. A period of contact loss is called an arch. The dynamics of this system is very complex and its complexity has become more interesting as the speed which trains run at increases[3].

In this study a part of the Norwegian Railway that is located between Soknedal and Støren will be investigated. This railway was built in 1919 and electrified in 1970[4], and was built on piecework. The part which has been investigated is called “Wire 152 Soknedal Station” by The Norwegian National Rail Administration. This part has been chosen due to its many irregularities.

1.1 The aim of the thesis

The primary aim of this thesis was to make a numeric model of a train running along a straight catenary section in three dimensions. This model should be able to run dynamic analyses to investigate the contact forces between the contact wire and the pantograph, and the vertical displacements of the contact wire along the whole section. It should be possible to include non-linearities in the model as well.

There are several important things which have to be studied to be able to model a catenary section in a way that gives answers that can match measured forces and displacements. Firstly, one needs to study the catenary systems mechanical and dynamical properties. Secondly, the pantographs mechanical and dynamical properties should be studied. Finally, the state-of-the-art for the catenary-pantograph interaction should be investigated.

The model should then be validated by comparing analyses results with measurements, literature and calculations.

1.2 The layout of the thesis

In Chapter 2 there will be presented the necessary theory about catenary systems in general and the specific catenary systems used in Norway to understand what is investigated later in the thesis. Chapter 3 describes how the numerical model has been made and why it is modelled as it is. Chapter 4 presents the methods used for obtaining the measurements. The results from both analyses and measurements will be presented and discussed in Chapter 5. The conclusion will be presented in Chapter 6.

A .zip-file will be included. This contains the .cae- and .jnl-file for the numerical model, two films of the pantograph running along the contact wire in the numerical model, and a Microsoft Excel-file describing the geometry. See Appendix F for a more detailed description.

2 Theory

2.1 The catenary system

The catenary system is, as mentioned in the introduction, the wire system above the railway track which consists of a contact wire, a messenger wire and a defined number of droppers. This system is held up by cantilevers which are fastened to poles on the side of the track. A model of a catenary system is displayed in Figure 3, and a picture of a real system is shown in the introduction, in Figure 1.

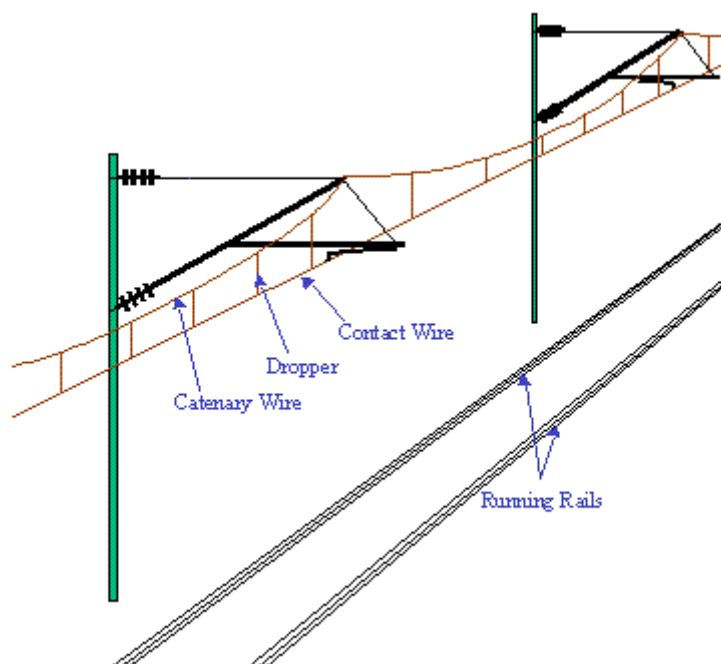


Figure 3 Model of a simple catenary system[5].

Some catenary systems also have parts called stitched wires. Stitched wires are connecting elements which are inserted between the catenary wire and the support. Their purpose is to make the contact wire height more equal along a span[3]. A catenary system with stitch wires is shown in Figure 4.

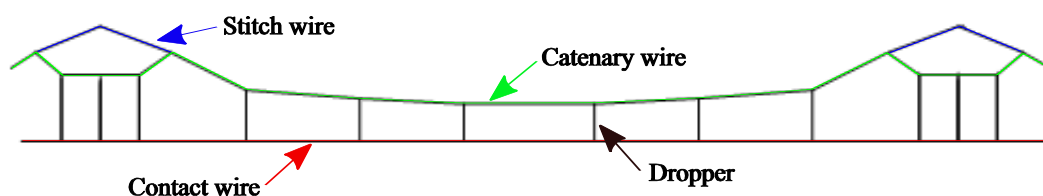


Figure 4 A catenary system with stitch wires[6], the green line describes the catenary wire, the red line is describes the contact wire, the black wires describes the droppers and the blue wires describes the stitch wires.

The different catenary systems used in Norway are called Table 54, System 35, System 20 and System 25. However, at present only the three latter can be chosen for building.[6]. The

technical regulations for the contact wire describe which system should be used for a specified railway section. The criteria that decide which system to use are the desired train velocity, the type of pantograph which are in use, the density of trains, and the type of tracks used[7].

There are two different types of System 35, one with stitch wires and one without. These systems are suitable for multiple pantographs, and velocities around 130 km/h. The maximum section length is 2 x 800 metres and the tension force is 7,1 kN in both the contact wire and the messenger wire[6].

System 20 is split into four different groups; A, B, C1 and C2. System 20 A is developed for one pantograph with speeds up to 200 km/h. This system includes the use of stitch wires and the radii of the curves should be larger than 800 metres. One section is allowed to maximum be 2 x 750 metres long. Both the contact wire and the messenger wire is subjected to a tension force of 10 kN[6]. One span of system 20 A is shown in Figure 5.

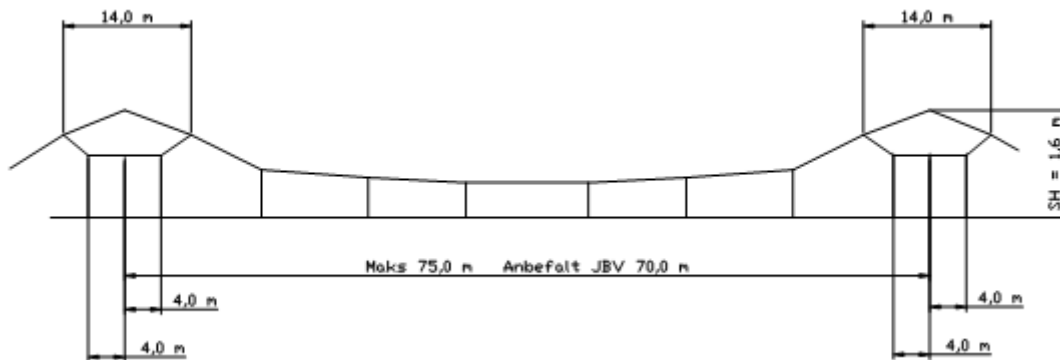


Figure 5 The catenary system "System 20 A". The maximum span length is 75 metres, but the recommended length is 70 metres[6]. The figure is not in scale.

System 20 B is dimensioned for train speeds up to 160 km/h with one pantograph, and there are no stitch wires. The system can be used with curvature radii below 800 metres, and the maximum length of a section is 2 x 650 metres. The tension force is 10 kN in both the contact wire and the messenger wire[6]. A model of one span of System 20 B is presented in Figure 6.

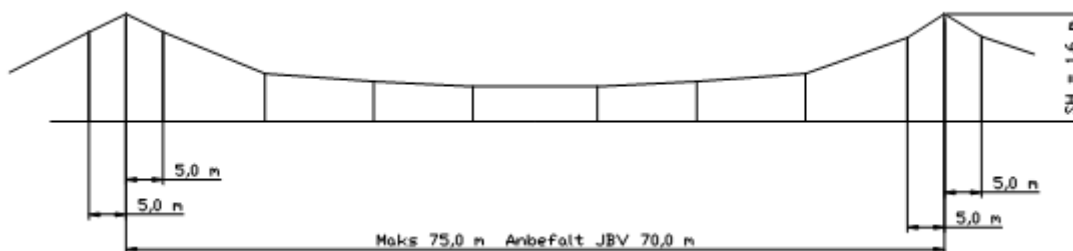


Figure 6 The catenary system "System 20 B". The maximum span length is 75 metres, but the recommended length is 70 metres[6]. The figure is not in scale.

System 20 C1 is designed for train speeds up to 200 km/h with one pantograph in sections inside tunnels. It can be built both with, and without, stitch wires, and the curvature radii should be larger than 5000 metres. The minimum height of the system is 0,75 metres and the tension force 13 kN in both the contact wire and the messenger wire. [6] An overview of one span of this system is shown in Figure 7.

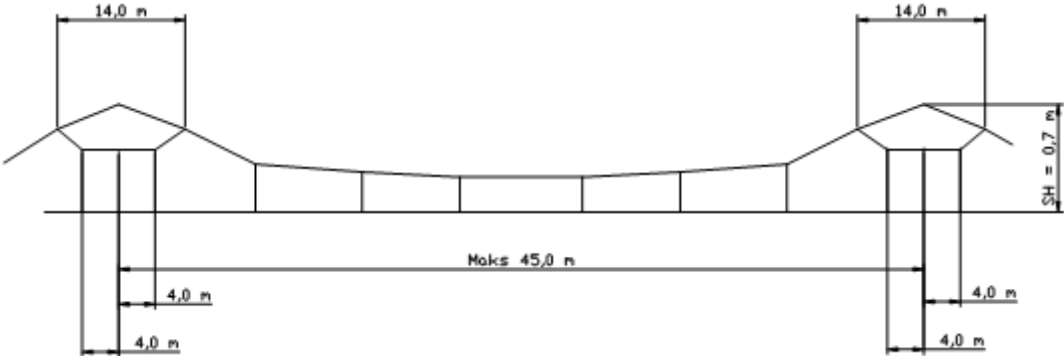


Figure 7 The catenary system "System 20 C1". The maximum span length is 45 metres. [6] The figure is not in scale.

System 20 C2 is also designed for use in tunnels. It allows a maximum train speed of 200 km/h, and the use of one pantograph. The system is built without stitch wires and the minimum height of the system is 0.30 metres. The tension force is 13 kN in both the contact wire and the messenger wire. [6] A span of System 20 C2 is displayed in Figure 8.

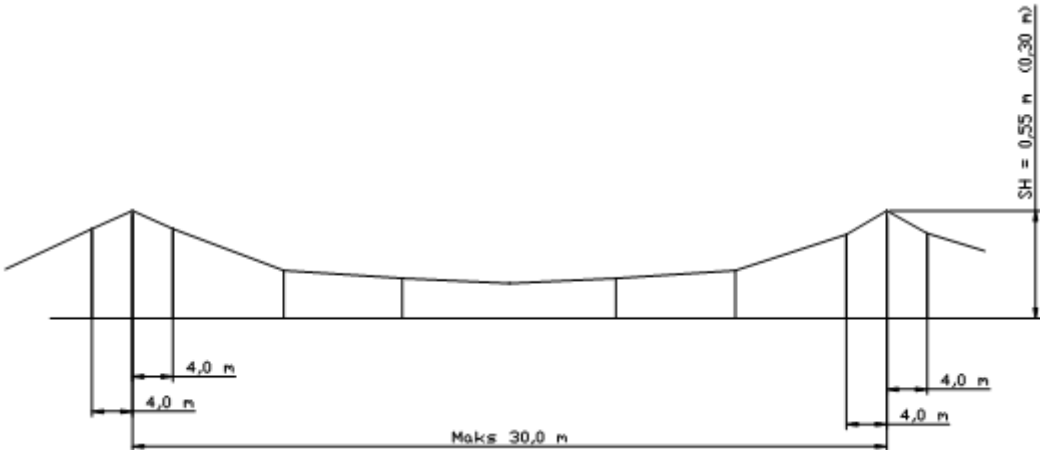


Figure 8 The catenary system "System 20 C2". The maximum span length is 30 metres. The system height is denoted SH[6]. The figure is not in scale.

The system called “System 25” is the catenary system in Norway designed for the highest train speeds. The maximum allowed train speed is 250 km/h, the system contains stitch wires and the minimum radii of the curvatures are 800 metres. The tension forces introduced are 15kN in both the contact wire and the messenger wire, and the maximum section length is 2 x 600 metres. [6] There is shown one span of System 25 in Figure 9.

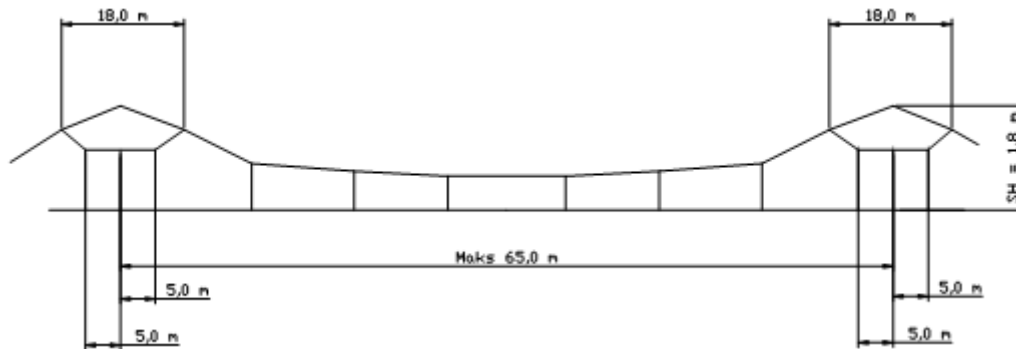


Figure 9 The catenary system "System 25". The maximum span length is 30 metres[6]. The figure is not in scale.

Table 54 is an old catenary system which is still in use in Norway, but not in new railway sections. The maximum train speed allowed is 130 km/h for this system. The original tension forces were 7,6 kN in both the contact wire and the messenger wire, but to cope with higher speeds they were changed to respectively 10 kN and 5 kN[8].

2.1.1 Case study – catenary section “Wire 152” at Soknedal station

The studied railway section is located just north of Soknedal station which is approximately 70 kilometres south of Trondheim, see Figure 10. The section is part of “Dovrebanen” which runs from Oslo to Trondheim.

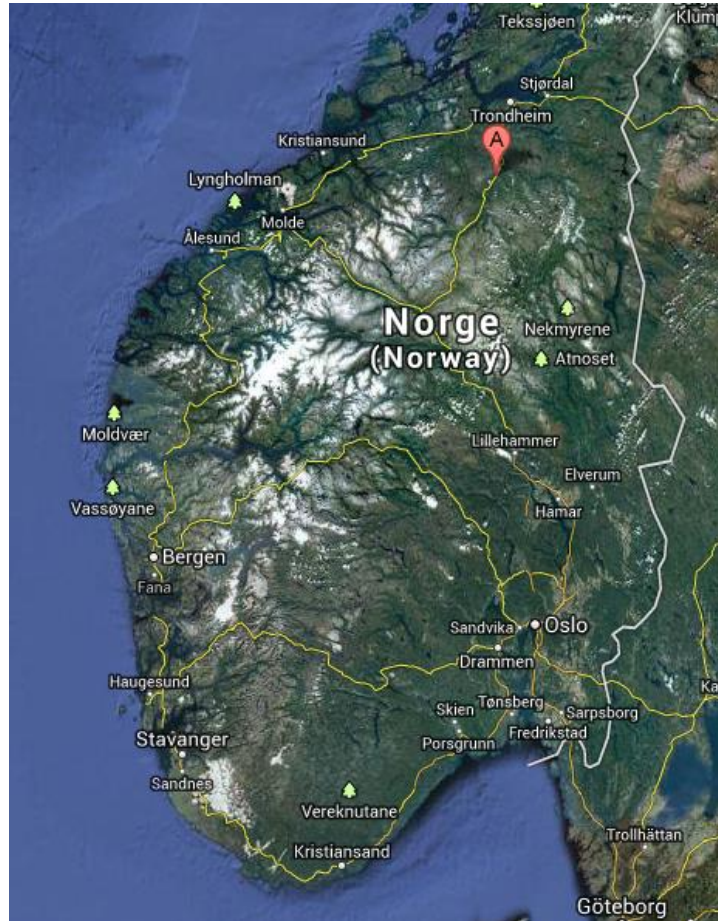


Figure 10 Location of Wire 152 at Soknedal station. The location is shown by the "A" in the red marker. The figure is based on [9].

The section was built with the catenary system “Table 54”, and it is 1451 meters long. The Norwegian National Rail Administration measurement of the position says that the section is between km 487.029 to 488.33. This is equivalent with between cantilever 1261 and 1288. The section is divided into twenty-six spans. The lengths of the spans are 40 and 60 metres.

In the studied railway section there is a part with very small curvature, $R=323\text{m}$, and there is a bridge where the contact wire has to be lowered to pass under. The position of the curve and the bridge along the section are marked in Figure 11. The small curvature is between km 487.75 and 488.18, and have span lengths of 40 metres. And the contact height starts to decrease at km 487.9. This is irregularities which reduces the allowed running speed on the section to 70 km/h. The rest of this sections geometry is described in detail in Appendix C-1, C-2, C-3 and C-4.[8].



Figure 11 The geometry of the studied railway section seen from above. The black line marks the track. The figure is based on [10].

2.1.2 The contact wire

The contact wires main task is to ensure transfer of electrical energy to the train without interruptions. In addition to this it is of great importance that the wear on both the contact wire, and the collection strips on the pantograph, is as low as possible to reduce maintenance costs[3]. There are two main things done to reduce this wear. Firstly, the contact wire has been mounted with zigzag, also called the stagger. This results in the wire travelling back and forth on the collection strips, decreasing wear. Figure 12 shows a typical zigzag on a section without curvature. In curvature the poles will be placed on the outside of the bend to obtain the same zigzag effect.[3] The geometry of the zigzag at “Wire 152” is presented in Appendix C-2.

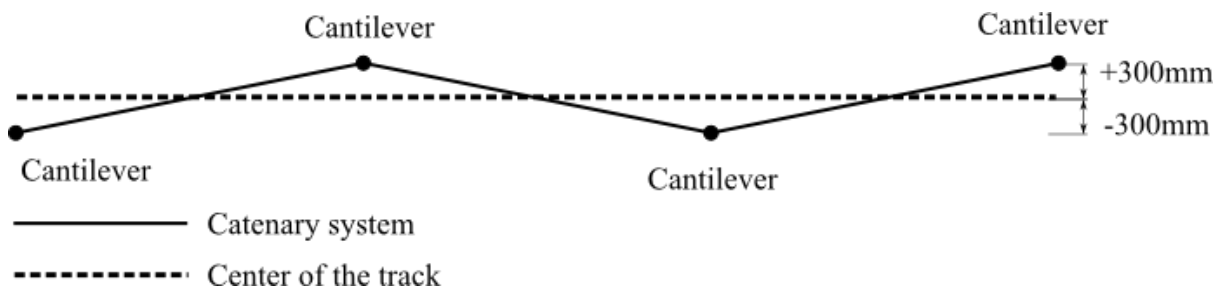


Figure 12 Zigzag of the catenary system

Secondly, the contact wire is designed to have a pre-sag, an initial vertical displacement, which is introduced to ensure contact without raising the mean contact force[3]. Pre-sag is described in detail later in the theory.

The contact wire used in “Table 54” is “Ri 100 Cu”. Its cross sectional area is not perfectly circular, but has grooves in the side to enable the dropper clips fasten to it as illustrated by Figure 13. This cross sectional area is given in the literature as 100 mm^2 [3, 6], but after modelling the cross section in AutoCAD, a software for computer-aided design, it was found to be 105.85 mm^2 , which is the value which will be used in this work. CrossX were used to find other cross sectional parameters. The moments of inertia were found to be $I_y=986.5 \text{ mm}^4$, and $I_z=839.2 \text{ mm}^4$. Whereas the St. Venant number (torsion constant) is $J=1511.5 \text{ mm}^4$.

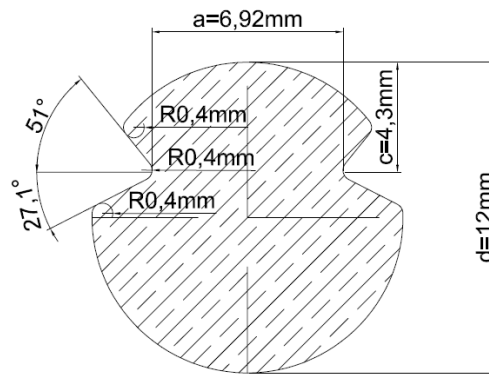


Figure 13 Cross section of the contact wire Ri 100 Cu[3]

According to rules in Norway the maximum mean value of the wear is given as 20% of the original cross sectional area before the wire has to be changed[11]. The new cross sectional area is then given as 80 mm^2 , but the calculated value from AutoCAD is 83.68 mm^2 , and it is this value that will be used here. Appendix A displays the figure that shows the size of the worn cross sectional area against the nominal diameter. The moments of inertia for the worn cross section were found to be $I_y=710.4 \text{ mm}^4$, and $I_z=503.3 \text{ mm}^4$. Whereas the St. Venant number (torsion constant) is $J=835.3 \text{ mm}^4$.

The specific weight of this contact wire is $8,9 \text{ N/m}$, the Young’s modulus, E , is $124 \cdot 10^9 \text{ Pa}$, Poisson’s ratio is 0.34 and the coefficient of thermal expansion is $1.65 \cdot 10^{-5} \text{ K}^{-1}$ [12].

2.1.3 The messenger wire

The messenger wire is the carrying wire, and is also referred to as the catenary wire in the literature. Its purpose is to lift the contact wire to the desired vertical position. The use of messenger wires permits longer spans and reduces the wear on the collection strips[3].

The messenger wire used in this work is “Cu 50/7”. It has a circular cross section with a diameter of 9 mm , its specific weight is $4,46 \text{ N/m}$ [6], the Young’s modulus, E , is $113 \cdot 10^9 \text{ Pa}$, Poisson’s ratio is 0.0 and the coefficient of thermal expansion is $1.7 \cdot 10^{-5} \text{ K}^{-1}$ [12].

2.1.4 The droppers

The droppers have the function of connecting the contact wire and the messenger wire so that the messenger wire can support the contact wire. The connection to the other wires is by dropper clips, such as the one shown in Figure 14. The droppers used here is Bz II 10/49, it has a circular cross section with the diameter of 4,5 mm, its specific weight is 0,89 N/m[6], the Young's modulus, E , is $100 \cdot 10^9$ Pa, Poisson's ratio is 0.0 and the coefficient of thermal expansion is $1.7 \cdot 10^{-5} \text{ K}^{-1}$ [12]. The different parts of a dropper are shown in Figure 15.



Figure 14 The dropper's connection to the contact wire at "Wire 152". The connection to the messenger wire is approximately the same.

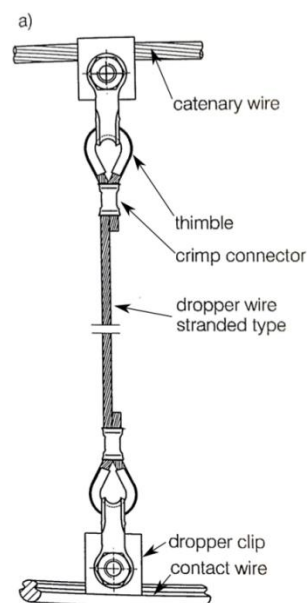


Figure 15 Description of a stranded type dropper[3]. In the studied section there are used dropper wires with massive cross sections.

2.2 The cantilever

The cantilever is the system which supports the messenger wire and the contact wire. It is mounted on a pole that stands up from the ground. An example of a cantilever with all its components is displayed in Figure 16. It is designed so that the top anchor is mostly subjected to tension forces and the cantilever tube only is subjected to compressional forces. The top anchor can in some situations be subjected to a small compressive force if the combination of the wind load and the effects of the curvature is larger than the tensile load resulting from the weight of the catenary system.[3]

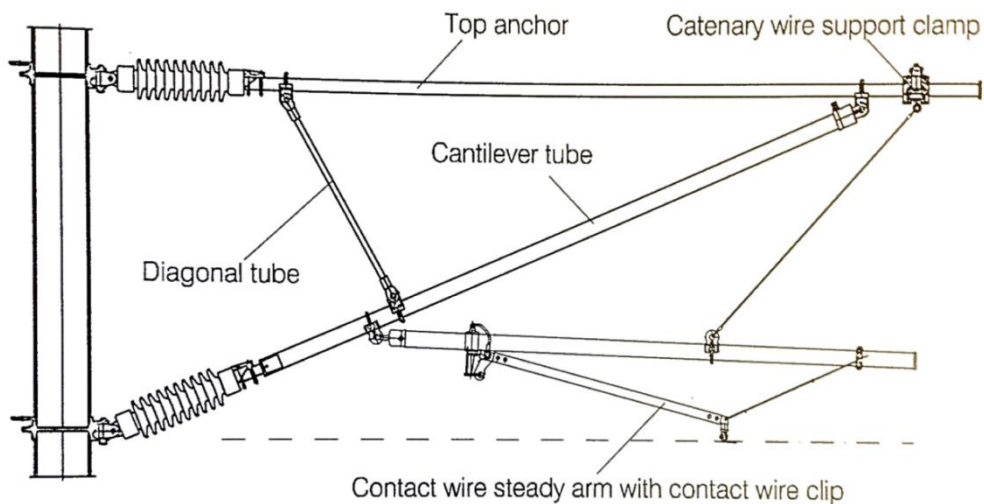


Figure 16 Description of a type of cantilever used in Norway[3]

The steady arm can be mounted in different directions, as shown in Figure 17, to either push or pull the contact wire into zigzag. Which way it is mounted depends on which way the forces acts, and then one mounts the arm so it will be in tension.[3]

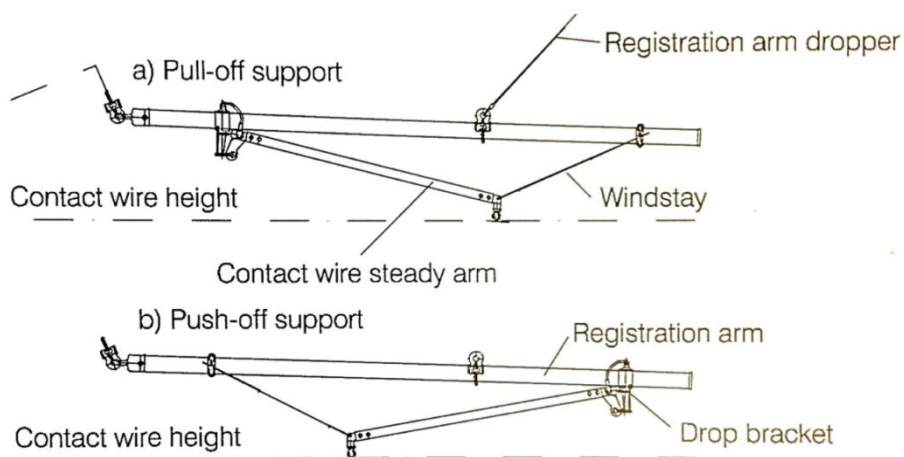


Figure 17 a) Pull-off support and b) push-off support on cantilevers[3]

2.3 Pre-sag

Some catenary systems are designed so that the centre of a span is lower than at the supports. This is called pre-sag. This ensures that the overhead contact line has more similar elasticity at the supports and in the middle of the span. The pantograph has to lift more in the centre of the span due to the pre-sag. And as a result the operating height of the pantograph varies less. It is found that at speeds lower than 200 km/h the pre-sag definitely provides better running quality. This because at those velocities the static behaviour is dominating, and the elasticity is then of great importance for the behaviour[3].

2.4 Pre-tensioning and midpoint anchor

To obtain the desired stiffness and geometry of the catenary system it is necessary to introduce tension in both the contact and messenger wire. This stress varies from system to system and the maximum permissible working tensile stress to be applied to a unworn contact wire should be calculated as the standard EN 50119 requires, see formula (2.1)[13].

$$\sigma_w = \sigma_{min} * n * K_{temp} * K_{wear} * K_{icewind} * K_{eff} * K_{clamp} * K_{joint} \quad (2.1)$$

Here σ_w is the maximum stress, σ_{min} is the minimum tensile failing strength, n is the safety factor, K_{temp} gives the relationship to temperature, K_{wear} gives the factor of maximum permitted wear, $K_{icewind}$ describes the effect of wind and ice loads, K_{eff} describes the efficiency of the tensioning equipment, K_{clamp} describes the efficiency of the tensioning clamps and K_{joint} describes the reduction of tensile strength in joints. The maximum value of the stress may not exceed 65% of the minimum tensile failing strength.[14]

The tension is obtained by using tensioning equipment at both ends of a wire length. The tensioning mechanism should be designed so that the tension does not vary more than 3% due to temperature changes[3]. The equipment used in the studied section is the same as the one presented in Figure 18. In addition to what is displayed in this figure a bar is used to distribute the right force to the messenger and contact wire, shown in Figure 19. The fastening position of the tensioning wire at the bar decides what the force will be in each wire, this due to force and moment equilibrium. The pre-tensional forces used at the site are 10 kN in the contact wire and 5 kN in the messenger wire[8].



Figure 18 Picture of the tensioning equipment used at “Wire 152”

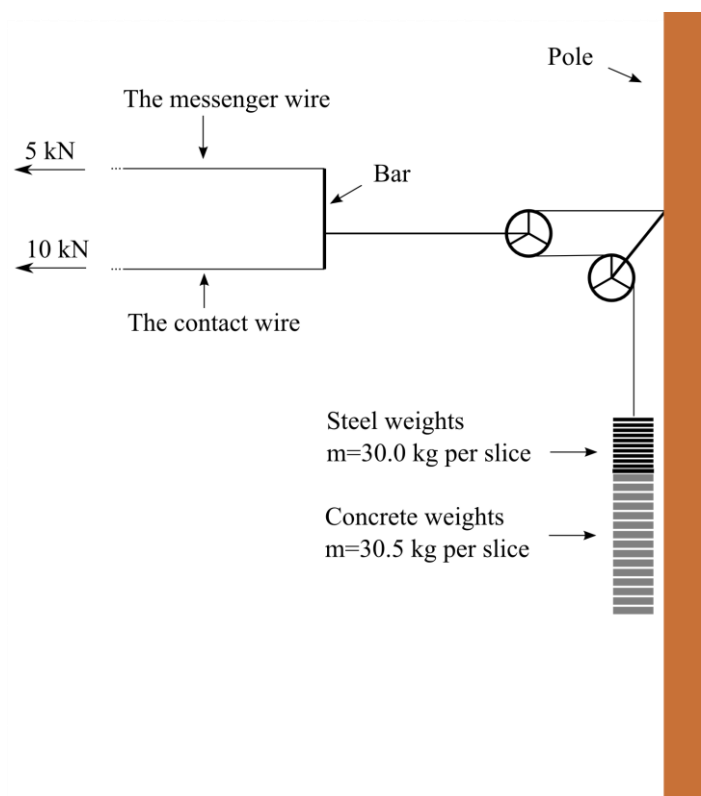


Figure 19 The tensioning equipment used at “Wire 152”

This tensioning device makes the catenary able to move in the longitudinal direction, which is undesirable. Consequently a mid-point anchor, which is placed approximately in the middle of the tensioning section, has been installed. This prevents the wires migrating towards the ends under changing loading conditions[3]. The mid-point anchor is introduced by fastening a wire on the contact wire, and then this wire is fastened to a pole.

2.5 Summary of the properties of the wires in Table 54

The components of Table 54 are described in Table 1.

Tabell 54	Type	Specific weight [N/m]	Diameter [mm]	Cross section [mm²]	Tension [kN]	Young's modulus	Poisson's ratio	Thermal expansion coefficient
Messenger wire	Cu 50/7	4.46	9.0	49.48	5.0	113*10 ⁹	0	1.7*10 ⁻⁵
Contact wire	Ri 100 Cu	8.9	12.0	100	10.0	124*10 ⁹	0.34	1.65*10 ⁻⁵
Dropper	Bz II 10/49	0.89	4.5	9.6		100*10 ⁹	0	1.7*10 ⁻⁵

Table 1 The components of Table 54[6]

2.6 The pantograph

The pantograph is the device on top of the train which purpose is to transfer electric energy from the contact wire to the electric traction unit on the train. One can simplify the pantograph into four components; the main frame, an arm, a pantograph head and a drive[3]. The pantograph studied is shown in Figure 20.

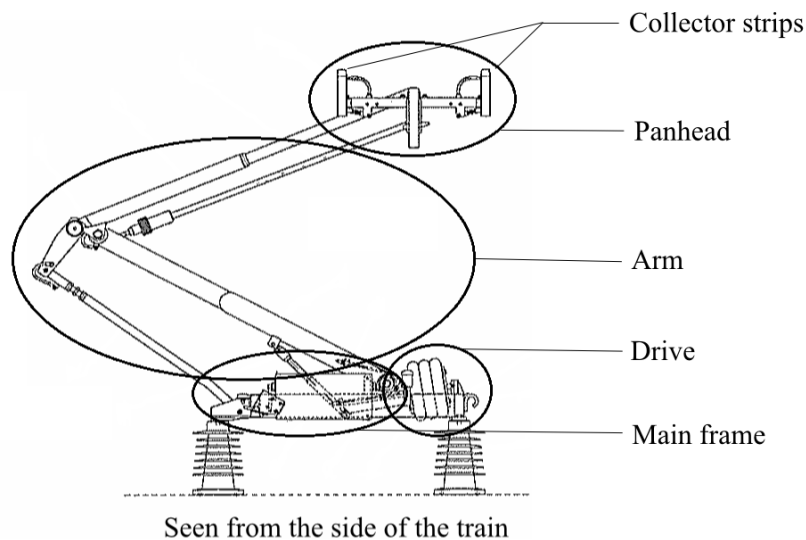


Figure 20 Simplified description of the pantograph, model WBL88[12], showing the collector strips, the pan head the arm, the main frame and the drive.

The pantograph is a complex mechanical system. At the bottom of the pantograph one has the fastening to the train's roof. This connection is very stiff and thus transfers forces and displacements to the bottom of the pantograph from the train. These forces and displacements are mostly due to irregularities in the track, crosswinds and the dynamic reactions in the train during motion.

The drive is the component which introduces the lifting force in the pantograph. The force is introduced by compressing the air inside the bellow[3]; thus it is a very stable force. When the pantograph moves up and down the drive will, in addition to introduce an upward force, function as a damper that is activated only by movement downwards. The reason it doesn't introduce damping on the way up is that the drive will be filled with more air as it does, and then counterbalance this effect[15].

The arm is fixed to the main frame and the drive, and it raises the pan head due to the force applied in the drive[16]. In addition to this there is also dry friction in the joint in the middle of the arm[17], which makes the system a bit more stable.

The pan head is fixed to the upper part of the arm by means of a pan tube. Two levers are fitted to the pan head on one end, and take up the collector strips at the other ends. The collector strips are raised up against weight and contact pressure by leaf springs[16]. These strips are the parts of the pantograph which are in directly contact with the contact wire, and they are the parts which transfer the power. On the current pantograph these strips are of plain carbon and are four centimetres wide and 1600 millimetres long[8].

2.7 The contact force

The term contact force describes the force that acts between the pantograph and the contact wire. In running situations this force varies according to many factors such as elasticity, the static force used, where the pantograph is along a span and which speed the train travels at. One differentiates between whether the train is in movement or not when describing the contact force. When the train stands still one is interested in the static force, which is measured as the force between the collector strips and the contact wire. Whilst the train is moving it is the dynamic force is looked at, and this force is divided into two contributions, the aerodynamic contact force and the dynamic interaction between the contact line and the pantograph. The aerodynamic contact force is defined as the sum of the static contact force and the resulting forces resulting from the aerodynamic effects of the running speed.[3] The contact wire slides on top of the pantograph as shown in Figure 21.



Figure 21 How the contact wire slides on top of the pantograph.

If the magnitude of the contact force is too low there will be times when there is no contact due to dynamic effects. Periods with no contact is called arcing. If the contact force is too high the contact will be well insured, but it will lead to undesirable rapid wear on the carbon collector strips. Thus the magnitude of the contact force is an interesting parameter to investigate.

The Norwegian National Rail Administration has given values for maximum, minimum and recommended mean force, and the standard deviation of the force[18]. These values are respectively shown in formula (2.2), (2.3) and (2.4), and in Figure 22 and Figure 23.

Maximum mean contact force[18]:

$$F_{mid,max} = 0,000586 * v^2 + 70 \text{ N for } 0 \leq v \leq 160 \quad (2.2)$$

Minimum mean contact force[18]:

$$F_{mid,min} = 0,00096 * v^2 + 50 \text{ N for } 0 \leq v \leq 250 \quad (2.3)$$

Recommended mean contact force[18]:

$$F_{mid} = 0,00104 * v^2 + 55 \text{ N for } 0 \leq v \leq 250 \quad (2.4)$$

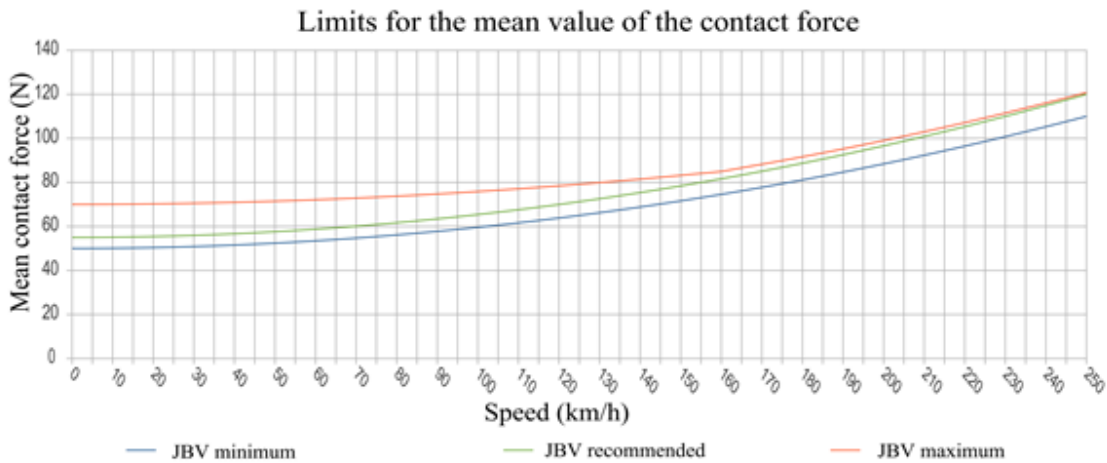


Figure 22 Limits for the mean value of the contact force[18]

The standard deviation(S) of the contact force should be maximum 20% of the maximum mean contact force for the given speed. This gives the values shown in Figure 23[18].

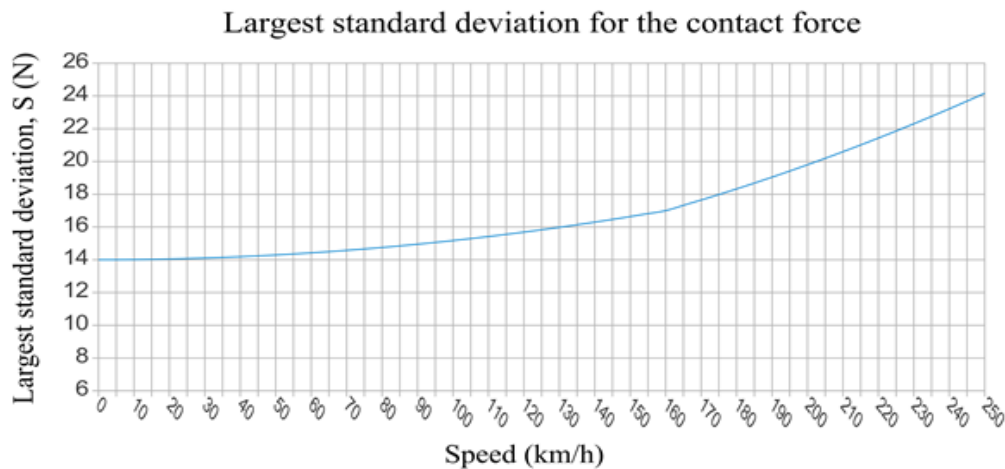


Figure 23 Largest standard deviation for the contact force[18]

In addition to this, the following demands apply[18]:

- 68,3 % of all the values shall be within ($F_{\text{mid,max}} + S$) and ($F_{\text{mid,max}} - S$).
- 95,5 % of all the values shall be within ($F_{\text{mid,max}} + 2*S$) and ($F_{\text{mid,max}} - 2*S$).
- 99,7 % of all the values shall be within ($F_{\text{mid,max}} + 3*S$) and ($F_{\text{mid,max}} - 3*S$).

The contact force demands for the train speeds of interest in this study is computed and shown in Table 2.

Speed (km/h)	70	90	130	200
Maximum mean contact force (N)	72.87	74.75	79.90	93.44
Minimum mean contact force (N)	54.70	57.78	66.22	88.40
Recommended mean contact force(N)	60.10	63.42	72.58	96.60
The standard deviation (N)	14.57	14.95	15.98	18.69
$F_{\text{mid,max}} + S$ (N)	87.45	89.70	95.88	112.13
$F_{\text{mid,max}} - S$ (N)	58.30	59.80	63.92	74.75
$F_{\text{mid,max}} + 2S$ (N)	102.02	104.65	111.86	130.82
$F_{\text{mid,max}} - 2S$ (N)	43.72	44.85	47.94	56.06
$F_{\text{mid,max}} + 3S$ (N)	116.59	119.59	127.85	149.50
$F_{\text{mid,max}} - 3S$ (N)	29.15	29.90	31.96	37.38

Table 2 Contact force demands at different velocities

2.8 The Elasticity

Elasticity is a term which is much used in railway literature. It is a measurement of how flexible the catenary system is in the vertical direction. This is measured in how many millimetres the contact wire is pushed upwards per Newton. In Humar [19] the exactly same thing is referred to as the flexibility influence coefficient. The flexibility matrix is the inverse of the stiffness matrix. A typical value for the elasticity of high-speed lines is 0.5 mm/N[3].

The elasticity of the system is a static entity. In dynamics it would be more interesting to look at the impedance (dynamic stiffness) of the system[20, 21]. The dynamic stiffness can be explained as the stiffness the structure has in a given dynamic situation. The dynamic stiffness has contributions from the static stiffness, damping and mass[22]. “The dynamic stiffness of the catenary is defined as the ratio of the load to the displacement caused by this load”[23]. The “dynamic elasticity” can then be found by computing the inverse of the dynamic stiffness.

2.9 The vertical displacement of the contact wire

The maximum uplift at support should be less than 120 mm according to The Norwegian National Rail Administration[24]. The normal uplift at support should be between 30 and 55 millimetres[8].

EN50318 also presents values for the maximum uplift, but these values are for train speeds of 250 km/h and 300 km/h[25].

2.10 Dynamic characteristics of typical overhead contact line designs

Dynamic characteristics of typical overhead contact line designs include the natural frequencies, f , the wave propagation speed, c , the reflection coefficient, r , the Doppler factor, α , the amplification coefficient, γ_A , the limiting speed, v_a , the non-uniformity, u , and damping [3].

2.10.1 The natural frequencies of catenary systems

The natural frequencies of the catenary system are numerous because of it has many degree of freedoms (DOFs) and there can be calculated one frequency for each DOF. In this work, where the geometry is very different from span to span, there will be expected to be even a larger number of frequencies. In EN 50318[25] the frequency range of interest is 0 to 20 Hz when the speed is between 250 km/h and 300 km/h and this range is also used in the literature[26, 27].

To check if the first natural frequencies are of the right order of magnitude one can use the formula presented in Kiessling [3], and shown below.

$$f_1 = \sqrt{\frac{H_{CW} + H_{MW}}{m'_{CW} + m'_{MW}}} / (2L) \quad (2.5)$$

Here f_1 is the first natural frequency, H_{CW} is the tensile force in the contact wire, H_{MW} is the tensile force in the messenger wire, m'_{CW} is the mass per meter in the contact wire and m'_{MW} is the mass per meter in the messenger wire.[3]

2.10.2 The wave propagation speed

The wave propagation speed, c , is the speed of a transversal impulse i.e. the local vertical movement caused by the pantograph moving[3]. If the train speed is so high that it catches up with the impulse the wire will get an infinite large vertical displacement[24]. It is computed as shown in formula (2.6).

$$c_{CW} = \sqrt{\frac{\sigma}{\gamma}} = \sqrt{\frac{H_0}{m'}}, \text{ m/s} \quad (2.6)$$

Where σ is the longitudinal stress (Pa), γ is the specific mass (kg/m^3), H_0 is the longitudinal force (N) and m' is the mass per meter (N/m) for the contact wire[3]. For the studied section the longitudinal force is 10 kN and the mass per meter is 0.89 kg/m[6]. This gives the studied system a wave propagation speed of 106 m/s or 382 km/h.

2.10.3 The reflection coefficient

The reflection coefficient, r , is defined in formula (2.7)[3].

$$r = 1 / \left(1 + \sqrt{\frac{H_{CW} m'_{CW}}{H_{MW} m'_{MW}}} \right) \quad (2.7)$$

Where H_{CW} is the longitudinal force (N) in the contact wire, H_{MW} is the longitudinal force (N) in the messenger wire, m'_{CW} is the mass per meter (N/m) for the contact wire and m'_{MW} is the

mass per meter (N/m) for the messenger wire[3]. The reflection coefficient for this system is thus 0.53.

2.10.4 The Doppler factor

The Doppler factor, α , is a factor which approaches zero as the velocity of the train approaches the wave propagation speed. It is defined in formula(2.8).[3]

$$\alpha = (c_{CW} - v) / (c_{CW} + v) \quad (2.8)$$

For the studied system this gives a Doppler factor of 0.69 at 70 km/h, 0.62 at 90 km/h, 0.49 at 130 km/h and 0.31 at 200 km/h.

2.10.5 The amplification coefficient

The amplification coefficient, γ_A , shows whether the change in the contact force will be less or more than the previous time the pantograph hit a reflecting transversal wave as the pantograph approaches the source of the reflection, e.g. a dropper. It is computed as in formula(2.9).[3]

$$\gamma_A = r / \alpha \quad (2.9)$$

For the studied system this gives an amplification coefficient of 0.77 at 70 km/h, 0.85 at 90 km/h, 1.08 at 130 km/h and 1.71 at 200 km/h.

2.10.6 The limiting speed

The limiting speed is given as the speed for which the amplification coefficient is equal to 1 and is computed as in formula (2.10).[3]

$$v_\alpha = c_{CW} \cdot \frac{(1-r)}{(1+r)} \quad (2.10)$$

The limiting speed for the studied system is then 117 km/h.

2.10.7 The non-uniformity

The degree of non-uniformity, u , can be an evaluation of the suitability of the overhead contact line for a specific application. This can be calculated as formula (2.11) shows[3].

$$u = \frac{(e_{\max} - e_{\min})}{(e_{\max} + e_{\min})} \cdot 100\% \quad (2.11)$$

Here e_{\max} and e_{\min} are the maximum and the minimum elasticity in a span[3].

2.10.8 Damping

The damping which occurs in the system is very important, but is difficult to measure and to model. It describes all energy-dissipating mechanisms in the system[28]. The amount of damping shows how fast the oscillations in the system reduces, and thus whether there will be a problem to use more than one pantograph on the same train[29].

Increasing the damping in the system, by inserting rubber damping hangers or friction damping hangers, has been tried as shown in Figure 24. The introduction of these components have been found by Aboshi, et al. [30] to reduce arcing and wear on the contact wire.

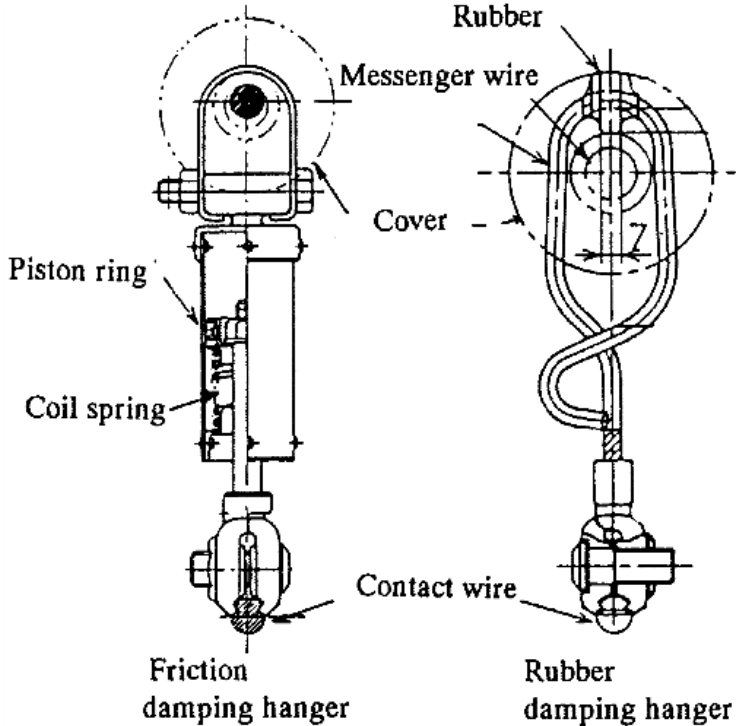


Figure 24 Friction damping hanger and rubber damping hanger[30]

3 Numerical modelling

The numerical model is primarily based on information which The Norwegian National Rail Administration and Schunk Nordiska have provided, see Appendix C-1 to C-4, and [6]. It is a model of “as planned”, not “as built”. Additional information has been taken from articles with similar problems. The finite element method program used to make the numerical model was Abaqus 6.12.

The required information for establishing this model is:

- The catenary geometry
 - Length of each span
 - Length and position of each dropper
 - The zigzag of the catenary
 - The height from track to contact wire
 - The radius of the curves, and how long they are
 - The length of a transition section
 - With or without stitch wires
 - Type of connections between wires
- The masts
 - Position relative to the track
 - Stiffness of the components
 - Type of connection to the wires
- The pantograph
 - The length and width of the bow strips
 - A numerical model of the pantograph
 - Damping values
 - Stiffness values
 - Masses
 - Friction
 - Static and aerodynamic uplift forces
- The mounting sequence

The camber, the height difference between the inner and outer track, which is present in curvature, has not been taken into account in this work. But it should be included in future work.

The model has been in constant development from the start of this work to its end. Changes have been made to improve the model, based on results of the analyses carried out.

The first model was a model of only one straight span, see Figure 25. This was done to get hold of how to model the different properties of the system. There were applied analyses to this model which has not been updated to match the properties of the final model.



Figure 25 Numerical model of one catenary system span.

The model of one span was then developed to model a whole section of spans in two dimensions. Analyses done on the whole section introduced new problems which had to be fixed, and the development of the model resulted in the final numerical model of the whole section in three dimensions.

3.1 The geometry of the railroad

The geometry of the system has been found by first making a simplified, but correct, global geometry of the track in Microsoft Excel. The global coordinates of the track, found in Excel, were then used to find the global coordinates of the positions of the masts and then the catenary system. A Matlab code was then used to obtain the track geometry with the preferred accuracy. Another Matlab code was made to export the global coordinates of the masts and the catenary system into .csv-files so it could easily be included in the numerical model. The steps for making this geometry in Abaqus are as follows;

- i. Choose the part one wishes to model
- ii. Choose “Create Wire: Point to point”
- iii. For both the messenger wire and the contact wire choose “Polyline and Chained wires”, for droppers choose “Polyline and disjoint wires” and for the track choose “Spline and Chained wires”.
- iv. Right click on the first cell and click on “Read from file” and find the correct .csv-file. The Matlab code is included in Appendix D, and the Excel file is included on the DVD. In Figure 26 the geometry of the numerical model is displayed with the y-axis scaled with a factor of five.

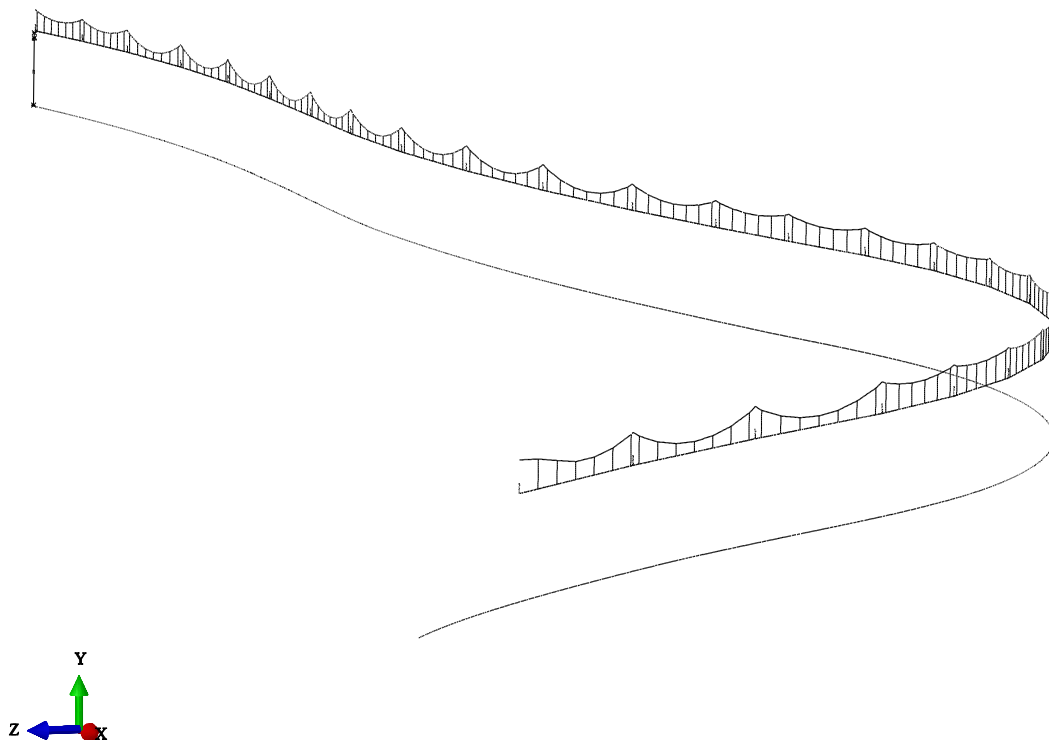


Figure 26 The obtained geometry for “Wire 152” in the numerical model in Abaqus; y-axis is scaled with a factor of five

For this particular railway section studied the geometry for each span was very different, and it is therefore difficult to make a generalized script to describe it. This is why Matlab was not used from the beginning. It is possibly easier to make a generalized Matlab script for newer systems, where the geometry is more alike. This should be considered in future work to reduce the time building a model.

In the first attempts to make a numerical model the geometry was not well defined. This was because the exact geometry from The Norwegian National Rail Administration had not yet been received. The geometry of the catenary system was then modelled in 2D, and then stretched out in 3D to obtain the zigzag. The droppers were modelled with the same length, and then stretched to the desired length by compressing them with the application of temperature. The stresses from this compression were removed after the right length was obtained. This worked for the given situation, but it was easier to model everything directly in three dimensions when the required information was available, and the duration of the analyses was reduced.

The numerical model is made with the x - z -plane as the horizontal plane where the x -axis starts tangential to the train movement, and the z -axis perpendicular to the train movement. The y -axis is the height with zero value at the top of the railway track.

Displacement in x - y - and z -direction will respectively be called U_1 , U_2 and U_3 , and rotations about the x -, y -, and z -axis will respectively be called UR_1 , UR_2 and UR_3 .

3.2 The catenary system

All the wire components, contact wire, messenger wire and droppers, are modelled as 3D deformable wires, and they are discretized by Timoshenko beam elements with hybrid formulation.

In theory it is likely that it would be sufficient to use Euler-Bernoulli beam elements instead of Timoshenko elements, since the main difference is the inclusion of shear deformations[31], and this is of a small magnitude in these wires. But in Abaqus all the analyses failed to converge when Euler-Bernoulli elements were used. Timoshenko elements were consequently used in all the wire components. Euler-Bernoulli beam elements is used in the literature[32], so it may be desirable to be able to use it in future work.

Hybrid formulation was used because it is designed to handle very slender situations, like wires, where the axial stiffness is very large compared to the bending stiffness of the beam. This formulation treats the axial force as an independent unknown to reduce the chance of errors and thus obtain convergence easier[33].

The mid-point anchor is modelled as a point that is fastened against all movement, except in the vertical direction. This is too rigid compared to the mid-point anchors real contributions. This entity should be modelled as two wires which are both fastened to the contact wire, and with the other end fastened to a pole each.

The reason the wires is not modelled as either shells or solids is that it would have introduced an extreme amount of degree of freedoms, which is undesirable for the analysis duration.

3.2.1 The contact wire

The cross-section of the contact wire is modelled as a generalized cross-section with profile properties obtained from the analysis program CrossX; see Appendix E-1 and E-2. The primary reason for using a generalized cross-section is that the geometry of the cross section was difficult or impossible to draw directly into Abaqus. Also it made it easier to introduce a worn cross-section afterwards.

The top surface of the collector strip was used as the master surface and the circumferential surface of the wire was used as the slave surface. The length of each contact wire element had to be very small compared to the total length in order to describe the contact with the pantograph sufficiently. If the length of each element were too large the master surface would go through the slave surface. Thus the element length had to be smaller than the width of the collector strip, which is four centimetres, to prevent this error. It was first tried with an element length of three centimetres, which described the system accurately for most cases, but in some of the analyses an error occurred which was believed to originate from a too long element length. An element length of two centimetres was consequently tried. This made all analyses terminate. The reason for this termination has not been adequately investigated, but due to experiences from other models one solution to fix this may be to enlarge the radius on the sides of the collector strips cross section, which is described later. The element length finally used in the analyses was then three centimetres.

3.2.2 The Messenger wire

The messenger wire is modelled with a solid circular cross section and the material properties described in the theory.

3.2.3 Droppers

The droppers were also modelled with beam elements to be able to describe the fact that it bends under compression. In addition to this it is important that the droppers have some kind of geometrical error to be able to bend before reaching buckling. This is included in this model as small errors in geometry that occurs at pre-tensioning. The tension in the messenger wire and the contact wire drags slightly differently, so the droppers will be slightly diagonal from the messenger wire to the contact wire, and this will be the geometrical error which is necessary.

The connections between the droppers, and the contact wire and the messenger wire are in practice free to rotate in any directions, but because this causes singularity in the model the rotational degree of freedoms had to be tied. Thus both the translational and the rotational degrees of freedom were tied in this connection. The masses of these connectors between the droppers and the CW and MW are not included in this work, but when they are included they should be included as point masses to include the effects of inertia forces.

At one time it was tried to model this connection with the connector type called "JOIN" in Abaqus. That appeared in the analyses to be too rigid, and caused many errors, and eventually termination of the job.

3.3 The cantilever

3.3.1 Registration arms

The registration arms are modelled as springs that follow the line of action; this is in order to enable effects in both horizontal and vertical directions to be included.

Their purpose is to hold the contact wire, solely to obtain the right geometry in the horizontal plane, not carry any significant weight in the vertical plane. Thus they do not have much stiffness and are consequently modelled as springs with little stiffness.

The springs are fastened to the rigid part of the mast with a connection fastened against all translational and rotational displacement. At the connection point with the contact wire they are fastened against all rotational displacement and displacement in U3-direction.

For later work it is desirable to model these components as bars that are free to rotate at their connection to the rigid mast. This would enable the model to describe whether the registration arm pushes the contact wire or pulls at it, which is necessary to include especially when the horizontal movement is to be analysed.

3.3.2 Brackets

In this work the brackets are modelled as rigid points, this because the movement of that point can be neglected. The messenger wire is fastened to the brackets so it is free to travel along its own length axis and to rotate about its normal directions. The other degrees of freedom are fixed.

This modelling of the brackets is too stiff compared to the actual stiffness. The error is not big, but it is desirable at a later point to model the whole mast as a truss system with the actual bars that are in use.

3.4 Pantograph

In this study the pantograph has been modelled in two slightly different ways shown in Figure 27. Both models are modelled as a mass-spring-damper system, and they both describe the pantograph called WBL 88 which is in use in the studied railway section.

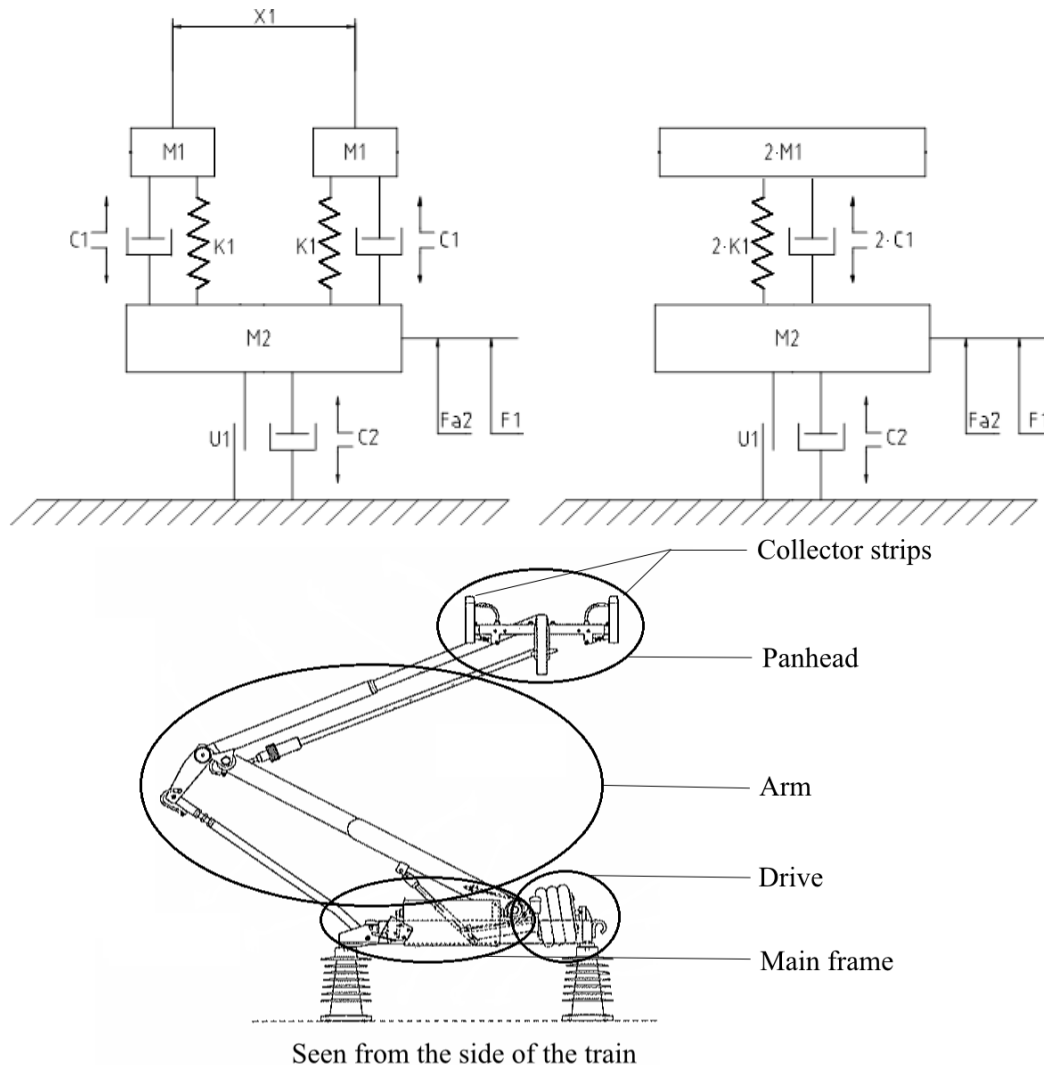


Figure 27 The upper left model is a numerical model of the pantograph WBL 88, the model to the upper right is a simplified version of the same model. They are numerical models of the figure at the bottom. M_1 and M_2 is masses, X_1 is the distance between the two collector strips, K_1 is a spring constant, C_1 and C_2 is damping constants, U_1 is a friction constant, F_1 is a static uplift force and F_{a2} is an aerodynamic uplift force, values for these parameters is displayed in Table 4.

M_1 describes the two pan heads and the second mass, M_2 , the mass of the pantograph arm. Both of these components are modelled as solids which later is made rigid by a constraint in Abaqus called “Rigid Body”.

The springs, K_1 and K_2 , and dampers, C_1 and C_2 , describe measured values of stiffness and damping between the respective components introduced. In the model received from Schunk Nordiska the damping between the arm and the main frame were modelled as C_2 when the

displacement were going down, and zero when the displacement were going up, this is not included in this work, but should be modelled in future work. The model received from Schunk Nordiska, with numerical values is displayed in [Appendix B](#).

Forces that are presented in this model are the static uplift, $F1$, which is introduced to ensure contact and the aerodynamic force, $Fa2$, which gives an extra lifting force when the speed increases. The aerodynamic force is in this work modelled as a constant force of 5N, which is the tested value at a wind speed of 100 km/h.

The dry friction in the arms joint, $U1$, is modelled as connector force which is assigned to a connector between the main frame and the arm.

The numerical values for the properties included in the model are shown in Table 3.

Parameter	Value
2*M1, mass of the pantograph	4*2,3 kg
X1, distance between collector strips	595 mm
C1, the damping between one collector strip and the arm	10 Ns/m
K1, the stiffness between one collector strip and the arm	3100 N/m
M2, mass of the arm	16,5 kg
U1, the friction force in the arm	17 N
F1, the static uplift force	55 N
Fa2, the aerodynamic uplift force	5 N (at 100 km/h)
C2, the damping between the arm and the main frame	63,5 Ns/m

Table 3 Numerical values for the used pantograph ([Appendix B](#))

The pan head is modelled as a solid beam with the cross section displayed in Figure 28. As presented in the theory, the width of each collector strip is 4 cm. However, in order to avoid problems in Abaqus regarding the contact between the contact wire and the collector strip, the width is modelled as 6 cm wide curves on the sides with a radius of one centimetre. This solution may be the cause of the problem described in the chapter about the contact wire. Therefore an attempt to model the curves with larger radius should be tried. The part is seeded with an approximate size of five millimetres. The mesh is shown in Figure 29.

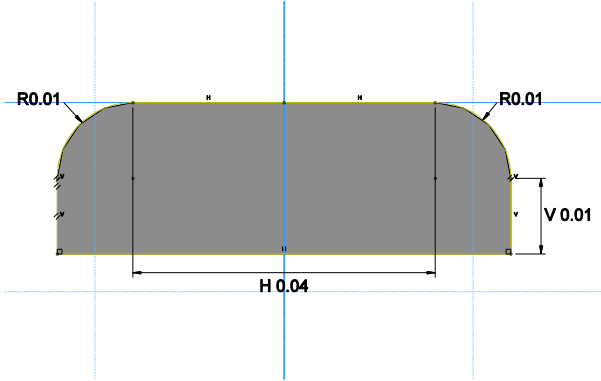


Figure 28 The cross section of the pan head obtained from the Abaqus model.

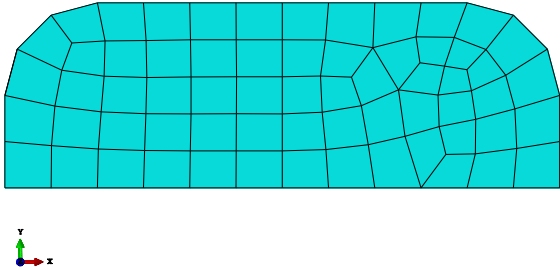


Figure 29 The mesh of the collector strip used in Abaqus.

This is a sufficient model to do quite accurate analyses, but to describe the pantograph better the pan head and the connection between the pan head and the upper part of the arm should be made more complicated. The pan head should be modelled with two bow strips that both have a spring and a damper in each end. This to include the pan heads ability to tilt to both sides. It is also desirable to model the pan head in this way because the measurements done along the track displays four forces, one for each end point on the collection strips. This is shown in Figure 30.

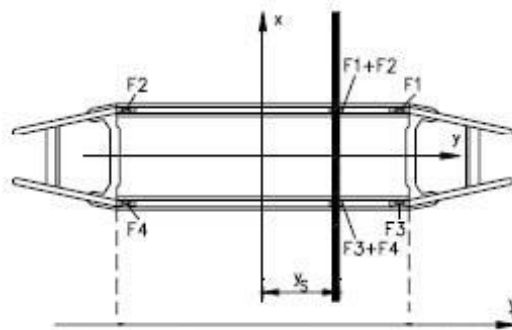


Figure 30 The positions where the force measurements on the pantograph are done are shown as *F1*, *F2*, *F3* and *F4*. The figure is of the pantograph seen from above.[12]

The aerodynamic forces that act on the pantograph can be significant in many situations. Pombo, et al. [34] show that there is a tendency that when wind loads are included the contact forces increases and the pan head is raised. They also observe that the variation of the contact force is increased when including wind loads. These loads are included as one load in this study, and it is modelled as a constant force. This is the usual way to introduce the force[35]. One should still aim to include the force as non-linear in future work to improve the models ability to predict what happens under different wind conditions and varying velocities.

The forces and displacements on the pantograph from the train which were presented in the theory are not taken into account in this model.

3.5 Damping of catenary systems

The catenary system is a structural system with very light damping thus the damping characterization is important[26]. The damping of the catenary system is included as Rayleigh damping [19, 28, 31]. It is usual to include the damping as proportional damping, such as Rayleigh damping, in the literature [26, 32, 36-42]. The Rayleigh damping matrix defines the global damping matrix as a linear combination of the mass matrix and the stiffness matrix as shown in formula (3.1)[28].

$$[C] = \alpha \cdot [M] + \beta \cdot [K] \quad (3.1)$$

To obtain values for α , the mass proportional damping coefficient, and β , the stiffness proportional damping coefficient, the natural frequencies of the global system had to be identified. Then the first natural frequency and a frequency a little lower than the maximum frequency of interest were used to computed them as shown in formula (3.2)[28].

$$\alpha = \zeta \frac{2\omega_1\omega_n}{\omega_1 + \omega_n} \quad \beta = \zeta \frac{2}{\omega_1 + \omega_n} \quad (3.2)$$

ζ is the damping ratio, ω_1 is the first natural frequency (rad/s) and ω_n is the higher frequency (rad/s). The motivation for choosing ω_n as close to the highest frequency of interest and not the highest is that this gives a more correct damping throughout the whole range of frequencies[28].

The values used for α , β and ζ in the literature differ. Damping values used in the literature is displayed in Table 4.

Article	α_{CW}	α_{MW}	β_{CW}	β_{MW}	ζ_{CW}	ζ_{MW}
Pombo and Ambrósio [32]	0.027	0.027	0	0	-	-
Wu and Brennan [23]	-	-	-	-	0.01	0.01
Yong Hyeon, et al. [15]	-	-	-	-	0.01	0.05
Cho [1]	-	-	-	-	0.01	0.05
J. Ambrósio [26]	0.027	0.027	0	0	-	-
Poetsch, et al. [29]	-	-	-	-	0.01	0.01
Jong-Hwi, et al. [41]	0.01	0.05	0.0001	0.0001	-	-
Zhang, et al. [43]	-	-	-	-	0.01	0.01
Sung Pil, et al. [44]	-	-	-	-	0.01	0.05
Y.H and T.C [45]					0.02	0.02

Table 4 Damping values used in the literature. α is the mass proportional damping coefficient, β is the stiffness proportional damping coefficient and ζ is the damping ratio.

Yong Hyeon Cho [46] has done research based on real data where the damping ratios were found to be between 0.01 and 0.04.

Based on this information the damping ratio used in this study is 0.01 in the contact wire and the droppers, and 0.05 in the messenger wire. In future work whether the damping is non-linear should also be investigated. Wu and Brennan [23] show that the damping ratio is not constant. It grows as the velocity increases. This is because the nominal natural frequency

decreases when the train speed increases. The non-linear damping will have a positive effect on the system's performance.

3.6 The pre-tensioning force

The pre-tensioning force is introduced in the model as pre-scribed temperature. This was done by calculating the necessary temperature in both the contact wire and the messenger wire to obtain respectively 10 kN and 5 kN. The temperatures calculated are specific for the given materials and cross sectional area, as one can see in the formula used, formula (3.3).

$$\Delta T = \frac{F}{EA\alpha} \quad (3.3)$$

Where ΔT is the necessary pre-scribed temperature, F is the desired tension force, E is Young's modulus, A is the cross sectional area and α is the thermal expansion coefficient.

This formulation requires that the temperature have to be calculated again if the cross-sectional area is reduced due to wear on the wire. It would be better to introduce the tensional forces in the same way they are introduced at site with weights at the end of each section. It should be aimed to include this in future work.

3.7 The contact force

In this work the contact between the contact wire and the pantograph is modelled with the hard contact that allows separation in the normal direction and with no friction in the tangential direction. It is crucial that the model can describe situations where there is no contact, thus the inclusion of separation in the normal direction. It is modelled in Abaqus with the following steps;

- i. Make an “Interaction Property”
- ii. Add tangential behaviour with the formulation “Frictionless”
- iii. Add normal behaviour as “Hard” Contact and check off “Allow separation after contact”
- iv. Make an “surface-to-surface contact” interaction
- v. Choose the collector strip(s) as the Master surface, and the contact wire as the Slave surface
- vi. Change the properties to match those in Figure 31.

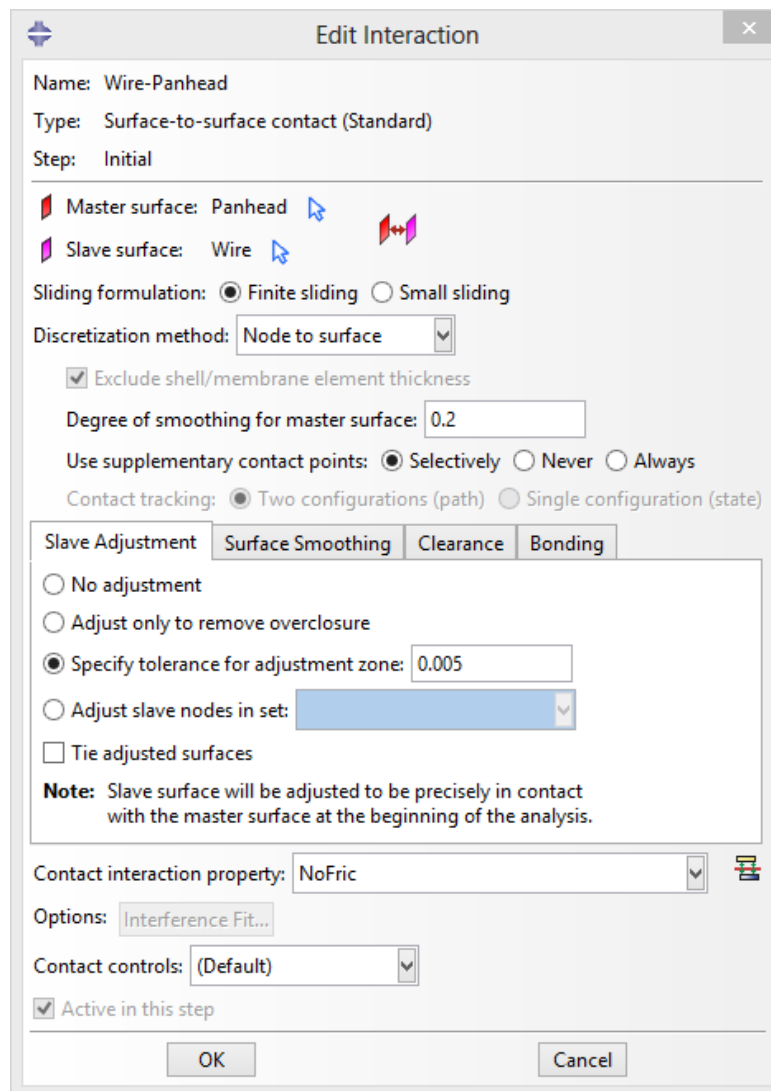


Figure 31 The interaction properties of the contact between the pan head and the contact wire

This formulation of the contact between the pan head and the contact wire is too simple considering its complexity. One thing that has to be included in future work is the friction force that emerges when the pan head slides under the wire. This friction force is especially important and significant in sections with curvatures of small radii[8]. In Ding, et al. [47] the friction coefficient of carbon rubbing against copper is of a value between 0.09 and 0.14 dependent on the temperature and the arc discharge. It is of great importance how this friction is included in Abaqus to be able to describe the highly non-linear properties of it.

Another which can be done with the formulation is that the normal behaviour could be defined in a function of the relative penetration between the two parts. This should be included by penalty formulation to allow loss of contact, which a kinematic constraint will not do[26]. Research should also be done on how the contact can be modelled differently to decrease the analysis duration. A proposition is to find out how one can model the wire as the master surface. If the wire could be made as the master surface one could possibly enlarge the length of each wire element, and this would reduce the duration of the analysis.

There have been tried to model the normal interaction with a spring stiffness in Abaqus/CAE, but this did not allow separation. It was therefore not used. This spring stiffness should be included in future work because it is included in EN50318:2002's reference model[25]. But it is essential that it still allows separation between the contact wire and the collector strip.

3.8 The numerical steps of the analyses

3.8.1 The first step

In the first step a little portion of the pre-tensioning force is introduced. This in order to obtain the necessary amount of stiffness required by the numerical analysis, before loads such as gravity can be introduced. The reasons for not introducing the whole magnitude of pre-tension at once is that this lifts the contact wire so high that numerical errors are introduced. And if gravity had been included without the pre-tensioning it is likely that the system would not have found equilibrium because of the very low stiffness in the wires. There was tried out in analyses how much tension to introduce in this first step to avoid numerical errors. The per cent of the total pre-tension introduced in this step were set at 20% for the contact wire and 28,5% for the messenger wire.

3.8.2 The second step

In the second step the rest of the pre-tension and the gravity of the wires were introduced simultaneously. The model is then as it would be without a train passing by.

After this the steps of the analyses differ. First the steps for studying the elasticity are presented, and then secondly the method for finding the natural frequencies will be shown. Finally, the method for doing the dynamic analyses with the moving train will be presented. Both the elasticity analyses and the frequency analyses are done without the train being present.

3.8.3 Elasticity analyses

The third step is to drag the contact wire up with a force of 150 N in fifteen selected points in a span, one at the time, and then measure the uplift in millimetres relatively to the position with pre-sag. The fifteen points are the two points at the registration arms, at each of the six droppers and in the middle between those eight points. The positions of these points along a span are shown in Figure 32.

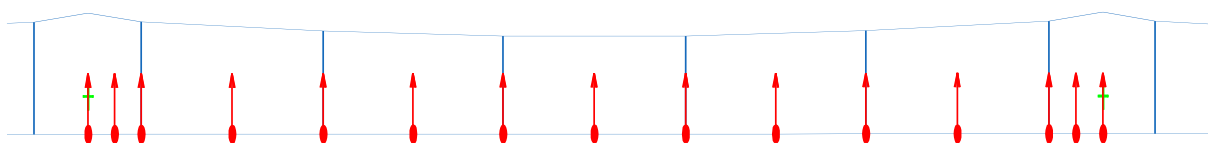


Figure 32 The points where the force is applied in the elasticity analyses. The red dots are the position, the red arrows are the forces and the blue lines are the wires; the top one is the messenger wire, the bottom one is the contact wire and the vertical lines are the droppers.

3.8.4 Frequency analyses

In these analyses there are two more steps. The third step computes the natural frequencies and the fourth computes the complex eigenfrequencies and the damping ratio.

First the analysis has to run only a frequency analysis to obtain the frequencies necessary for calculating the Rayleigh damping coefficients. Then the analysis can run again including the step with the complex frequency analysis. After running some analyses the number of interesting frequencies was set to be 2000.

3.8.5 The dynamic analyses

3.8.5.1 The third step

The third step consists of applying the static uplift force and the mean aerodynamic force on the pantograph. The aerodynamic force is included in this step because in the next step the train has constant velocity from time step one and the force will then need to be introduced before the train starts moving.

3.8.5.2 The fourth step

The fourth step is when the train moves. The method used for moving the train (pantograph) at the right speed along the right path in the numerical model were to use pre-scribed displacements. In this model the degree of freedoms (DOFs) needed to be pre-scribed were U1, U3 and UR2, but the method is applicable to all six degrees of freedom. To know the exact displacements per time step the Matlab code made for the description of the track was used. The Matlab script was adjusted to write out an input file, .inp, which describes the amplitude of displacements/rotations for each time step in Abaqus. This input file was included into the main input file in Abaqus by the use of the keyword *INCLUDE as shown in Figure 34. The displacement of each DOF were included separately, and the magnitude of the displacement were describe by using the keyword *AMP. Figure 33 shows parts of the additional input file, which describes the amplitude of each displacement or rotation. In the same input file one can see how the amplitudes are assigned their respective displacement/rotation with the use of “*Boundary”.

```
*Amplitude, name=U1
0, 0, 0.02, 0.38889, 0.04, 0.77778, 0.06, 1.16667
0.08, 1.55556, 0.1, 1.94444, 0.12, 2.33333, 0.14, 2.72222
0.16, 3.11111, 0.18, 3.5, 0.2, 3.88888, 0.22, 4.27777
0.24, 4.66666, 0.26, 5.05554, 0.28, 5.44443, 0.3, 5.83331
*Amplitude, name=U3
0, 0, 0.02, 6e-05, 0.04, 0.00024, 0.06, 0.00055
0.08, 0.00097, 0.1, 0.00152, 0.12, 0.00218, 0.14, 0.00297
0.16, 0.00388, 0.18, 0.00491, 0.2, 0.00606, 0.22, 0.00733
0.24, 0.00872, 0.26, 0.01023, 0.28, 0.01187, 0.3, 0.01362
*Amplitude, name=UR2
0, 0, 0.02, -0.00047, 0.04, -0.00078, 0.06, -0.00109
0.08, -0.0014, 0.1, -0.00171, 0.12, -0.00202, 0.14, -0.00233
0.16, -0.00265, 0.18, -0.00296, 0.2, -0.00327, 0.22, -0.00358
0.24, -0.00389, 0.26, -0.0042, 0.28, -0.00451, 0.3, -0.00482
** Name: U1 Type: Displacement/Rotation
*Boundary, op=NEW, amplitude=U1
Train, 1, 1, 1.
** Name: U3 Type: Displacement/Rotation
*Boundary, op=NEW, amplitude=U3
Train, 3, 3, 1.
** Name: UR2 Type: Displacement/Rotation
*Boundary, op=NEW, amplitude=UR2
Train, 5, 5, 1.
```

Figure 33 Parts of the input file which is included in the main input files

```
** BOUNDARY CONDITIONS
**
*INCLUDE, INPUT=SpanMast1261to1288SoknedalStasjonAmplnp1.inp
```

Figure 34 The keyword which include the extra input file into the main input files

4 Measuring methods

4.1 Geometry

Selected geometry properties of some of the spans along the studied railway section have been measured with varying accuracy. Three geometry properties; the stagger, contact wire height and the elevation of the outer rail, were measured in the three spans between pole 1276 and 1279. In addition the distances between droppers in span between pole 1277 and pole 1278 were measured.

The stagger was measured as the horizontal distance from the middle of the track to where the contact wire was at each position measured. The contact wire height was measured as the height from the top of the inner rail to the bottom of the contact wire. The camber (the elevation of the outer rail) was measured as the height difference between the inner rail and the outer rail. This was measured with the use of a laser, a bubble level and an inch rule the way Figure 35 displays it. The laser could be moved from side to side so the laser beam could hit the contact wire.

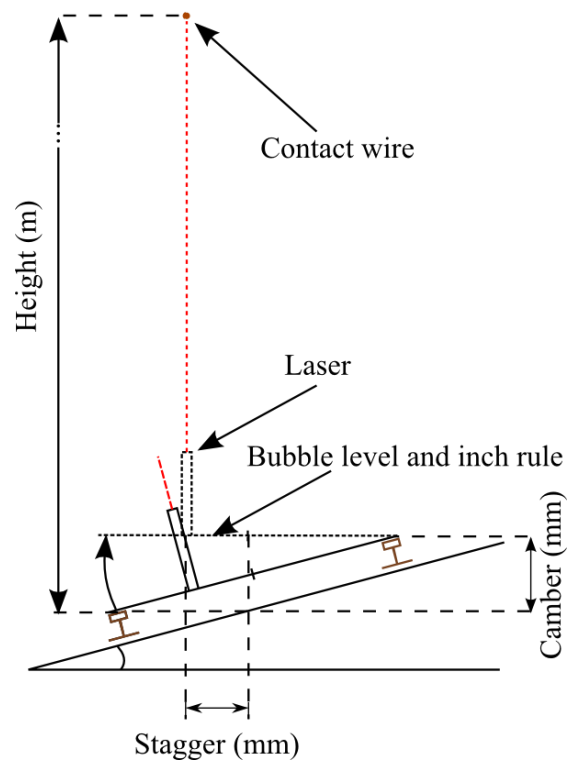


Figure 35 The method for measuring different geometrical values on the catenary system

The distance between the droppers were also measured with the laser, and were measured standing on the top of a train.

4.2 Tension in the contact wire

The tension in the contact wire was measured with a tension measuring device which is shown in Figure 36. The device used was CableBull[48]. To measure the force one has to first measure the diameter of the wire, and adjust the device to this diameter. Then the device is mounted on the contact wire as shown in Figure 36, and the axial tension force is measured.



Figure 36 Tension test at site with the device CableBull[48].

4.3 Elasticity

The elasticity was measured on sight by dragging the contact wire up with a measured force, and then the displacement of that point where measured for that force. The elasticity was then calculated as the displacement (mm) per Newton (N). The force was introduced by one person lifting the wire with a dynamometer, and then reading of the force on the dynamometer and the displacement of that point simultaneously. The margin of error for this measurement method is large, but it is fast and easy to obtain results. The dynamometer used is shown in Figure 37.



Figure 37 Dynamometer, Pesola PHS040[49]

The elasticity was also measured in the numerical model, by pushing the contact wire up with a defined force at fifteen points in a selected span; at each registration arm, each dropper and between each dropper. The displacement were found the respectively points and the elasticity was found.

4.4 Modal parameter identification

One measurement series has been done in order to try to identify the modal parameters of the catenary system. This has been done using a modal hammer, Figure 38, and an accelerometer, Figure 39. The modal hammer is designed to excite and measure impact forces on medium to very large structures[50]. And the accelerometer yields simultaneously dynamic acceleration and force measurements from exactly the same location on the structure[51]. Both the accelerometer and the modal hammer were wired to a power supply/signal conditioner, see Figure 40 and then wired to a NI dynamic module which was standing in a NI chassis as shown in Figure 41. The dynamic module was then connected to a PC by an USB-port. The program used to read these measurements were LabView with the extension called “Record Impact Testing FRF data.vi”[52].



Figure 38 Modal hammer, Brül and Kjær type 8208[51]



Figure 39 Accelerometer, Kistler type 8770A50[50]



Figure 40 Signal conditioner/power supply, Kistler Type 5134[52]



Figure 41 NI chassis type cDAQ-9174 with the NI dynamic mounted[53]

The whole system described above was set up on the roof of a railway wagon to be able to do the measurements at that height, 5,6 metres above ground. The accelerometer was fastened to one additional dropper clamp, and this was then fastened to the contact wire between to existing droppers, see Figure 42. The contact wire was then hit with the modal hammer for each meter away from the accelerometer and up to twenty one meters away. After the measurements were done, the analysis of them should be done in LabView “Modal Parameter Identification.vi”[52]. The programs ability is to do a force response frequency analysis to obtain the natural frequencies and their modal damping ratio. The theory for force-response frequency analyses can be found in Chopra [28].



Figure 42 The fastening of the accelerometer the contact wire. The accelerometer is the grey thing on the top of the dropper clamp. The white cable sends the measured information to the computer.

5 Results and discussion

In this chapter the results will be presented and discussed one by one.

In all the analyses with reduced cross sectional area, the pre-scribed temperatures which introduce the pre-tension were not adjusted. Thus the tension forces in these analyses are too low.

5.1 Natural frequencies and modes

Three natural frequency analyses have been performed in this work. They will be presented after a short presentation of theoretical values for the first natural frequencies of one span. After the presentation of the analyses the results from these will be presented and discussed.

The first natural frequency of the system, computed as presented in the theory, should for a span of 60 metres be;

$$f_1 = \sqrt{\frac{H_{CW} + H_{MW}}{m'_{CW} + m'_{MW}}} / (2L) = \sqrt{\frac{10000N + 5000N}{0.89kg/m + 0.446kg/m}} / (2 * 60m) = 0.883Hz \quad (5.1)$$

And for a span length of 40 metres be;

$$f_1 = \sqrt{\frac{H_{CW} + H_{MW}}{m'_{CW} + m'_{MW}}} / (2L) = \sqrt{\frac{10000N + 5000N}{0.89kg/m + 0.446kg/m}} / (2 * 40m) = 1.325Hz \quad (5.2)$$

In the theory the frequency range of interest was presented as between 0 and 20 Hz.

5.1.1 The numerical analyses

5.1.1.1 Analysis 15

Analysis 15 found natural frequencies of “Wire 152” when it was modelled as a straight section and without wear on the contact wire. This analysis has taken into account 300 frequencies in the range between 0 Hz and 4 Hz. Analysis 15 has not been updated since it first was developed, so it does not have the exactly same properties as the other analyses. Differences compared to the other analyses may occur due to this. In future work this analysis should be updated to have the same properties as the other analyses, and to include frequencies between 0 Hz and 20 Hz.

5.1.1.2 Analysis 26

Analysis 26 computed the natural frequencies of “Wire 152” when it was with curvature and without wear on the contact wire. The analysis was designed to take out the first 2000 frequencies, which were found to be in the range 0 Hz to 18 Hz.

5.1.1.3 Analysis 33

Analysis 33 calculated the natural frequencies of “Wire 152” when it was modelled with curvature and with 20% wear on the contact wire. This analysis has also been designed to take out 2000 frequencies, and these frequencies were between 0 Hz and 18 Hz.

5.1.2 Results and discussion of the natural frequencies

The frequencies found in the three analyses, Analysis 15, Analysis 26 and Analysis 33, are presented respectively in Figure 43, Figure 44 and Figure 45. One can see from these figures that there are extremely many natural frequencies present in the catenary section. The reason for this high number of frequencies in the desired interval is, as mentioned previously, that nearly no span has the same geometry and axial tension which results in many frequencies in the same area of interest. The frequencies are almost continuous in the whole range of frequencies computed.

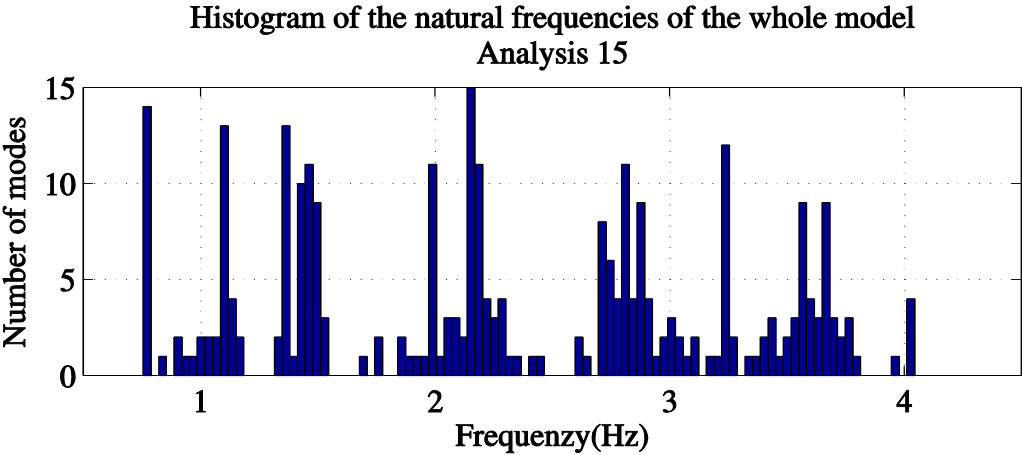


Figure 43 The natural frequencies from 0 Hz to around 4 Hz of the whole section found in Analysis 15. This is the first 300 natural frequencies of the model.

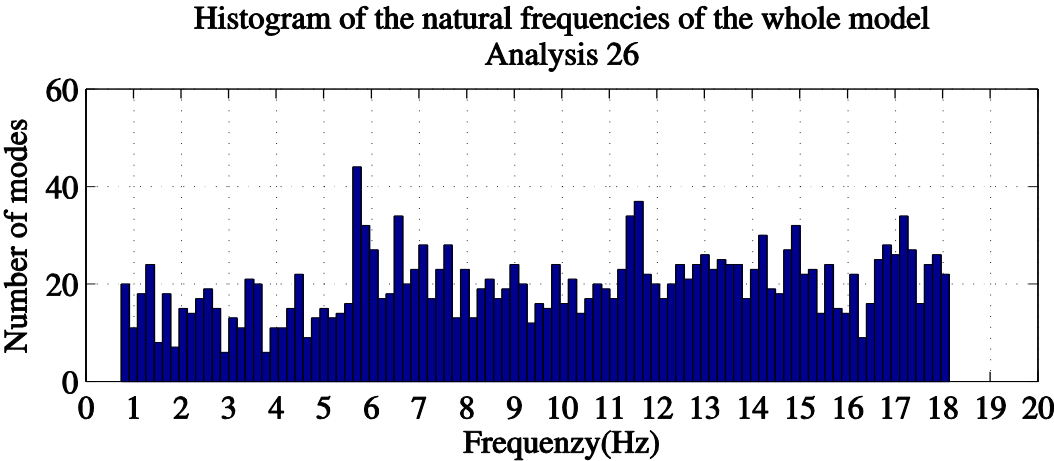


Figure 44 The natural frequencies from 0 Hz to around 18 Hz of the whole section found in Analysis 26. This is the first 2000 natural frequencies of the model.

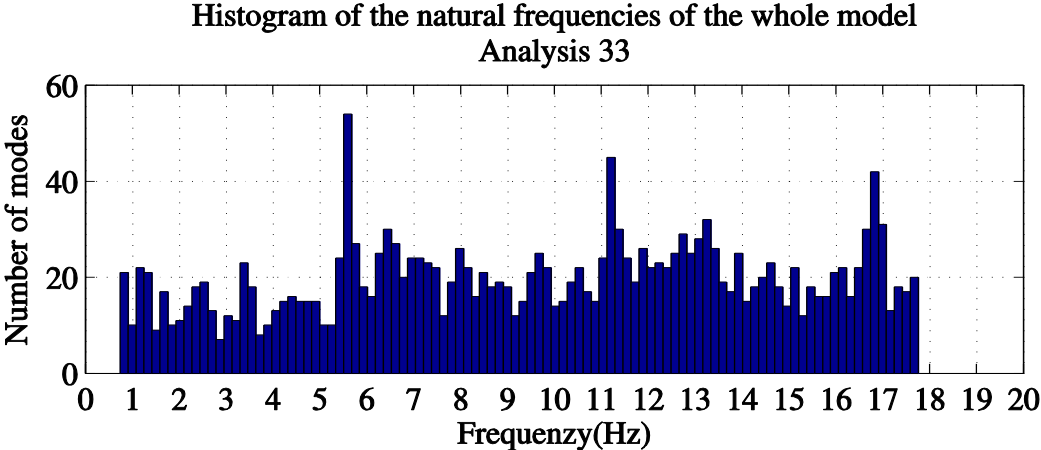


Figure 45 The natural frequencies from 0 Hz to around 18 Hz of the whole section found in Analysis 33. This is the first 2000 natural frequencies of the model.

The difference in frequencies for the model with and without a worn cross section is not major, as seen in the histograms above. The frequencies in the analysis with a worn cross section are slightly lower, than for the analysis without wear. They are even lower for the model done on the straight section. The first natural frequencies are 0.70085 Hz for Analysis 15, 0.74104 Hz for Analysis 26 and 0.74364 Hz for Analysis 33. This shows that the first natural frequency is of the same magnitude in all analyses, and that the difference between worn and unworn contact wire does not affect the natural frequencies much. This can also be shown by looking at the magnitude of the last frequency computed which is 18.138 Hz for Analysis 26 and 17.761 Hz for Analysis 33.

One can clearly see by comparing the histograms that the number of frequencies found when “Wire 152” was modelled as a straight section is considerably less than when including curvature. This confirms that differences in geometry and tension due to curvature results in a higher number of modes in the same frequency range.

To find the range of natural frequencies which are of importance the corresponding generalized mass ratio for each frequency in Analysis 26 and 33 is computed. They are respectively shown in Figure 46 and Figure 47. Analysis 15 is not included because there are too few frequencies included.

By looking at the generalized mass one can determine the resistance the catenary system has against an applied acceleration with a given frequency. A relatively low generalized mass means that at the given frequency the impact on the catenary system will be low[3].

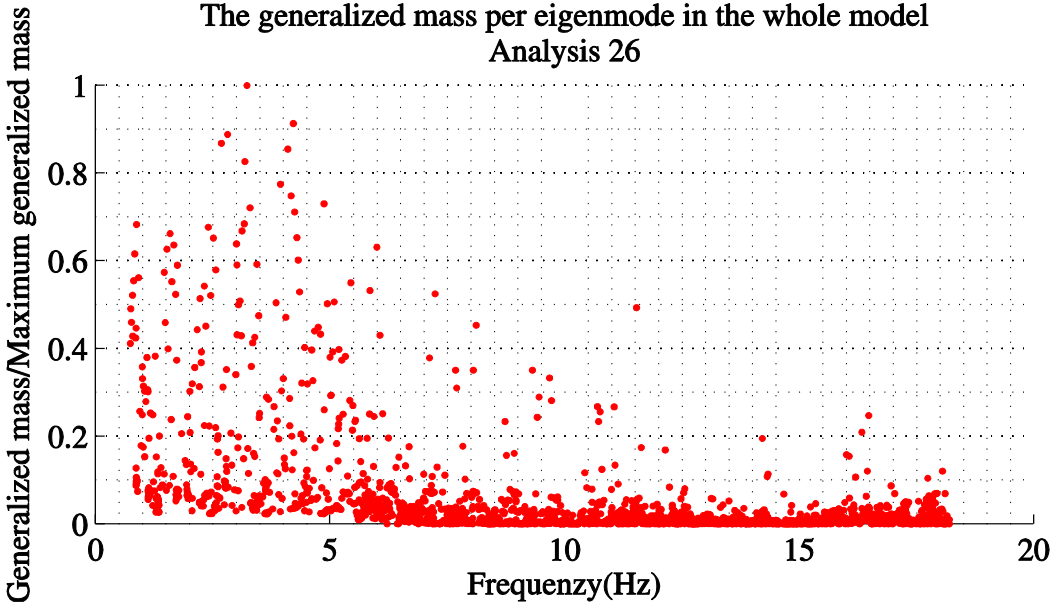


Figure 46 The generalized mass ratio plotted against its natural frequency from Analysis 26. The ratio is computed as the generalized mass for each mode divided by the maximum value for the generalized mass. The cross section of the contact wire is unworn.

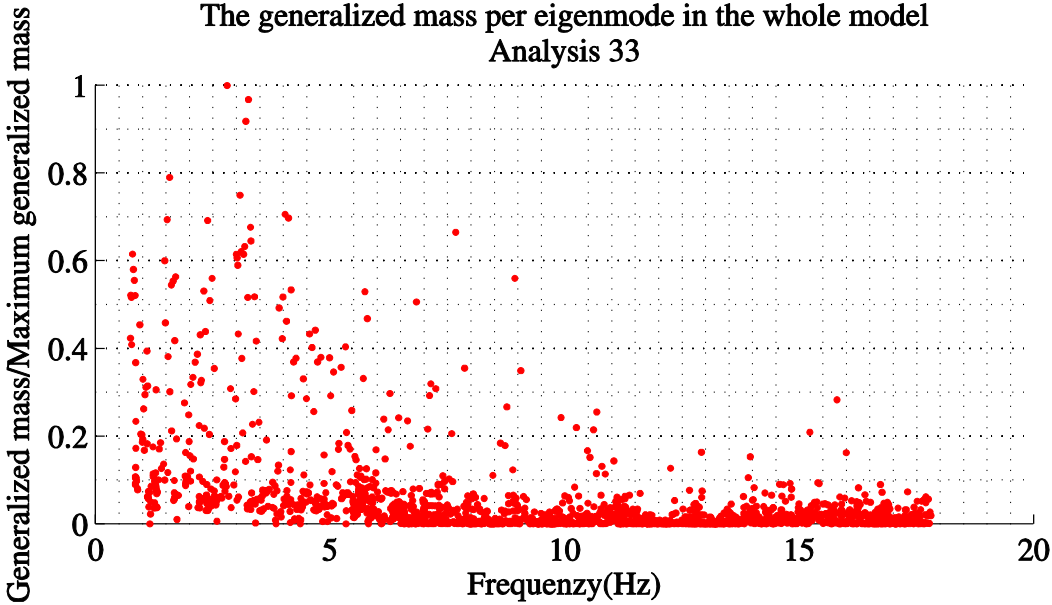


Figure 47 The generalized mass ratio plotted against its natural frequency from Analysis 33. The ratio is computed as the generalized mass for each mode divided by the maximum value for the generalized mass. The cross section of the contact wire is worn by 20%.

From the figures presented above one can see that the frequencies below 6 Hz are the frequencies with the highest corresponding masses. And thus the catenary system will primarily be affected by these frequencies. This is the same result which Kiessling [3] has presented. It can also be seen that the number of frequencies above 12 Hz considerably affecting the system are very low. The frequency range of interest looks approximately the same for both Analysis 26 and 33.

The frequencies of the most interesting magnitude, shown above to be between 0 Hz and 6 Hz, are displayed for Analysis 15, 26 and 33 in respectively Figure 48, Figure 49 and Figure 50.

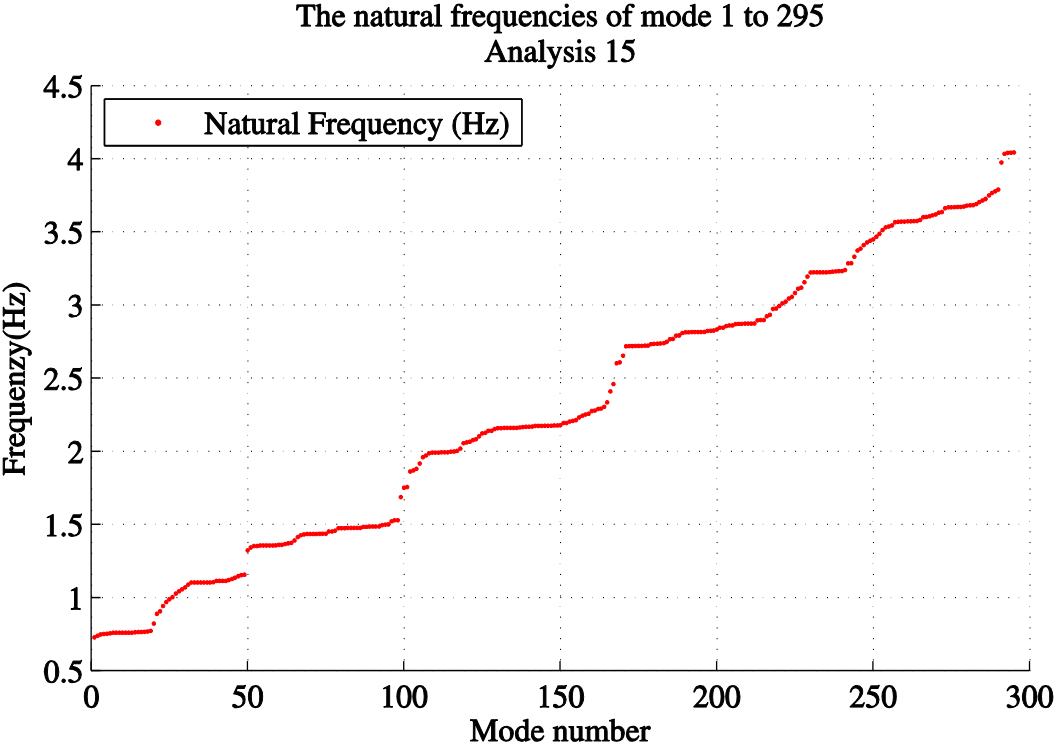


Figure 48 The natural frequencies between 0 Hz and approximately 4 Hz from Analysis 15.

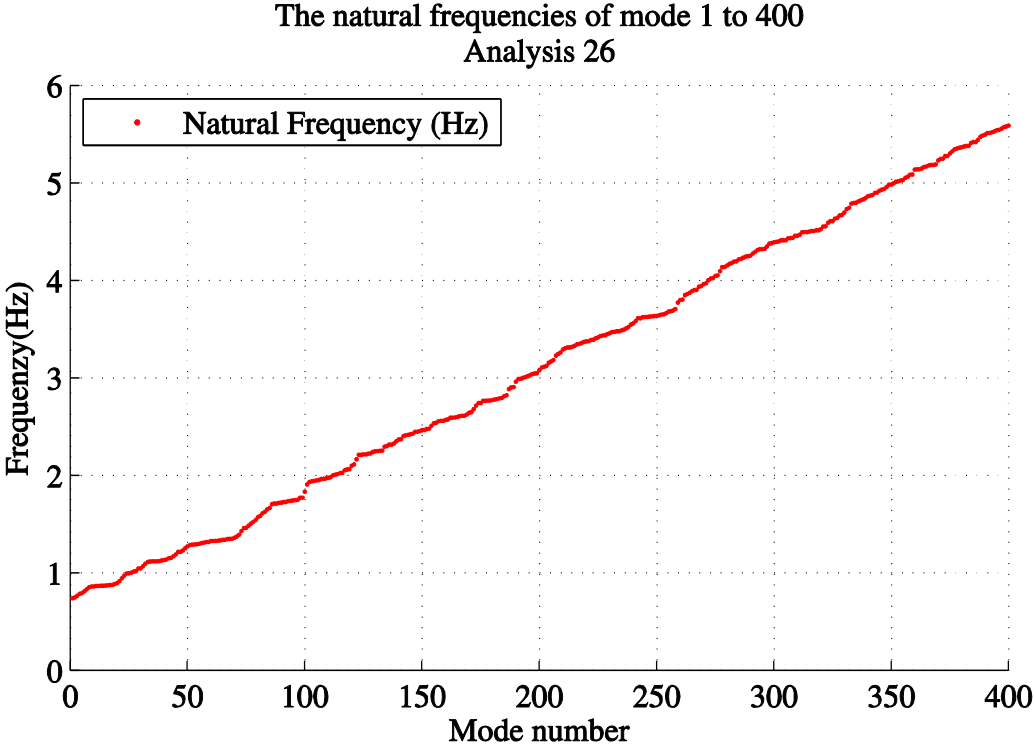


Figure 49 The natural frequencies between 0 Hz and approximately 6 Hz from Analysis 26.

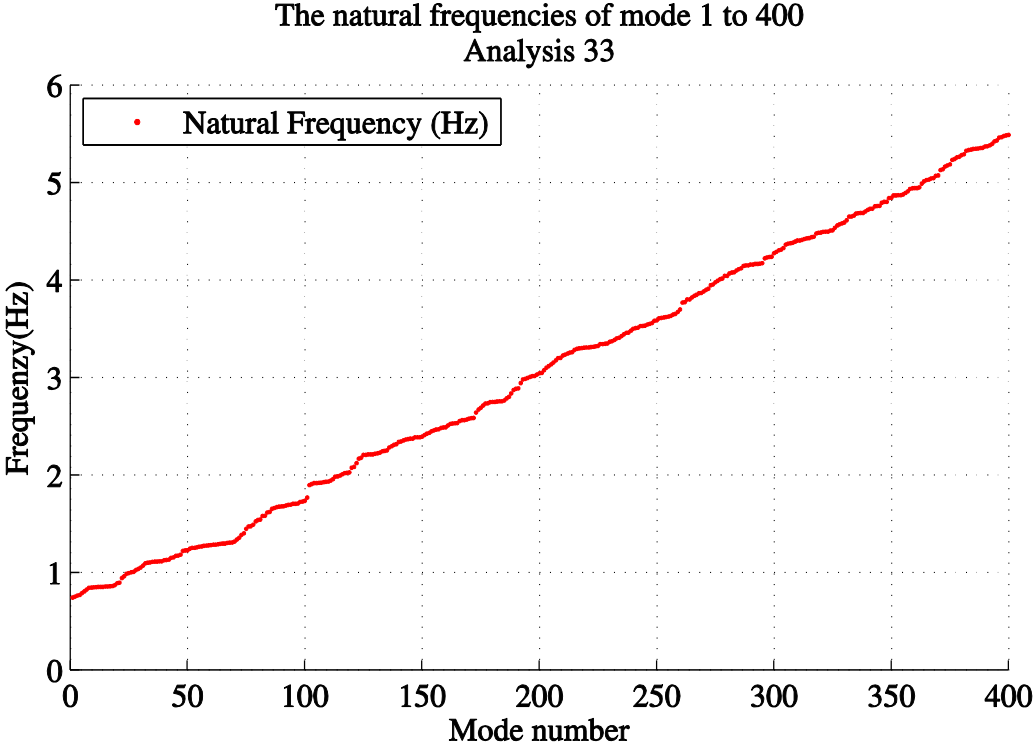


Figure 50 The natural frequencies between 0 Hz and approximately 6 Hz from Analysis 33.

5.1.2.1 Analysis 15

From Figure 48 one can clearly see that there are accumulations of eigenmodes around some frequencies in Analysis 15. The first clear accumulation is in the range between 0.70 Hz and 0.77 Hz. These frequencies are the first natural frequencies for 60 metres long spans in the contact wire. The next accumulation is between 1.10 Hz and 1.15 Hz, and these are the first natural frequencies of the contact wire were the spans are 40 metres.

5.1.2.2 Analysis 26

From Figure 49 one can see that there are accumulations of modes around some frequencies in Analysis 26, but it is not as clear as for Analysis 15. This is the effect of including curvature in the analysis, which makes the geometry of every span different. The first accumulation is around 0.87 Hz, the second around 1.32 Hz, the third around 1.72 Hz and the fourth around 2.0 Hz.

The frequencies in the area around 0.87 Hz is found to excite the spans with a length of 60 metres both in and out of plane. In Figure 51 the corresponding mode to the frequency of 0.87 Hz is shown. One can clearly see in this figure that the mode shape is a half sine wave. This is also found to be the case for the frequencies around 0.87 Hz. The mode shape for the frequencies around 1.32 Hz is also found to be shaped as a half sine wave, but it excites the spans with a length of 40 metres. The frequencies between around 0.87 Hz and 1.32 Hz can be looked at as fundamental frequencies of the different spans.

The next accumulation of frequencies around 1.72 Hz is found to give modes shaped like a full sine wave in the spans of 60 metres. The corresponding mode shape for the natural frequency of 1.75 Hz is shown in Figure 52. The frequencies around 2.0 Hz have also corresponding modes shaped like a sine wave, but they excites the spans of 40 metres.

It is found when regarding the mode shapes in Abaqus that the first natural frequencies of the droppers are around 6.6 Hz, and thus outside the most interesting range of frequencies.

The eigenmode which have the highest generalized mass is shown in Figure 53. One can clearly see that the impact on the system at its natural frequency will be large since it excites almost the whole catenary section.

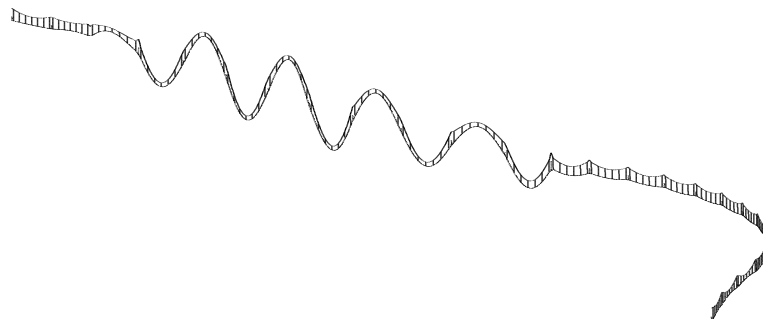


Figure 51 Eigenmode 15 with frequency=0.87 Hz from Analysis 26. This displays half sine waves of the 60 metres long spans.

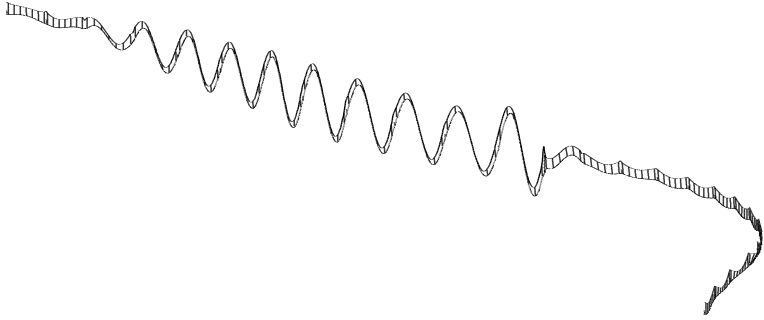


Figure 52 Eigenmode 95 with frequency=1.75 Hz from Analysis 26. This displays sine wave modes of the 60 metres long spans in the model.

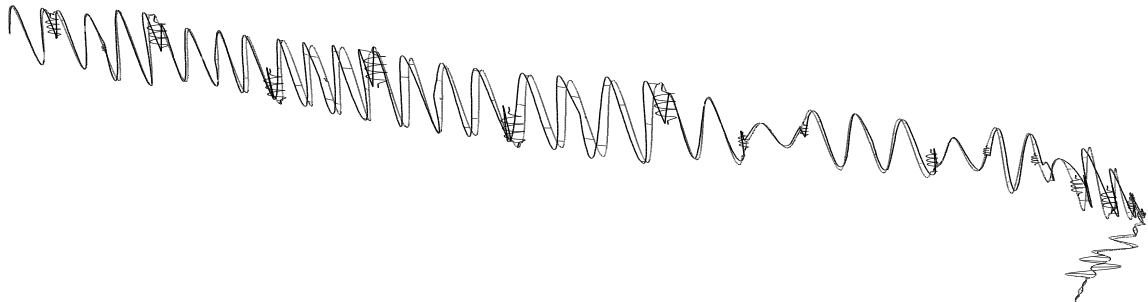


Figure 53 The eigenmode which has the highest generalized mass in Analysis 26. This is eigenmode 212 and the frequency is 3.23 Hz.

5.1.2.3 Analysis 33

It is clear from Figure 49 and Figure 50 that the natural frequencies found in Analysis 26 and 33 are approximately the same. The mode shapes is also found to be similar for the first, second, third and fourth area of frequency accumulation in both analyses. The results from Analysis 33 will thus only be presented in Table 5.

Natural Frequencies	Frequency (Hz)
First accumulation of frequencies	0.85
Second accumulation of frequencies	1.29
Third accumulation of frequencies	1.69
Fourth accumulation of frequencies	1.92
The frequency with the highest generalized mass	3.26

Table 5 Frequency areas with accumulation of modes in Analysis 33.

The small difference in the natural frequencies of the model with and without a worn contact wire indicates that it is difficult to use frequency analyses to measure the magnitude of wear. It should be noted that with the correct axial tension force in the worn contact wire the result would have been slightly different. Since the tension force is too low it is likely that the frequencies are too low as well. This is due to a lower geometrical stiffness than with the correct tension force.

5.2 Damping

The damping included in the analyses is, as mentioned earlier, Rayleigh damping. Two plots of the effective damping ratios for each natural frequency are obtained from Analysis 26 and Analysis 33, and shown respectively in Figure 54 and Figure 55, together with plots of the introduced Rayleigh damping, the mass proportional damping and the stiffness proportional damping.

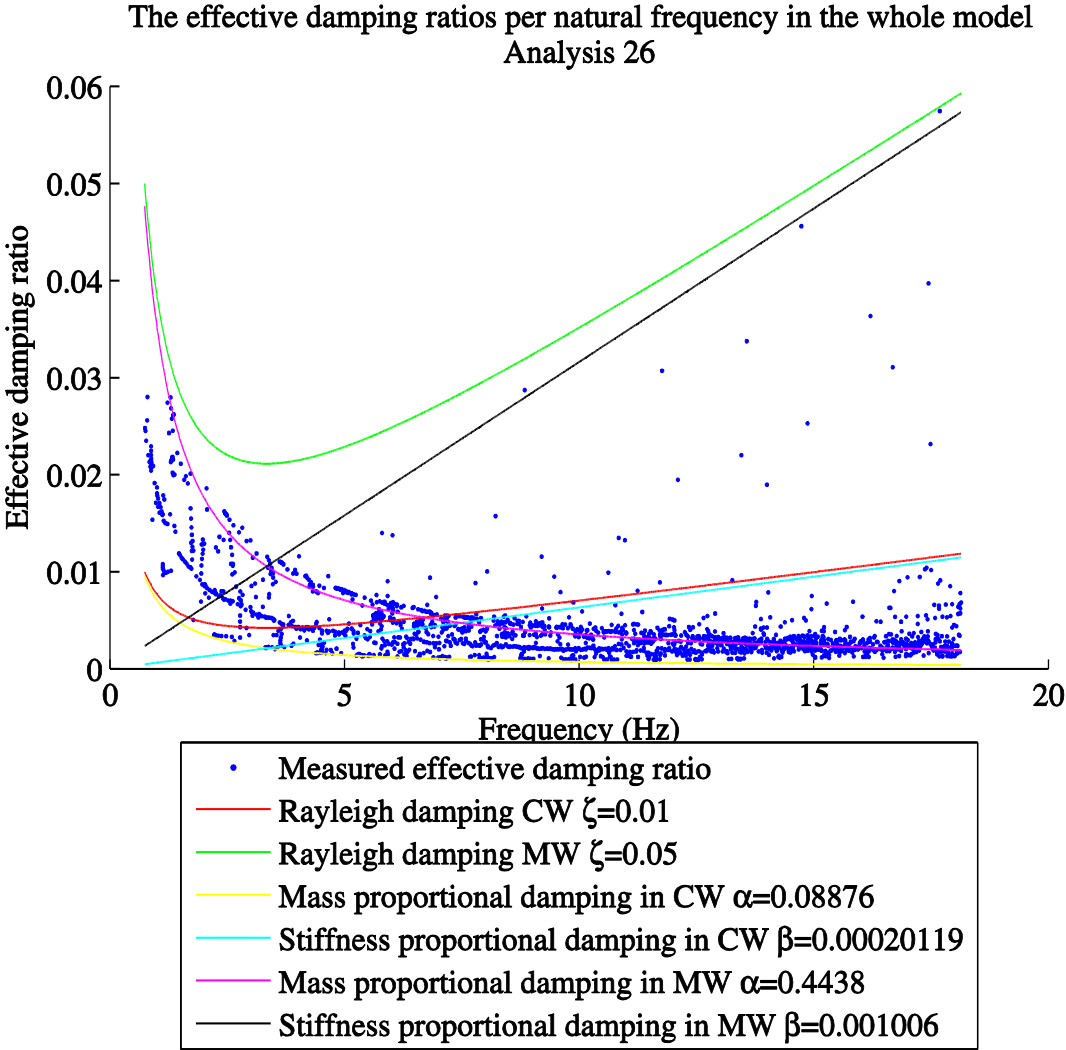


Figure 54 The effective damping ratios for each natural frequency in the whole model from Analysis 26.

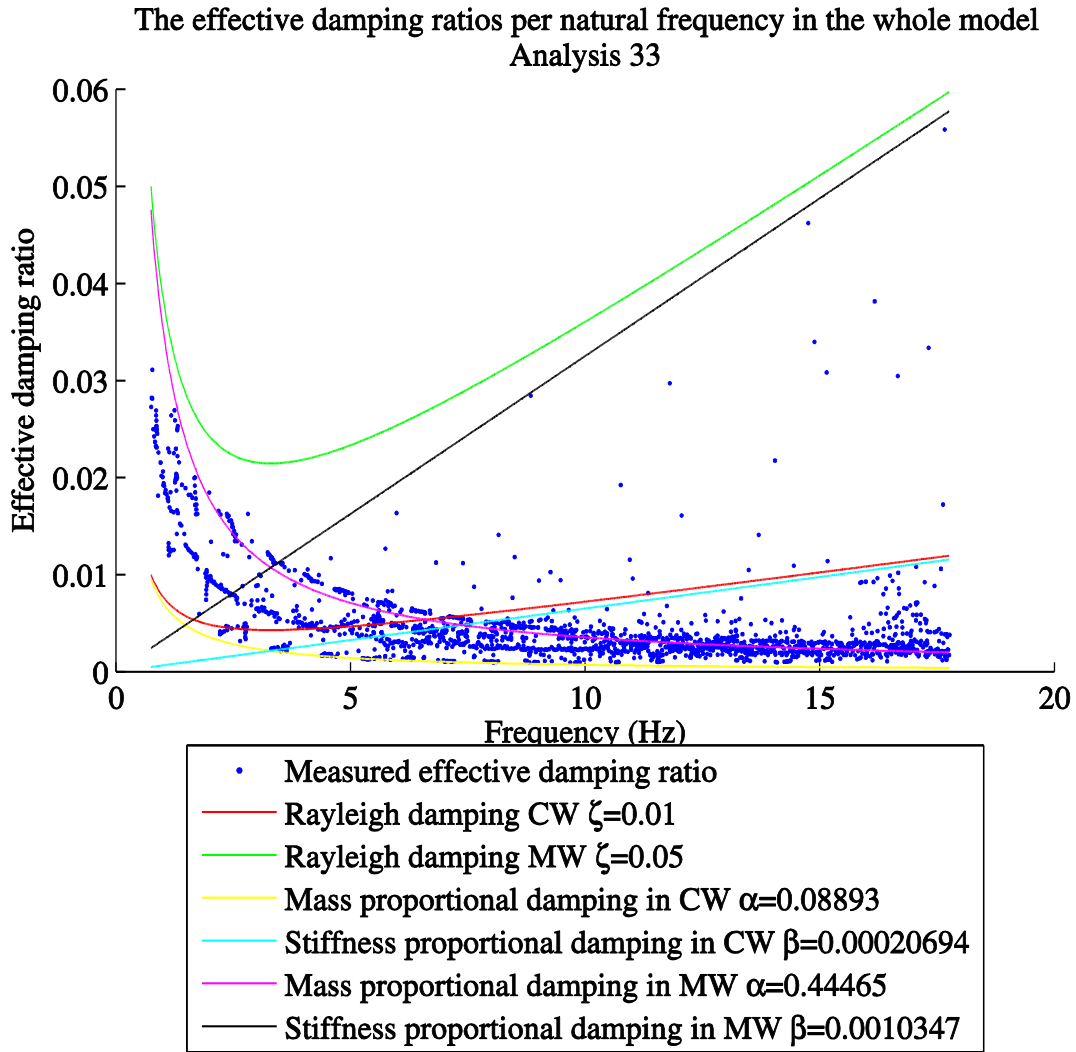


Figure 55 The effective damping ratios for each natural frequency in the whole model from Analysis 33.

Based on the figures above, it is difficult to tell if the damping which is introduced is correct or not. In theory the effective damping ratios, blue dots, should have followed the path of the Rayleigh damping function. But because one damping ratio is used for the messenger wire, and one for the contact wire, two Rayleigh graphs are present, red and green line. It is then difficult to say where the blue dots should have been. To have more control on the damping it is generally smarter to operate with one damping ratio for the whole model. However, based on these figures it is possible to tell that the damping is mostly mass-dependent. This because the measured effective damping ratios of the most interesting frequencies, 0-6 Hz, can be seen to follow the mass proportional part of the Rayleigh curve.

In Abaqus there is a general problem with introducing the damping as Rayleigh damping when the contribution from the geometrical stiffness to the total stiffness matrix is considerable. This is because the β -value is only multiplied by the stiffness matrix without the geometrical stiffness contribution when used in the analyses.

The damping ratios used in the models was 0.01 in the contact wire and 0.05 in the messenger wire. It is found that it is easier to describe and have control over the actual damping if only one value is used. It is suggested that this damping ratio in future work should be 0.01.

5.2.1 Measurements

Frequency-response measurements were taken on site. Modal parameter identification with these measurements was tried. This identification was difficult since the program used did not allow small enough mesh to obtain accurate results. In Figure 56 the interface of the program is shown, and two frequencies and their corresponding damping ratios displayed. These results are plausible, but, as previously mentioned earlier, not very accurate.

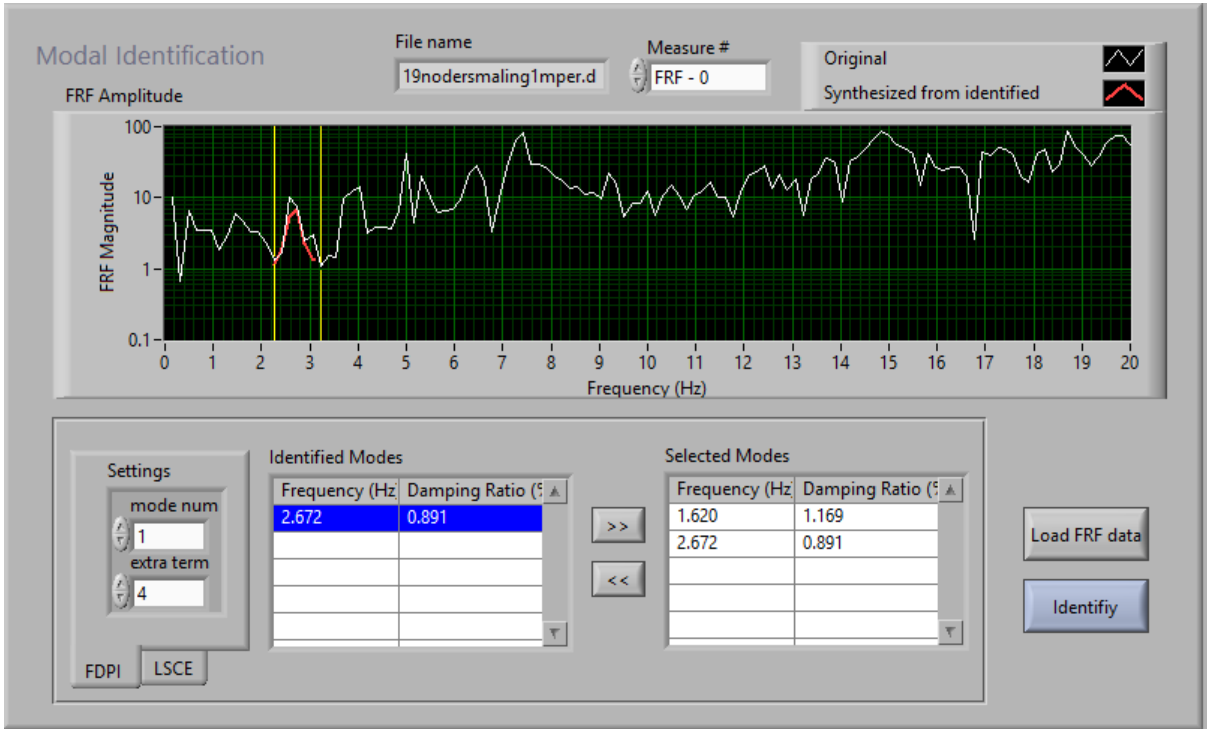


Figure 56 Interface of the modal parameter identification program with one of the measurements done at the site. In the figure one can see that there is found a natural frequency of 2.67 Hz and a corresponding damping ratio of 0.00891.

5.3 Elasticity

5.3.1 Numerical analyses

The numerical analyses of the elasticity were performed by applying a static uplift load of 150 N to selected points along the span between pole number 1277 and 1278, and finding the displacement at those points. Two elasticity analyses were done, Analysis 28 and Analysis 34. Analysis 28 was applied when the contact wire was unworn, and Analysis 34 was applied when the contact wire was worn 20%. In Figure 57 one can see a screen shot of how the test was performed in the numerical model.

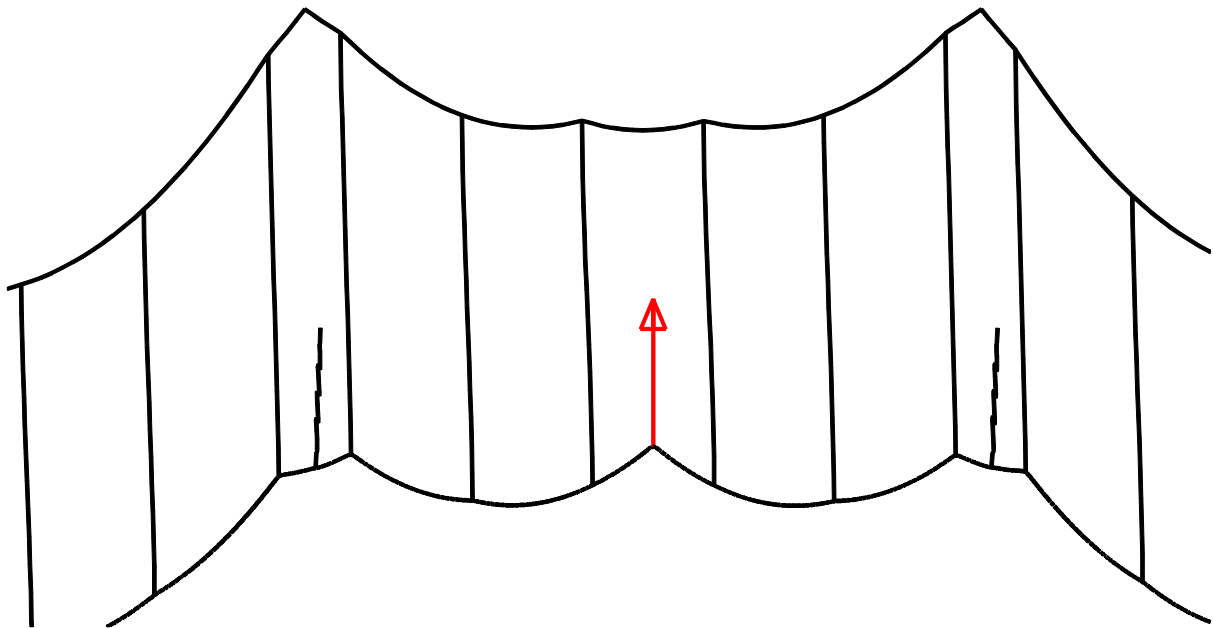


Figure 57 Elasticity test in the middle of the span between pole 1877 and 1278 with the displacement shown and the red arrow illustrates the uplift force. The uplift force was 150 N. The y axis is scaled up with a factor of 20, and the deformation is scaled up by a factor of 5.

The result from Analysis 28 gives a maximum elasticity of 0.9955 mm/N which occurs in the middle of the span. The mean value for the elasticity in the span was 0.6111 mm/N. In Figure 58 the obtained elasticity for the whole span from Analysis 28 is displayed.

Analysis 34 gives a maximum elasticity of 0.9883 mm/N and a mean value of 0.604 mm/N. The maximum elasticity was found in the middle of the span. The elasticity for the whole span found in Analysis 34 is displayed in Figure 58.

5.3.2 Measured values

The measured results have, as explained previously, a large margin of error due to imprecision in the simultaneous readings of the force and displacement. The maximum elasticity was found in the middle of the span, and was 0.9 mm/N. The mean value found was 0.506 mm/N.

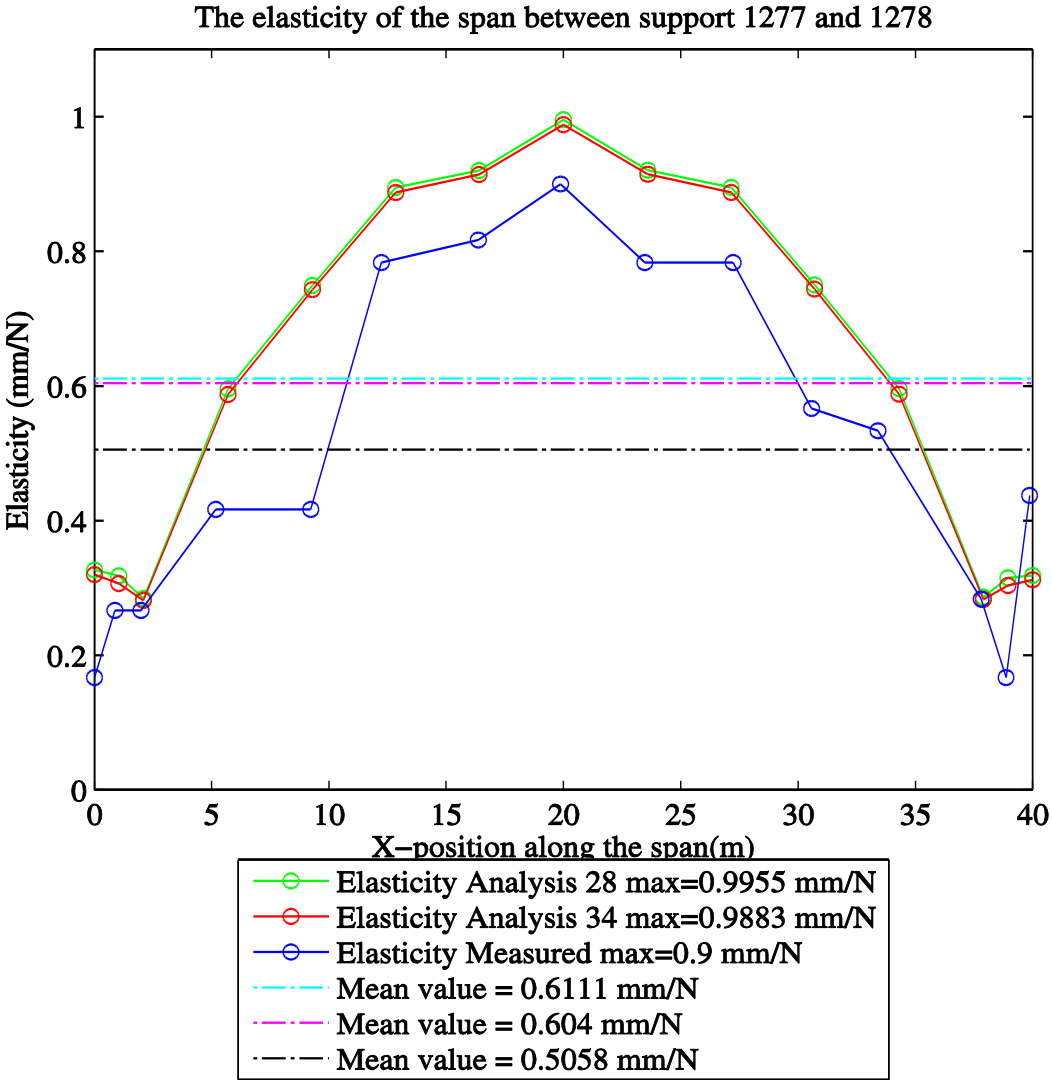


Figure 58 The elasticity results from Analysis 28, Analysis 34 and the measurements at site.

5.3.3 Discussion of the elasticity

The figure clearly illustrate that the elasticity obtained in the numerical model is close to the reality. But it would be preferable to do the measurements at the site with higher precision to, reduce the margin of error and thus have better results for validation of the numerical model.

5.4 The tension force in the contact wire and the messenger wire

The introduced pre-tensioning force in the contact wire and the messenger wire were respectively 10 kN and 5 kN. In addition to this the gravity load and the geometry gives the total tension in the wires. In Figure 59 the tension forces in the model without wear are displayed. The maximum value in the contact wire was 14.8 kN.

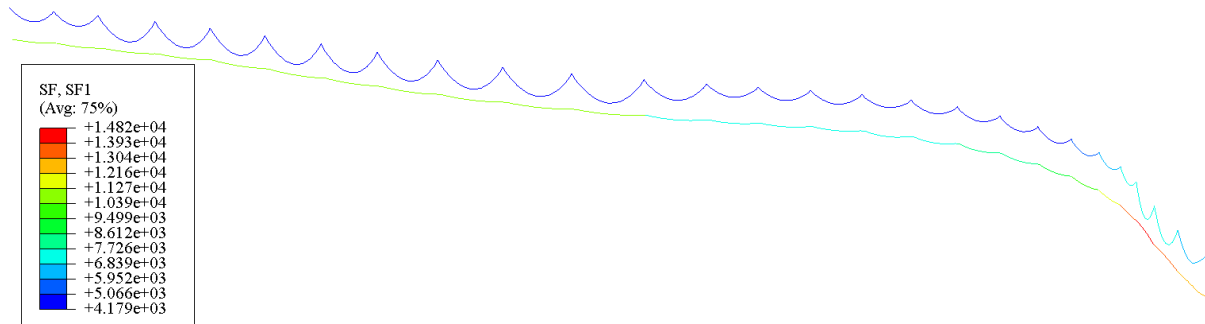


Figure 59 Tension forces in the numerical model without wear. The legend on the left shows which magnitude each colour describes.

The tension force measurements obtained from the studied railway section are shown in Table 6 together with obtained tension forces from the numerical model.

Span	1272/ 1273	1276/ 1277	1277/ 1278	1278/ 1279	1279/ 1280	1281/ 1282
Span from the right in Figure 59.	15	11	10	9	8	6
Measured tension in contact wire (kN)	16.5	17.2	17.2	17.3	17.3	17.7
Measured tension in contact wire in per cent of maximum value	93.2%	97.2%	97.2%	97.7%	97.7%	100.0%
Tension in contact wire from numerical model (kN)	7.1	7.3	7.5	7.8	8.3	10
Tension in contact wire from numerical model in per cent of maximum value	71.0%	73.0%	75.0%	78.0%	83.0%	100.0%

Table 6 Tension forces in the contact wire, both from measurements at site and from the numerical model.

One can see that the differences between the measured values and the values from the numerical values are far from the same. Due to the fact that the contact wire should have approximately 10 kN as the maximum tensioning force it is reasonable to believe that the measurements are incorrect. Despite this it is important to look at the loss of tension in the system. In both the measured results and the results from the model the tension decreases when considering spans further away from the sections end. This is correct because it is at the ends the tension is applied. The difference in tension is much larger in the numerical model than in the measured results. The reason for the large decrease of tension in the model should be investigated and fixed in future work. It is possibly due to accumulation of forces at the supports.

5.5 Wear

The wear of the contact wire was measured at seven points along the studied section, six of them in the middle of the span, and one at a support. The results of the measurements done in the middle of the spans are presented in Table 7. The wear found at support 1277 was 9.75%.

Span	1272/1273	1276/1277	1277/1278	1278/1279	1279/1280	1281/1282
Wear	4.17%	5.83%	6.25%	5.67%	6.00%	5.92%

Table 7 The measured wear of the contact wire in six different spans.

All the measured values of the wear are inside the limit of 20%. But it is interesting to see that the wear is larger at the support than in the middle of the span. This reflects that the contact force at the support is possibly larger than in mid span.

5.6 Pre-sag

The pre-sag have been measured at site, and found in the analyses both for a worn contact wire and an unworn contact wire. The results are displayed in Figure 60.

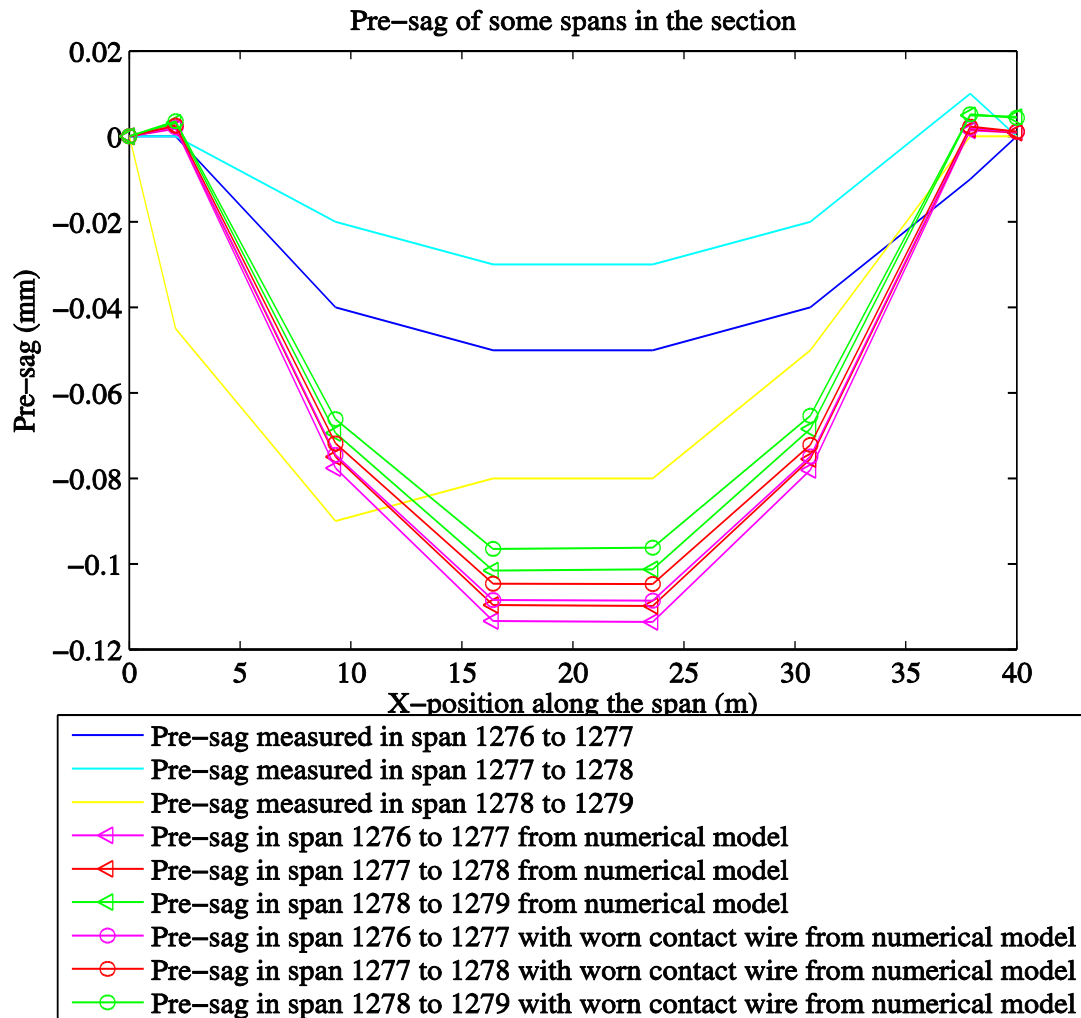


Figure 60 Pre-sag of some spans in the catenary section. There is included pre-sag found from measurements, analyses with and without a worn contact wire.

It is clear from the figure above that the pre-sag obtained in the numerical model is too large in the examined spans. In span 1278 to 1279 the model is quite close to reality. The pre sag there is 26.5% too large in the model without wear, and 20% too large when wear is included. The respective values for span 1277 to 1278 are 266% without wear and 349% with wear. And in span 1276 to 1277 it is 127% and 117%. The reason for this large error may be that the tension force is too low in the model. However, the shape of the pre-sag is correct.

As a result of different dropper design in the spans some of the spans in the numerical model have shown a pre-lift instead of a pre-sag. This effect occurs in span three, four and five from the south, and in span two, three and four from the north. This may be a result of differences in the geometry of the droppers. A small dropper height in the middle of the span will result in a high vertical component of the pre-tensioning force, and thus a large lift of the wire. This effect has not been checked at site, but should be checked in future work.

5.7 Implicit dynamic analyses

Nine different dynamic analyses have been performed on the numerical model of “Wire 152” in this work. These nine analyses are presented below. One should be aware that the real running speed of the train is normally between 70 and 90 km/h at this railway section. So the railway section is not designed to run at speeds of 130 km/h and 200 km/h. Most of the analyses were done using parallel processing which with testing were found to reduce the duration of each analysis. There was not a linear relation between the duration and the number of processors used. Thus if one only wished to reduce the total time of the analyses it would be more efficient to run all at the same time with one processor each.

First each dynamic analysis will be presented, and then the results from these analyses will be displayed and discussed one by one.

5.7.1.1.1 Analysis 10

Analysis 10 was an early analysis of the section Wire 152 when it was modelled as a straight section. Many parameters have been changed after this version of the numerical model was made. The main differences are that the pantograph model was of different pantograph from the one used in Norway, and that it was run along a straight section. The train was driven at 200 km/h and there was no wear on the contact wire. The maximum time step used was 0,01 second for the dynamic part of the analysis. The results from this analysis will not be shown because it is difficult to compare its results with the other analyses due to big differences in the modelling.

5.7.1.1.2 Analysis 27

Analysis 27 was the only analysis which included two bow strips on the pantograph. The train was driven at 70 km/h and there was no wear on the contact wire. The maximum time step used was 0,01 second for the dynamic part of the analysis. The results of this analysis will not be displayed because the friction force used in the pantograph was pointed the wrong way. And due to time limitations it was not possible to run it again after the error was fixed.

5.7.1.1.3 Analysis 29

Analysis 29 was run with one bow strip on the pantograph. The train was driven at 70 km/h and there was no wear on the contact wire. The maximum time step used was 0,01 second for the dynamic part of the analysis. The duration of the analysis was approximately 70 hours when three logical processors were used.

5.7.1.1.4 Analysis 30

Analysis 30 was run with one bow strip on the pantograph. The train was driven at 70 km/h and the contact wire was worn 20%. The maximum time step used was 0,01 second for the dynamic part of the analysis. The results of this analysis will not be shown for the same reasons as for Analysis 27.

5.7.1.1.5 Analysis 31

Analysis 31 was run with one bow strip on the pantograph. The train was driven at 90 km/h and there was no wear on the contact wire. The maximum time step used was 0,008 second for the dynamic part of the analysis. The duration of the analysis was approximately 109 hours with one logical processor used.

5.7.1.1.6 Analysis 32

Analysis 32 was run with one bow strip on the pantograph. The train was driven at 130 km/h and there was no wear on the contact wire. The maximum time step used was 0,005 second for the dynamic part of the analysis. The duration of the analysis was approximately 62 hours with three logical processors used.

5.7.1.1.7 Analysis 35

Analysis 35 was run with one bow strip on the pantograph. The train was driven at 200 km/h and there was no wear on the contact wire. The maximum time step used was 0,003 second for the dynamic part of the analysis. The duration of the analysis was approximately 59 hours with three logical processors used.

5.7.1.1.8 Analysis 36

Analysis 36 was run with one bow strip on the pantograph. The train was driven at 90 km/h and the contact wire was worn 20%. The maximum time step used was 0,008 second for the dynamic part of the analysis. The duration of the analysis was approximately 57.5 hours with three logical processors used.

5.7.1.1.9 Analysis 37

Analysis 37 was run with one bow strip on the pantograph. The train was driven at 130 km/h and the contact wire was worn 20%. The maximum time step used was 0,005 second for the dynamic part of the analysis. The duration of the analysis was approximately 50 hours with three logical processors used.

5.7.2 The contact force

The contact forces computed in the analyses are taken out by extracting all the contact forces which acts on the collector strip, sum them for each time step and thus obtain the total contact force in each time step. The results from Analysis 29, 31, 32, 35, 36 and 37 are respectively shown in Figure 61, Figure 62, Figure 63, Figure 64, Figure 65 and Figure 66. In these figures the contact forces will be displayed at the position they act along the railway track between Oslo and Trondheim. Thus the x-axis displays the distance from Oslo in kilometres. This is done to more easily compare the numerical results with the measured results which are displayed in the same way.

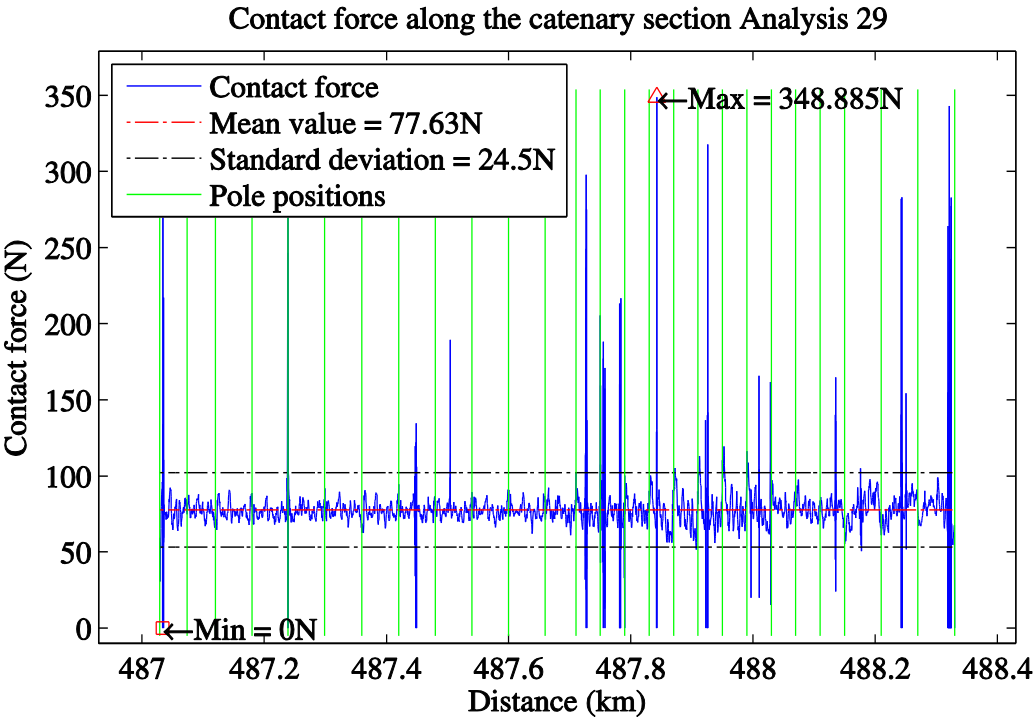


Figure 61 The contact force along the section from Analysis 29, speed=70km/h and full cross section.

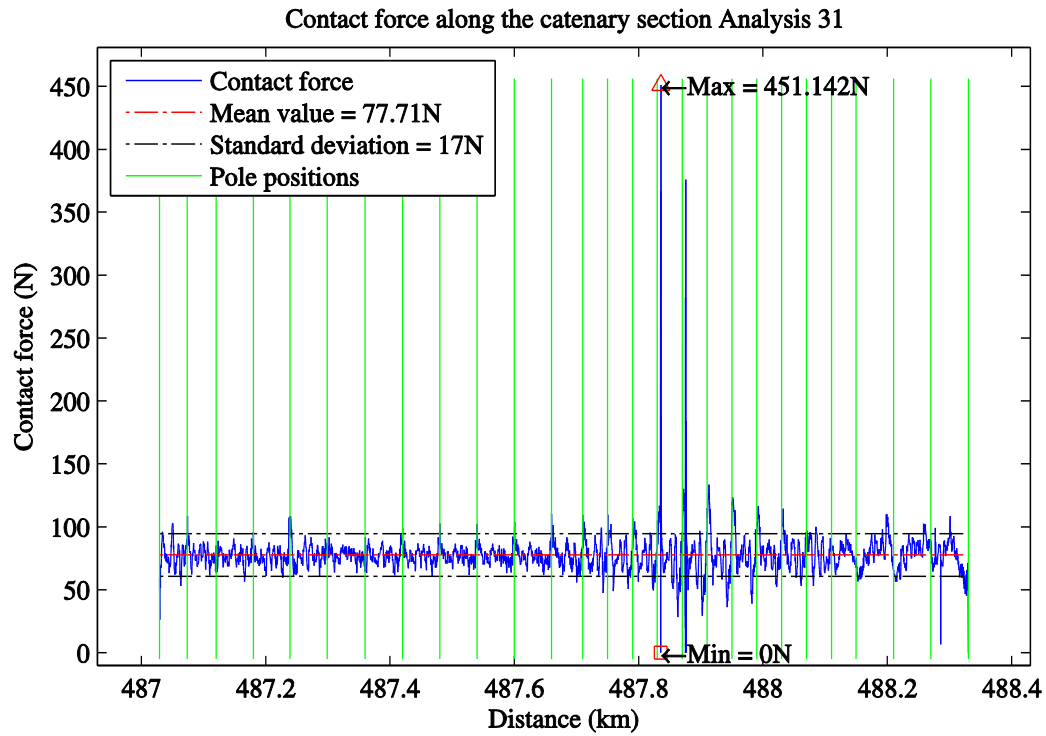


Figure 62 The contact force along the section from Analysis 31, speed=90km/h and full cross section.

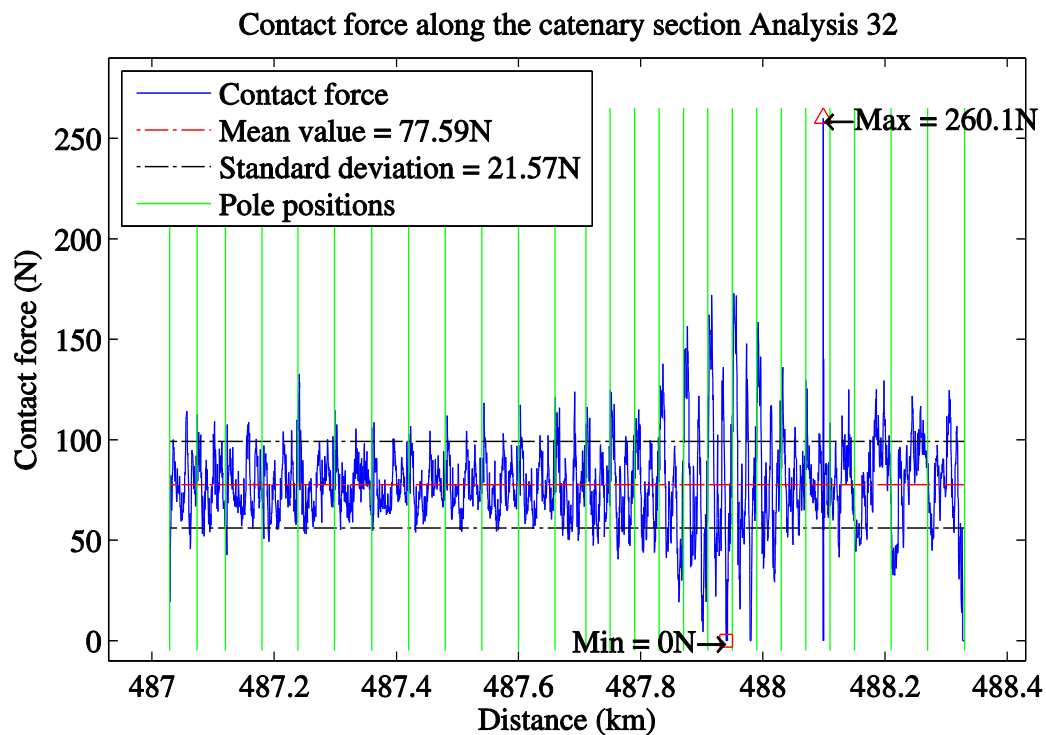


Figure 63 The contact force along the section from Analysis 32, speed=130km/h and full cross section

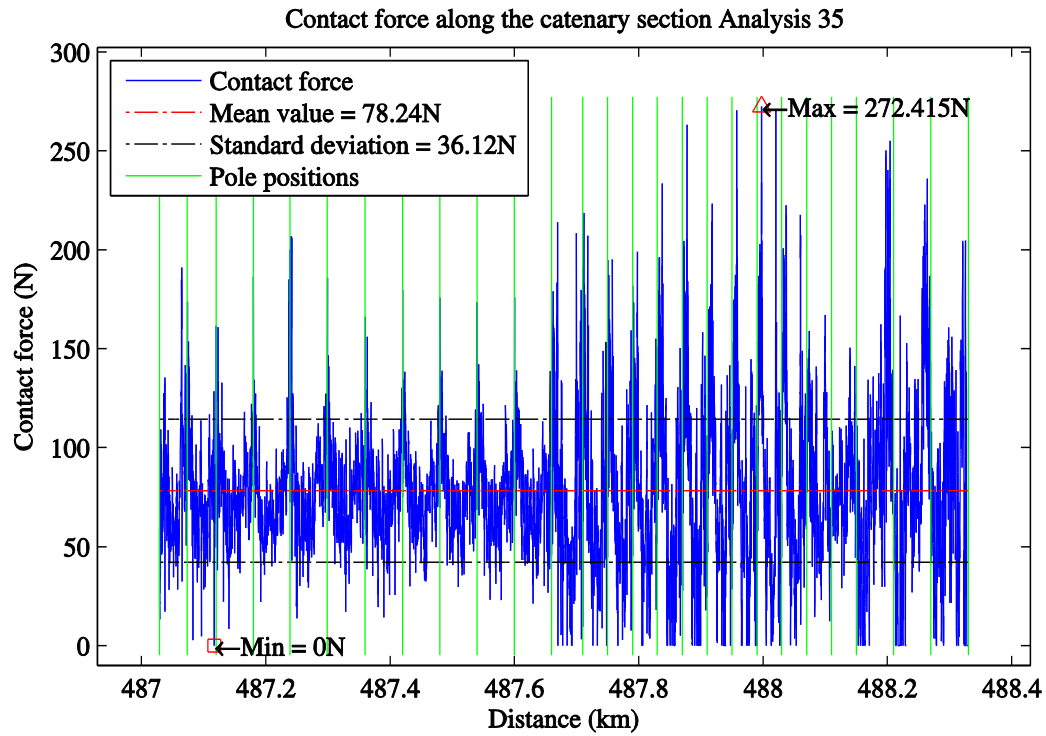


Figure 64 The contact force along the section from Analysis 35, speed=200km/h and full cross section

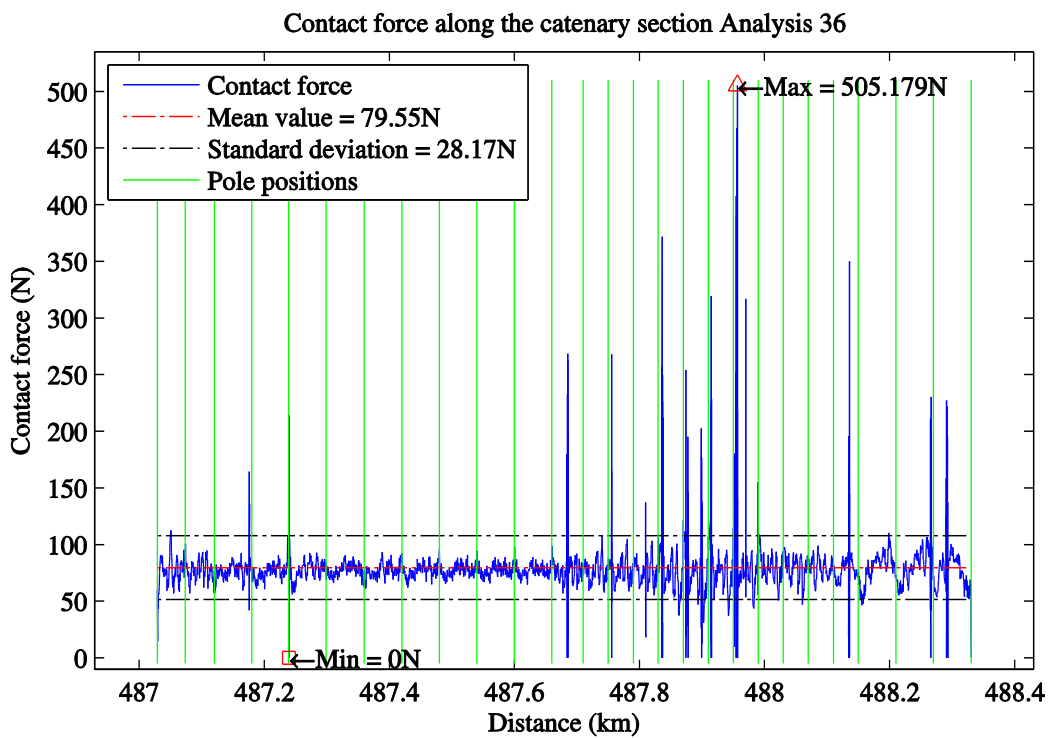


Figure 65 The contact force along the section from Analysis 36, speed=90km/h and 20% worn cross section.

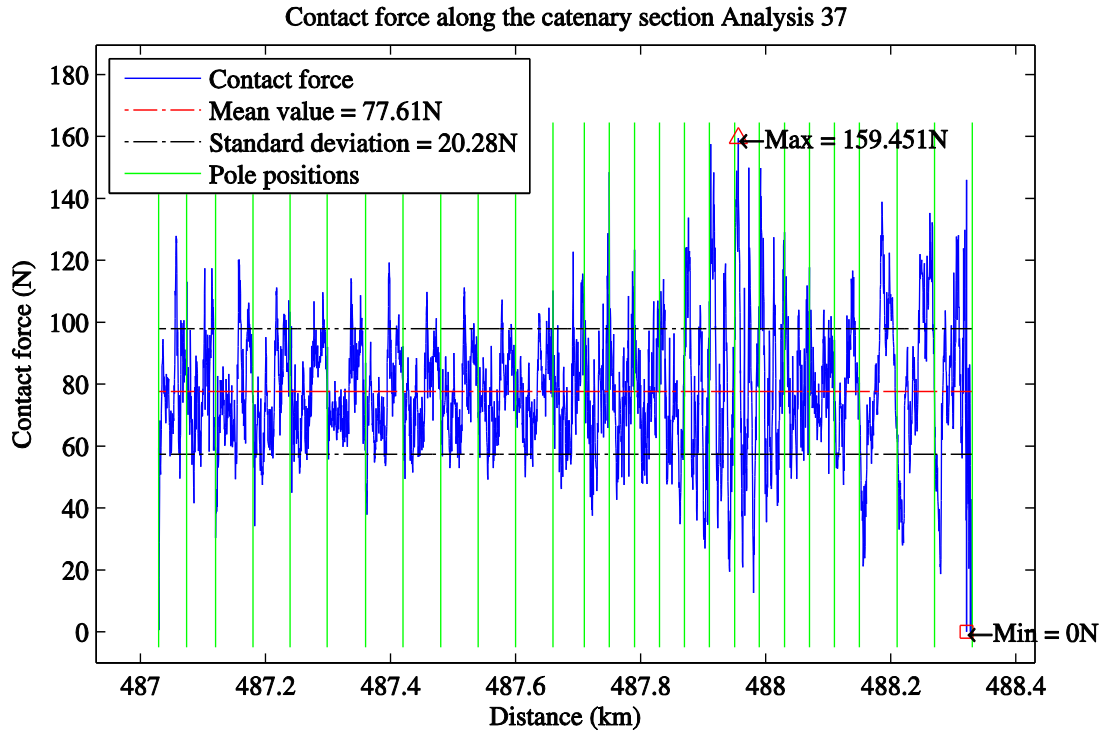


Figure 66 The contact force along the section from Analysis 37, speed=130km/h and 20% worn cross section.

There have been measurements done of this contact force for the given catenary section. These measurements have been done by The Norwegian National Rail Administration with a train speed of 90 km/h. The results from one measurement are presented in Figure 67.

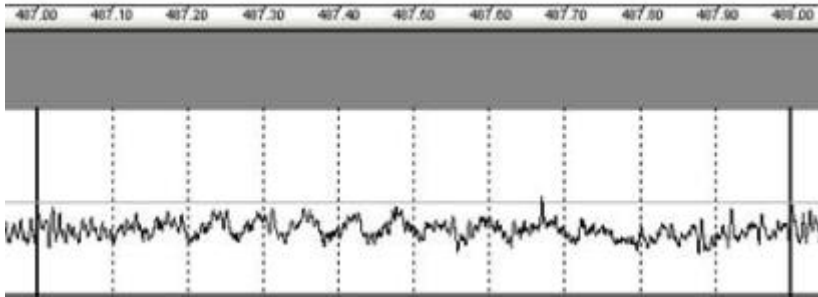


Figure 67 Measurement of the contact force occurring along Wire 152 at 90 km/h. This is measured by The Norwegian National Rail Administration.[8]

The statistical values obtained from the measurement above are shown in Figure 68.

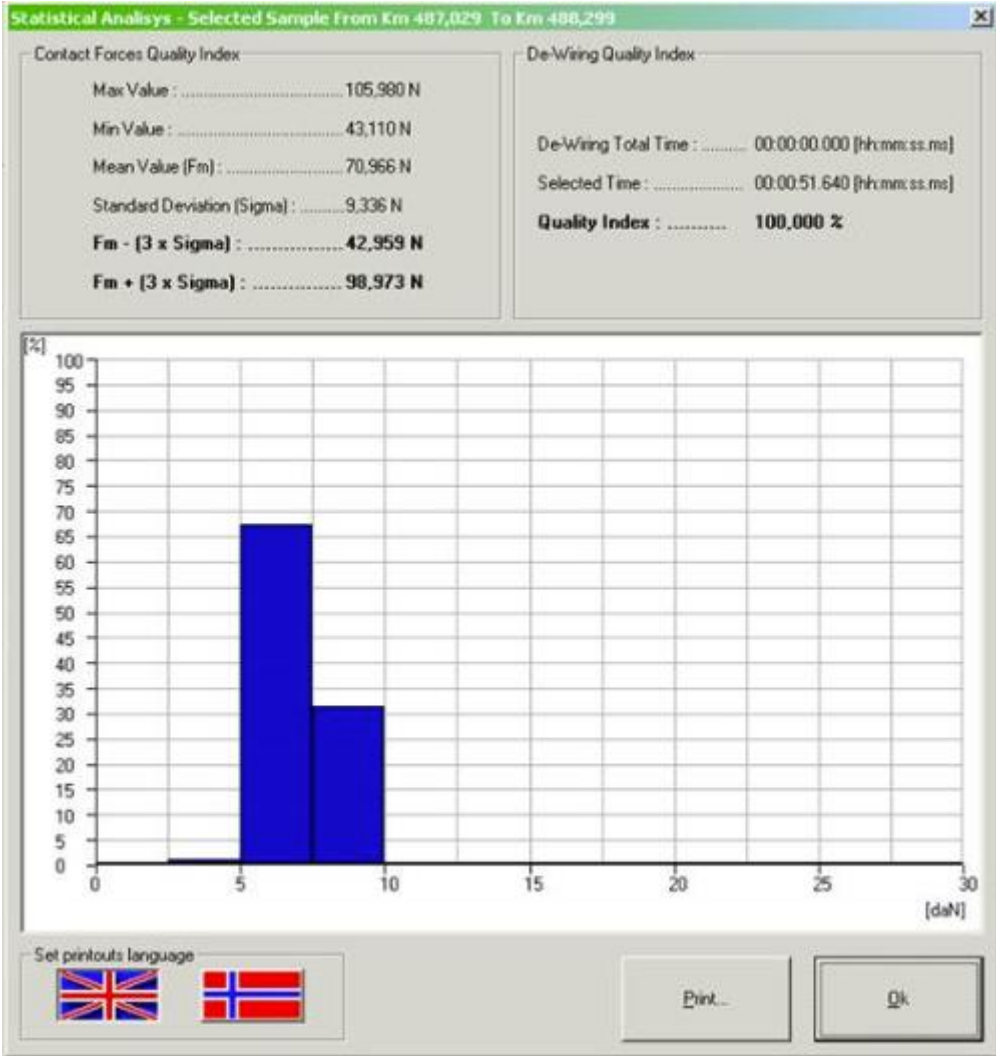


Figure 68 The statistical analysis of the measurement of the contact force occurring at Wire 152 at 90 km/h. This is measured by The Norwegian National Rail Administration.[8]

5.7.2.1 Discussion of the contact force

In the analyses above one can see that the contact force suddenly have high peaks, these high forces are not real. This is because the measured maximum value at 90 km/h were 105.98 N as presented in Table 8, and the maximum values are much larger than this. The high peaks are possibly due to a numerical error in the contact interaction formulation. And it is very likely that this error is the reaction of the collector strip getting hooked a little bit by the contact wire. Numerical it is the master surface which fastens a bit in a slave node. The effect of this error is that the standard deviation can be raised; this is especially seen in Analysis 29 and 36. It also results in too high maximum values for the contact force, and contact losses which should not have occurred.

In Table 8 there is displayed a selection of important contact force values for all the numerical analyses.

	Analysis 29	Analysis 31	Analysis 32	Analysis 35	Analysis 36	Analysis 37
Train speed (km/h)	70	90	130	200	90	130
Mean value of the contact force (N)	77.63	77.71	77.59	78.24	79.55	77.61
Standard deviation of the contact force (N)	24.5	17	21.57	36.12	28.17	20.28
Maximum value of the contact force (N)	348.9	451.14	260.1	272.4	505.2	159.45
Approximately maximum value without the errors	120	130	175	272.4	100	159.45
Minimum value of the contact force (N)	0	0	0	0	0	0
Wear of the contact force	0	0	0	0	20%	20%

Table 8 Summary of important contact force values obtained from the numerical analyses.

The mean contact force was found to be almost the same for all the analyses, with a value around 77.7 N. Compared to the measured value of 70.996 N, the magnitude of the numerical result is thus very close to the reality.

One can clearly see that the standard deviation of the contact force is dependent on the velocity of the train. The only value that differs from this is the standard deviation in Analysis 29 which is clearly erroneous due to the suddenly high and low values which occur. The standard deviation obtained in the numerical model is twice as high as the measured one at 90 km/h. The main reasons for this is probably due to an over simplified contact interaction formulation, numerical errors, lack of wear in Analysis 31 and a too low a tension force in Analysis 36.

The maximum values shown in the figures are mostly wrong because they are a reaction to the numerical problem of the contact formulation. But if one adjusts the values for this error, as done in Table 8, one can see that the maximum values are only slightly different from the measured one.

The contact force along one span can be seen to vary in patterns. The pattern gets clearer as the train speed is increased. It is easiest to see the pattern in Figure 63. For most spans the highest contact force occurs just after the train have passed a support. This is because the contact force increases when the pan head suddenly change vertical direction and is pressed down by the pre-sag of the contact wire. In the rest of the span the contact force reacts on the stiffness of the wire. Around the droppers the stiffness is higher, and the contact force increases. In the same way the force decreases between the droppers, and has its minimum value in the middle of the span. In the spans were the pre-sag have become a pre-lift, the contact force is largest in the middle of the span due to the high stiffness here. It has its

minimum value just after the support, when the pantograph stretches out again to follow the contact wire up.

Another effect in the model is that the contact forces increases from the first span in the area with small curvature, at km 487.75, until the middle of the curve, at km 487.96. Then it decreases until it reaches the same contact force values at the end of the curve, at km 488.18, as it had before the curve. This effect can be seen in all the plots of the contact force. But this effect is not clear in the measurement. The reason may be that the speed of the train when the measurements were done was too low to show a clear effect. And that the effects of wear are highly important. As presented before, the wear at support was larger than the wear at mid span. This can reflect that the wear where the contact forces is highest have the most worn cross sections, and thus the biggest reduction in elasticity. The elasticity then becomes more even along the span, and may reduce this effect seen in the numerical analysis without wear. Another answer to the difference between the numerical results and the measurements is that the effect in the model is erroneous.

It is crucial that the model could describe separation of the contact, as presented in the chapter about numerical modelling. This is equivalent to describing the contact force as zero. It is easy to see that the model allows this when regarding the plots. It is a good thing that there are no real losses of contact in the models with a train speed of 70 or 90 km/h because that is the real train velocity at the site.

5.7.3 The uplift of the contact wire at support 1277

The relative vertical displacement for the contact wire at support 1277 is here shown in Figure 69, Figure 70, Figure 71, Figure 72, Figure 73 and Figure 74 for the different analyses that have been run. It is computed as the displacement of the contact wire point relative to the pre-sag condition.

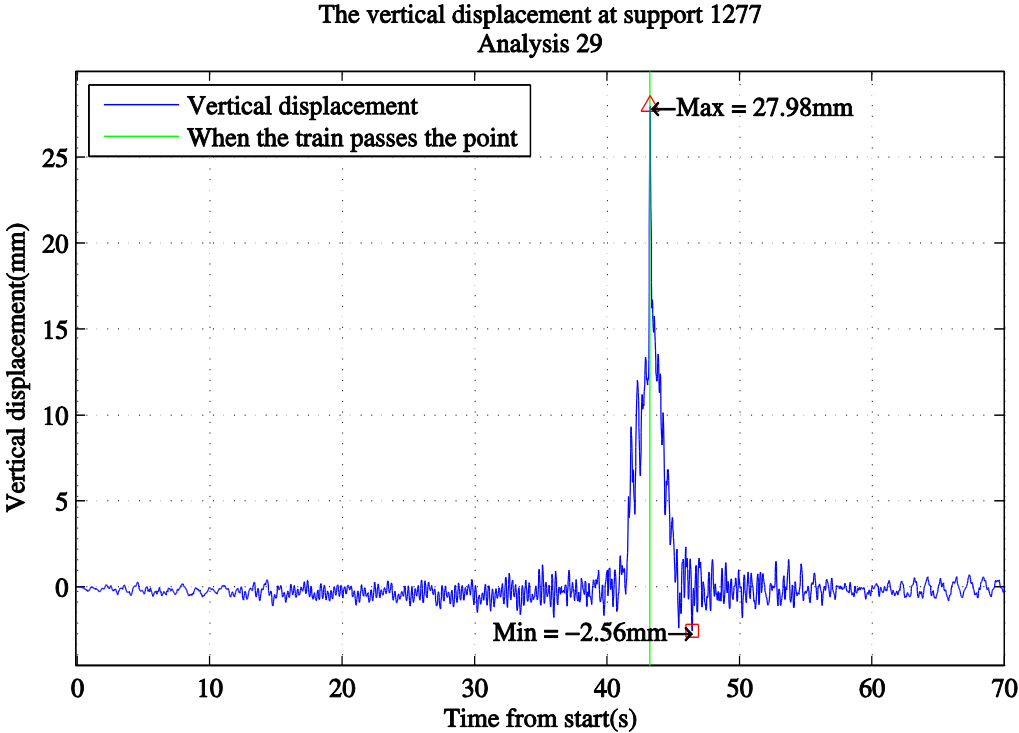


Figure 69 The vertical displacement of the contact wire at support 1277 in Analysis 29, speed=70 km/h and full cross section

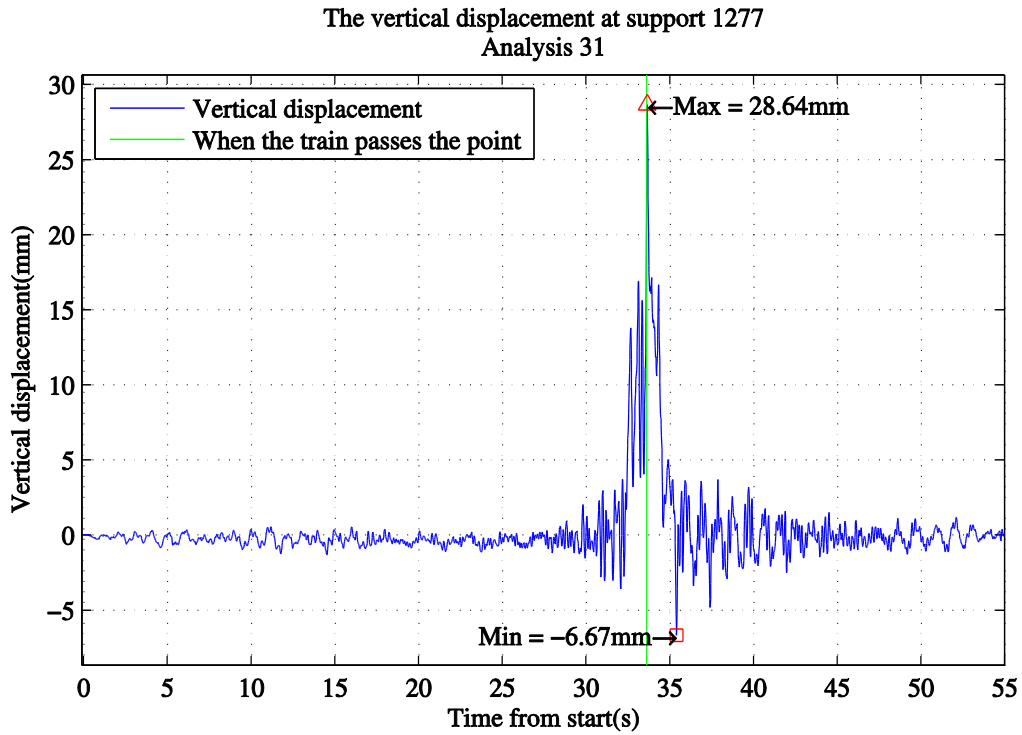


Figure 70 The vertical displacement of the contact wire at support 1277 in Analysis 31, speed=90 km/h and full cross section

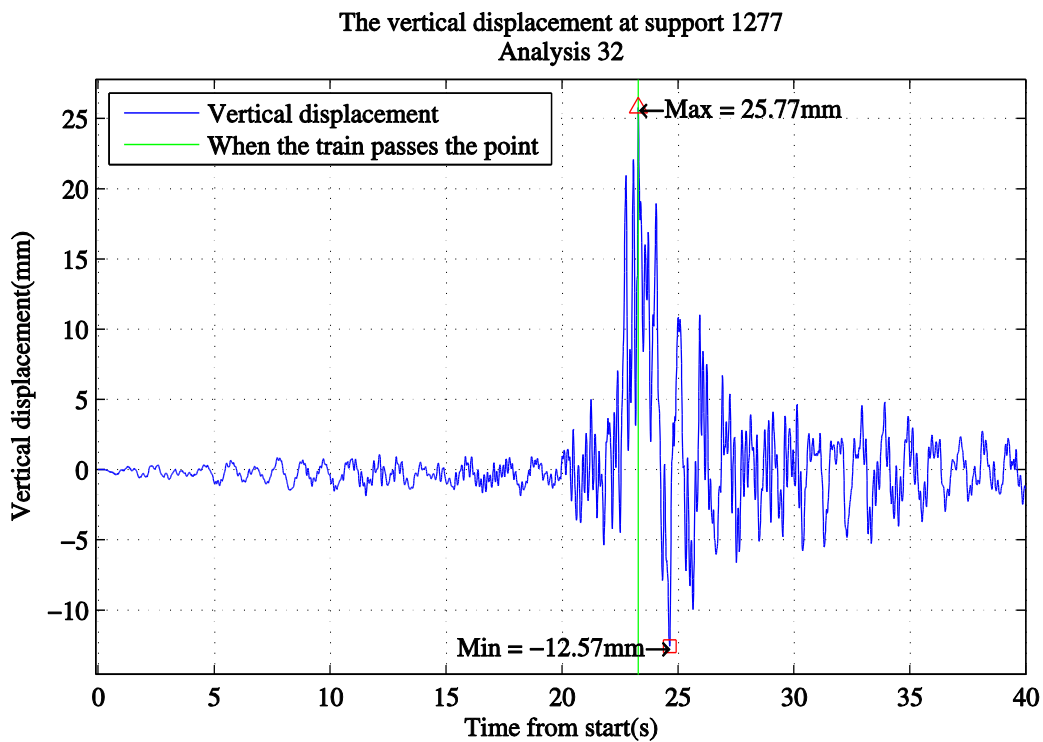


Figure 71 The vertical displacement of the contact wire at support 1277 in Analysis 32, speed=130 km/h and full cross section

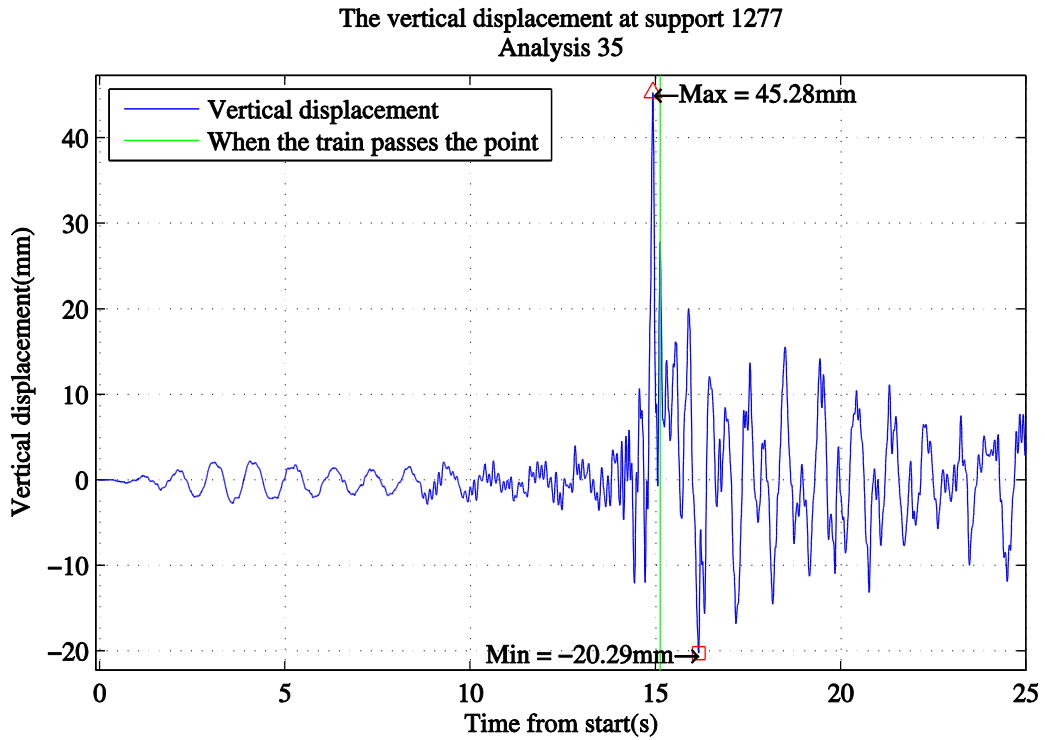


Figure 72 The vertical displacement of the contact wire at support 1277 in Analysis 35, speed=200 km/h and full cross section

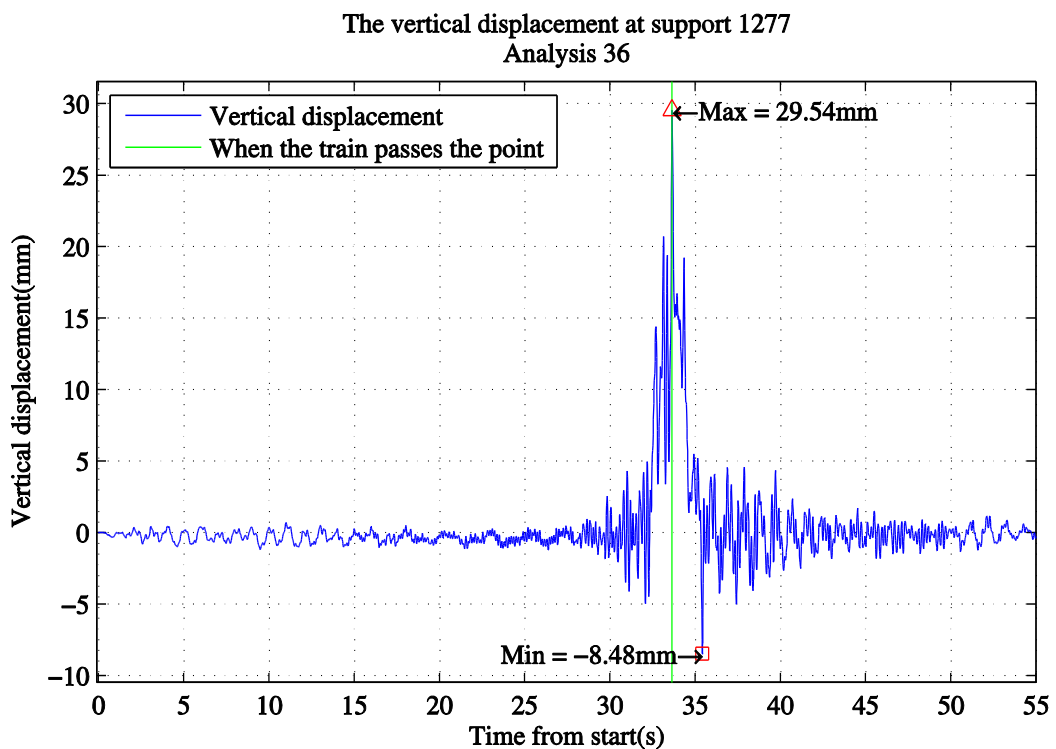


Figure 73 The vertical displacement of the contact wire at support 1277 in Analysis 36, speed=90 km/h and 20% worn cross section

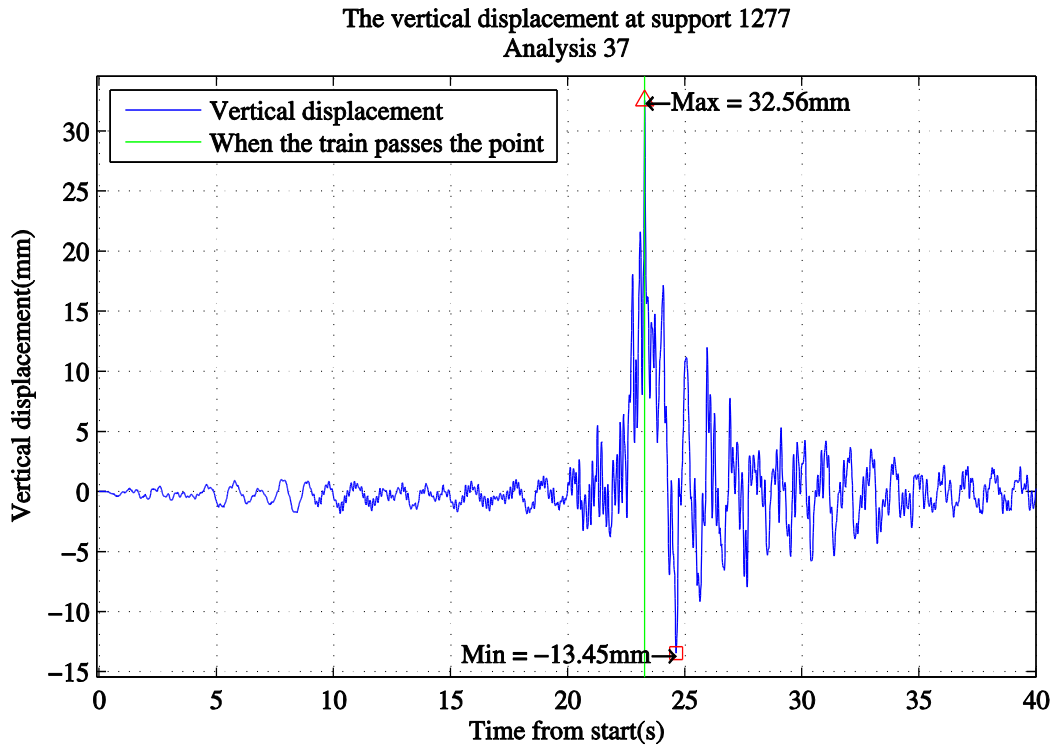


Figure 74 The vertical displacement of the contact wire at support 1277 in Analysis 37, speed=130 km/h and 20% worn cross section.

The first displacements which occur in the plots above have to be because of an impulse induced by the train. The reasoning for this is that the displacements before the train passes the support clearly grows with increasing train speed. But it is not due to the impulse which travels with the transversal wave propagation speed. This impulse travels at 382 km/h, as presented in the theory, and is therefore at support 1277 after 7.9 seconds. The excitation of the point starts to happen after about 0.25-0.29 seconds in all the analyses. This period time indicates that the oscillation is due to longitudinal waves in the wire. They are introduced by starting the train at a given velocity, and not increased steadily from zero to the desired speed. The longitudinal wave velocity can be computed by formula (5.3).[54]

$$c = \sqrt{\frac{E}{\rho}} \quad (5.3)$$

Where c is the longitudinal wave velocity (m/s), E is the Young's modulus (MPa) and ρ is the density (kg/m^3). The speed is then computed to be 3726 m/s or 13415 km/h. With this speed the wave uses 0.226 seconds to the support. When the inertia is taken into account it is very likely that the speed is lowered slightly, and thus this wave is the reason for the early oscillations of the wire. The amplitude of the oscillation is dependent of the magnitude of the force introduced, and is then clearly dependent on the velocity of the train. This effect is likely to happen in the real world as well. But it is then initiated by catenary section changes, friction and geometrical errors on the contact wire.

The transversal impulse of the wave propagation speed can also clearly be seen in Figure 72 after 7.9 seconds. Based on theory presented earlier this is correct. It is difficult to see in the plots with lower train speeds, but it is present as very small displacements with high frequency compared to the other movement. The fact that the displacements introduced by this impulse increases with velocity is good, because higher velocity results in a larger impulse.

The extreme values of the displacements take place when the pantograph is beneath the studied point for every analysis except Analysis 35. In this analysis the speed is so high that the amplitude of the transverse impulse is increased due to the amplification factor presented in the theory. That can result in a large displacement just before the support. The support is shown by the green line. After the pantograph has passed the point the wire continue to oscillate due to the dynamic properties of the system. If the dynamic oscillations damp out before the analysis is over, the remaining oscillations are possibly due to a combination of the transversal impulse, longitudinal impulse and movement with at frequencies with approximately zero damping.

It is interesting to look at the development of the displacements magnitude as the speed of the train increases. In the analyses with a train speed of 70 km/h and 90 km/h it is clear that the behaviour is quasistatic. This is due to the fact that the amplitude of the oscillations after the train has passed is very small. The amplitude of the dynamic oscillations is around 2 millimetres at 70 km/h and around 4 millimetres at 90 km/h, and is mostly a reaction of the transversal and longitudinal impulses. The small increase between 70 and 90 km/h are due to an increase in the impulses causing the movement, as stated earlier. In Analysis 32, where the speed is 130 km/h, one can clearly see that the oscillations are significantly larger, both before the train passes, and after the train has passed. The increase which happens before the passing of the train is a consequence of a train speed which is larger than the limiting speed of 117 km/h. This results in an amplification factor of more than 1.0, and therefore the amplitude grows as the train approaches the source of reflection, the support. An effect due to this is that the maximum value is actually less than for the analysis done at lower speeds because the train has probably passed the support when the transversal impulse was on its way down again.

When the train speed is increased to 200 km/h in Analysis 35 the dynamic response increases considerably. This indicates a resonant behaviour of the wire. The maximum value happens, as previously stated, before the train passes the support. The displacement when the train passes is 27.8 millimetres and thus almost the same as for the other analysis. The natural period of damped vibration is approximately one second, which gives a frequency of 1 Hz[28]. This is the same as the first natural frequency for the nearby spans. The viscous damping ratio, ζ , is found by the use of four cycles after the train have passed. It can be found by formula (5.4).[19]

$$\zeta = \frac{\delta_n}{\sqrt{4\pi^2 n^2 + \delta_n^2}} \text{ where } \delta_n = \ln\left(\frac{u_i}{u_{n+i}}\right) \quad (5.4)$$

Where u_i denotes the displacement at peak i and n describes the number of cycles included. The damping ratio in Analysis 35 has then been calculated to be 0.0234. This means that there is a 50% reduction of in the displacement amplitude after 4.7 cycles, which is equal to 4.7 seconds since the period is 1 second. This is calculated with formula (5.5) [28].

$$j_{50\%} \approx 0.11 / \zeta \quad (5.5)$$

This is a very important parameter to check. It gives information about whether the amplitude of the displacement has decreased enough before the next pantograph passes the same point. In this case; if the distance between two pantographs was 200 metres, the train speed could maximum be 153 km/h if the second pantograph was to pass the same point after the amplitude has been reduced by 50%.

The magnitude of the displacements found at the support is lower than the maximum tolerated uplift of 120 mm for all analyses. The uplift found in the implicit dynamic analyses is of the same magnitude as the usual uplift in the catenary system “Table 54”, which is presented in the theory to be between 30 and 55 millimetres.

It is generally difficult to discuss the results in the analyses with a worn contact wire because the tension force introduced there was wrong. Both the wear and the reduction of the tension force results in a reduced stiffness and thus a higher elasticity. The effect this has on the displacement is that it is generally larger compared to the other analyses with the same train speed.

5.7.4 The displacement at mid span between support 1277 and 1278

The relative vertical displacement for the contact wire point in the middle of the span between support 1277 and 1278 is here shown in Figure 75, Figure 76, Figure 77, Figure 78, Figure 79 and Figure 80 for the different analyses run. It is computed as the displacement of the contact wire point relative to the pre-sag condition.

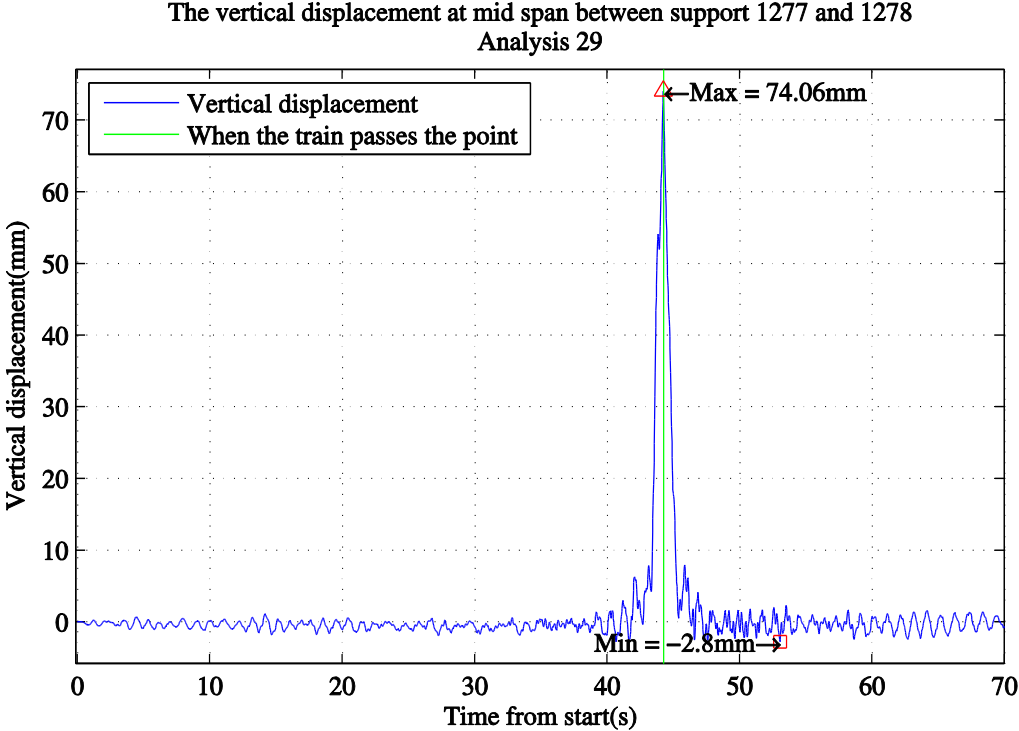


Figure 75 The vertical displacement at mid span between support 1277 and 1278, Analysis 29 speed=70 km/h and the cross section is full

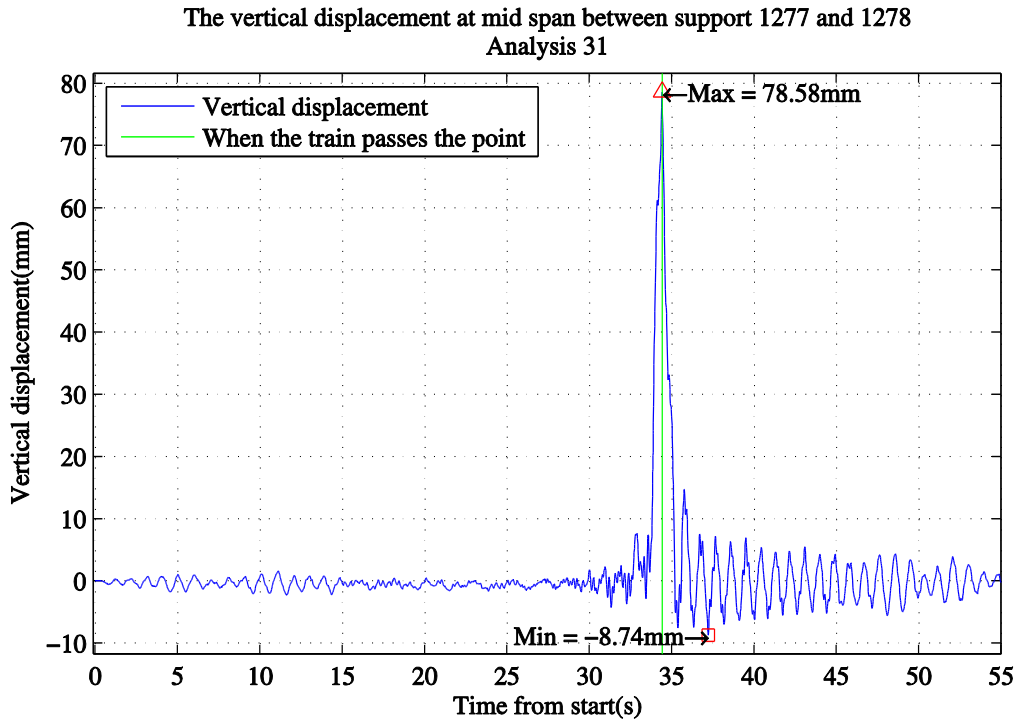


Figure 76 The vertical displacement at mid span between support 1277 and 1278, Analysis 31 speed=90 km/h and the cross section is full

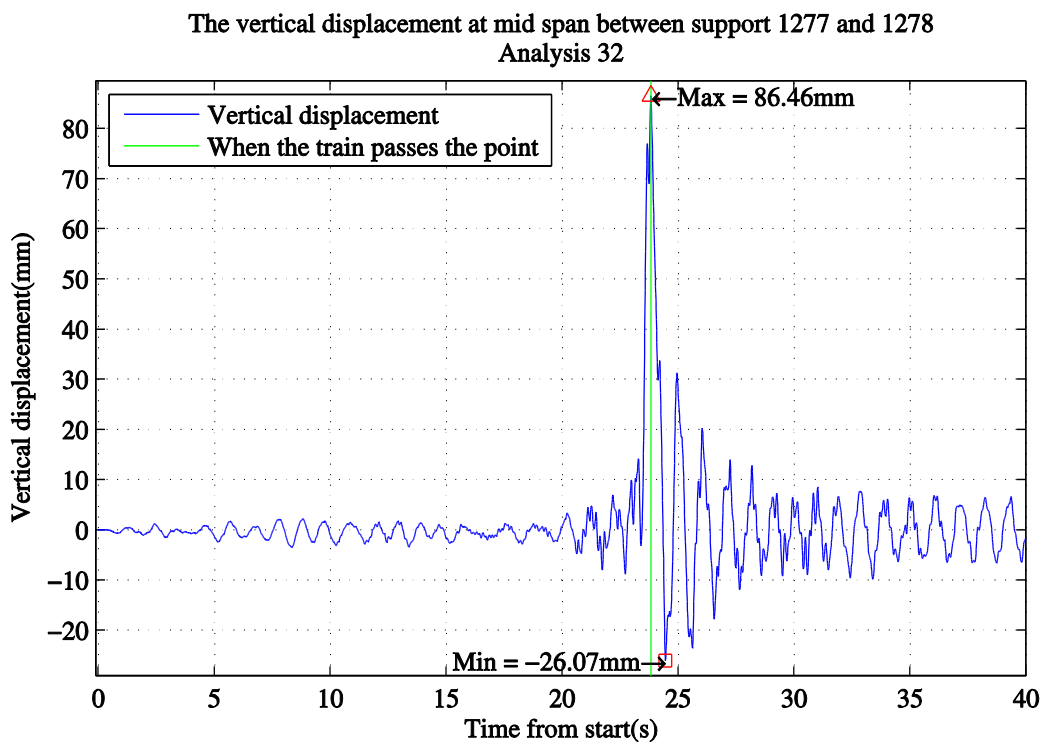


Figure 77 The vertical displacement at mid span between support 1277 and 1278, Analysis 32 speed=130 km/h and the cross section is full

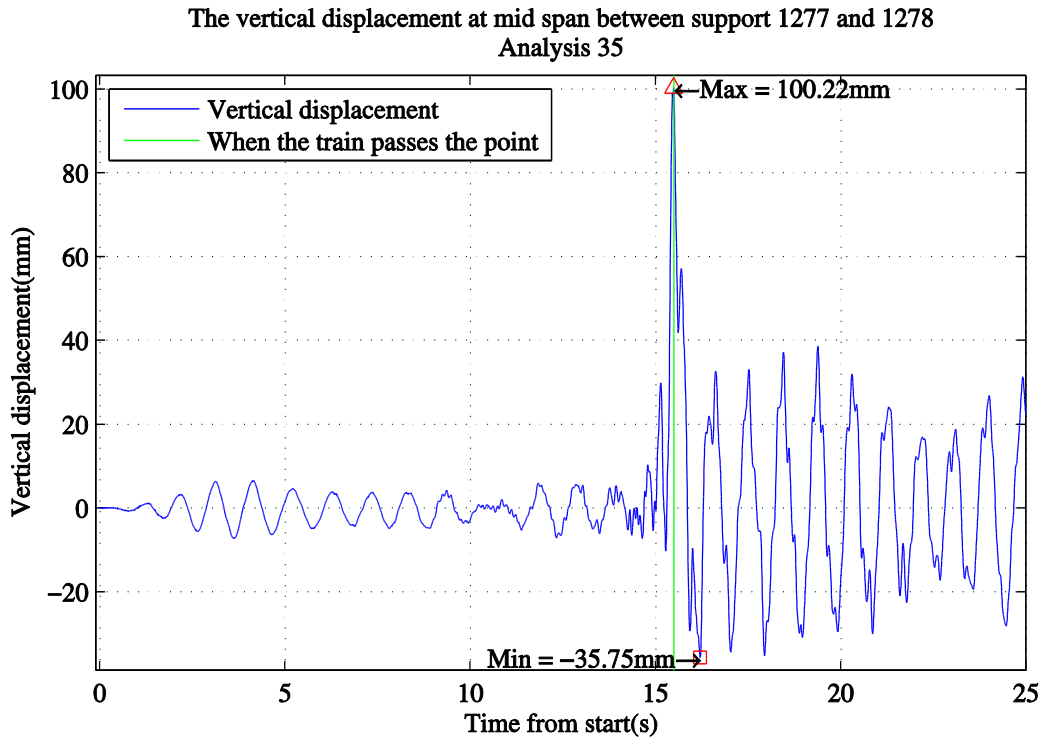


Figure 78 The vertical displacement at mid span between support 1277 and 1278, Analysis 35 speed=200 km/h and the cross section is full

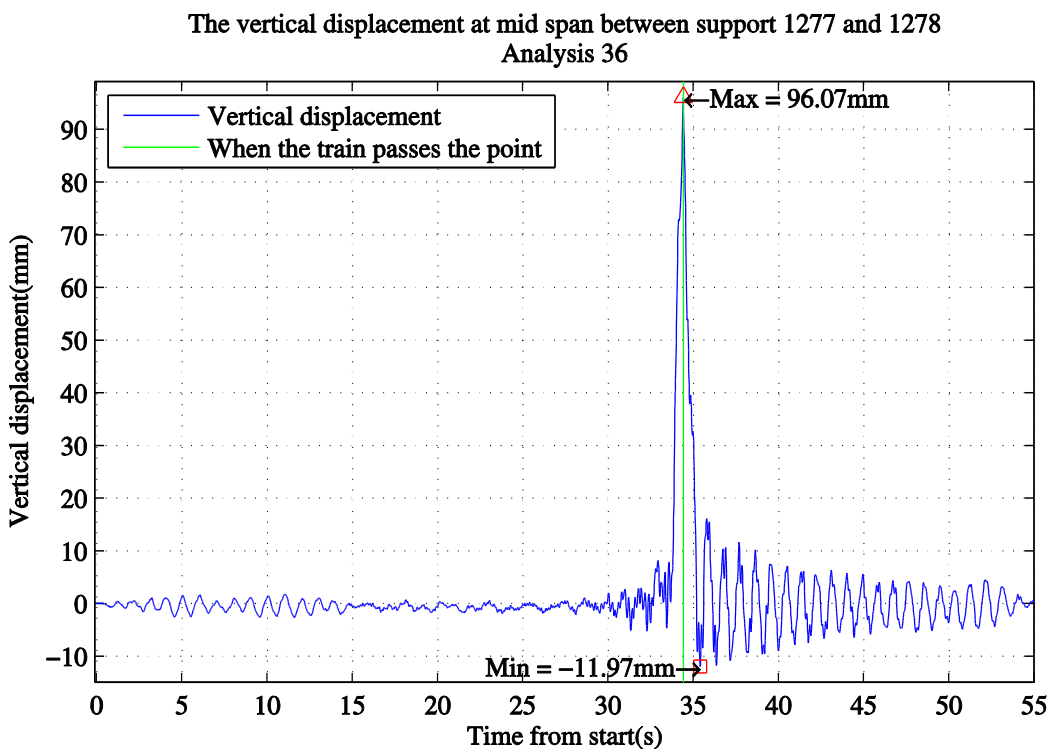


Figure 79 The vertical displacement at mid span between support 1277 and 1278, Analysis 36. Speed=90 km/h and 20% worn cross section.

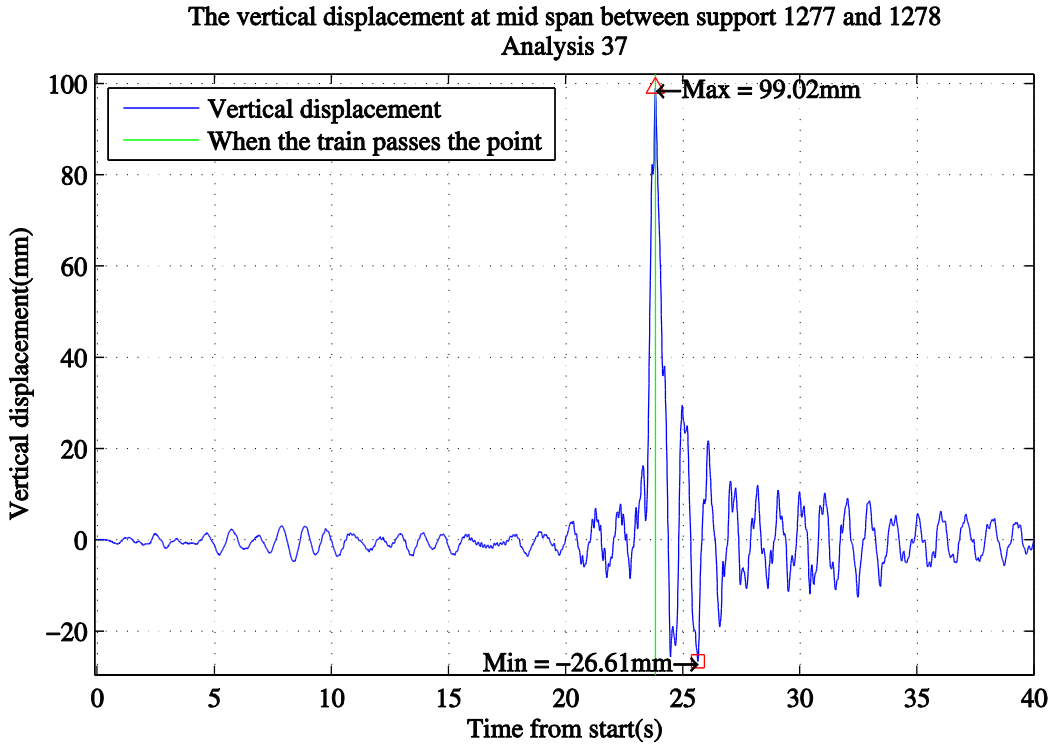


Figure 80 The vertical displacement at mid span between support 1277 and 1278, Analysis 37. Speed=130 km/h and 20% worn cross section.

The shape of the plots of the vertical displacement in the middle of the span is very similar to the plots of the vertical displacement at support. The biggest difference is that the displacements are larger. The displacement which occurs earliest in the plot is thus due to longitudinal waves and transversal waves in the material as presented earlier. It is also clear that the dynamic response increases due to the train speed. Especially in Analysis 35 the dynamic response is large, and, as seen in Figure 78, there seems to be little or no damping present. To study the damping more thoroughly one should let the system vibrate for a longer time period after the train has passed.

The maximum displacement of the contact wire can from the figures clearly be seen to increase with velocity. There have not been found any measurements of the maximum displacement in the middle of one span, so the obtained cannot be validated. They are probably of the right magnitude when comparing these values to the values at support. These values are generally larger and that should be the case because the elasticity is bigger in the middle of the span.

An interesting observation is that there are no clear magnifications of the transversal impulse. This is because this point is not close to any source of reflection, and will therefore not have the same effect as at support.

5.7.5 The trajectory of the contact point between the pan head and the contact wire

The trajectory of the contact point describes the position of the collector strip in the vertical direction whilst the train moves in the horizontal direction. The point of reference is the top of the railway track beneath the contact wire. The red line plotted in the figures below describes the initial position of the contact wire before gravity and tension is applied. It would have been better to show the vertical geometry after these loads had been applied, but this was not possible due to time limitations.

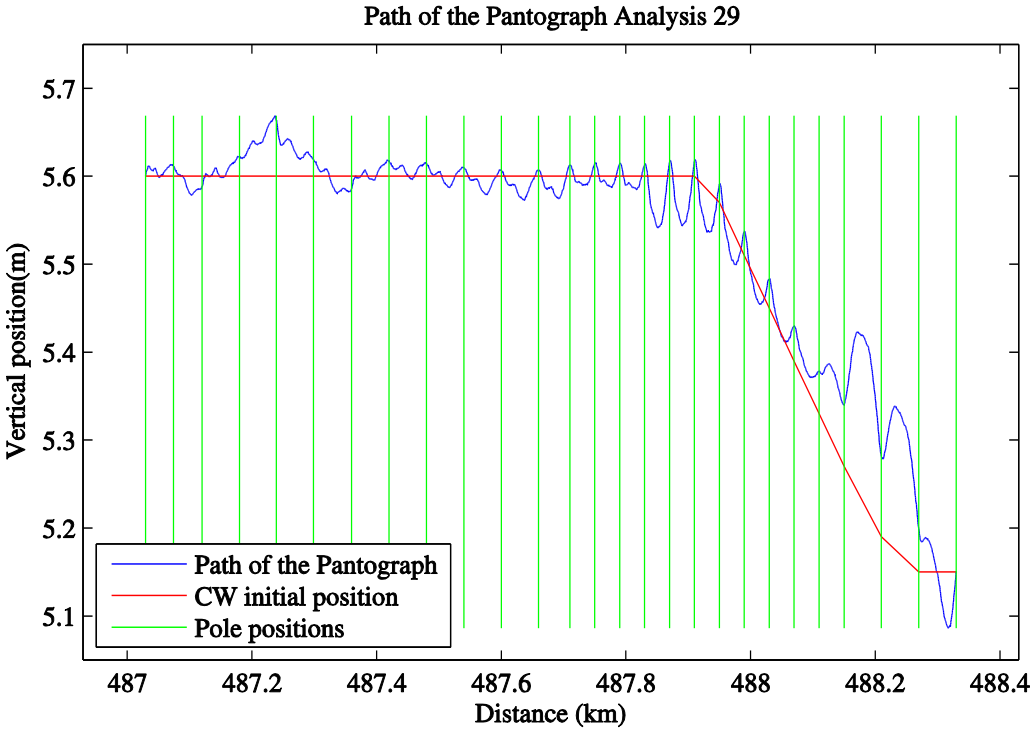


Figure 81 The path of the pantograph in Analysis 29, speed=70 km/h and full cross section

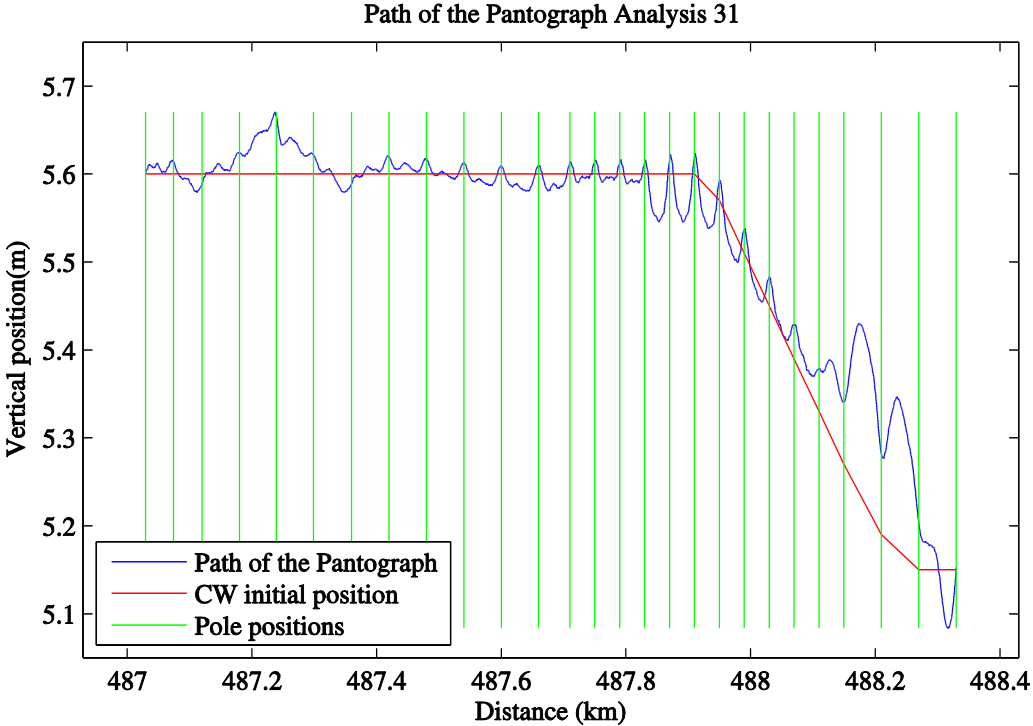


Figure 82 The path of the pantograph in Analysis 31, speed=90 km/h and full cross section

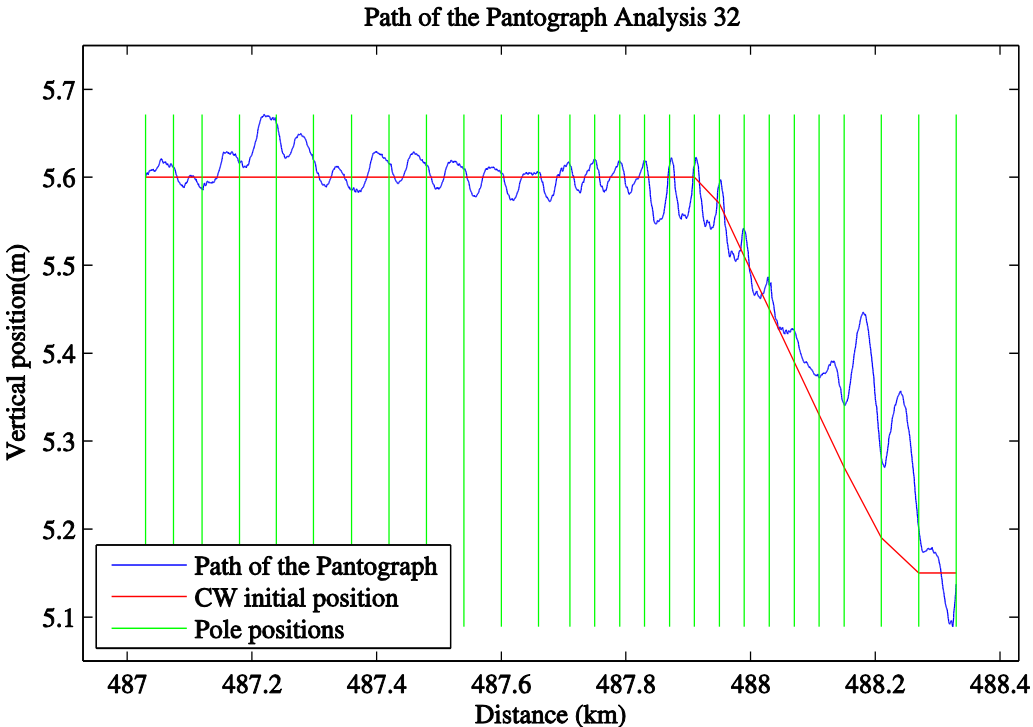


Figure 83 The path of the pantograph in Analysis 32, speed=130 km/h and full cross section

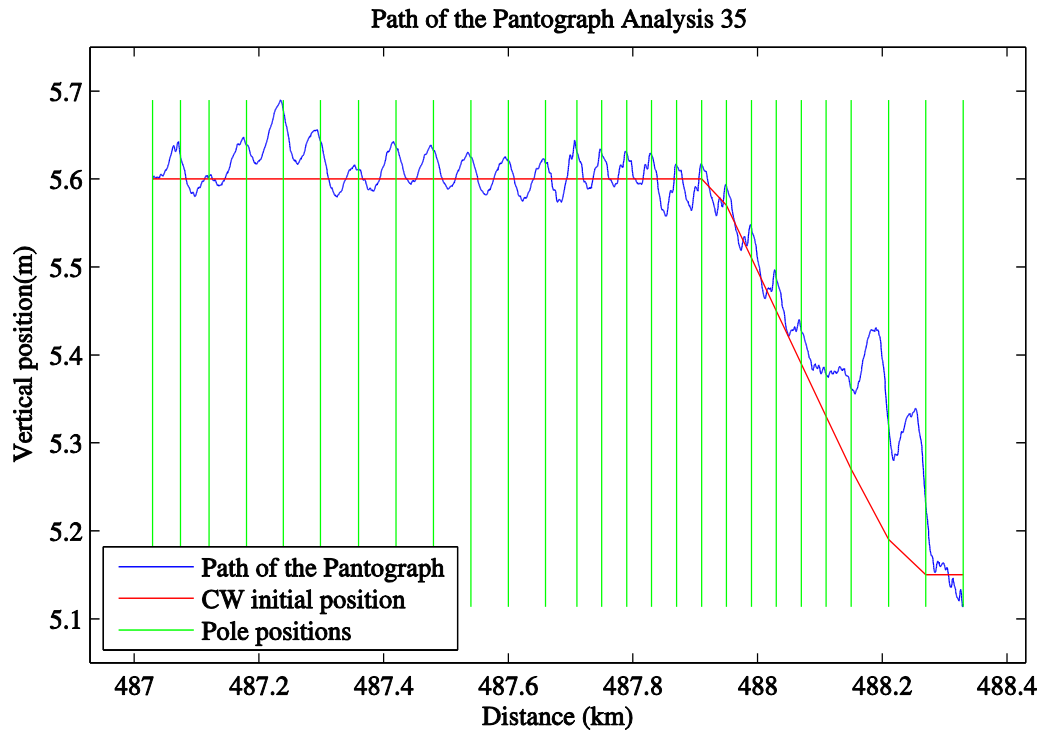


Figure 84 The path of the pantograph in Analysis 35, speed=200 km/h and full cross section

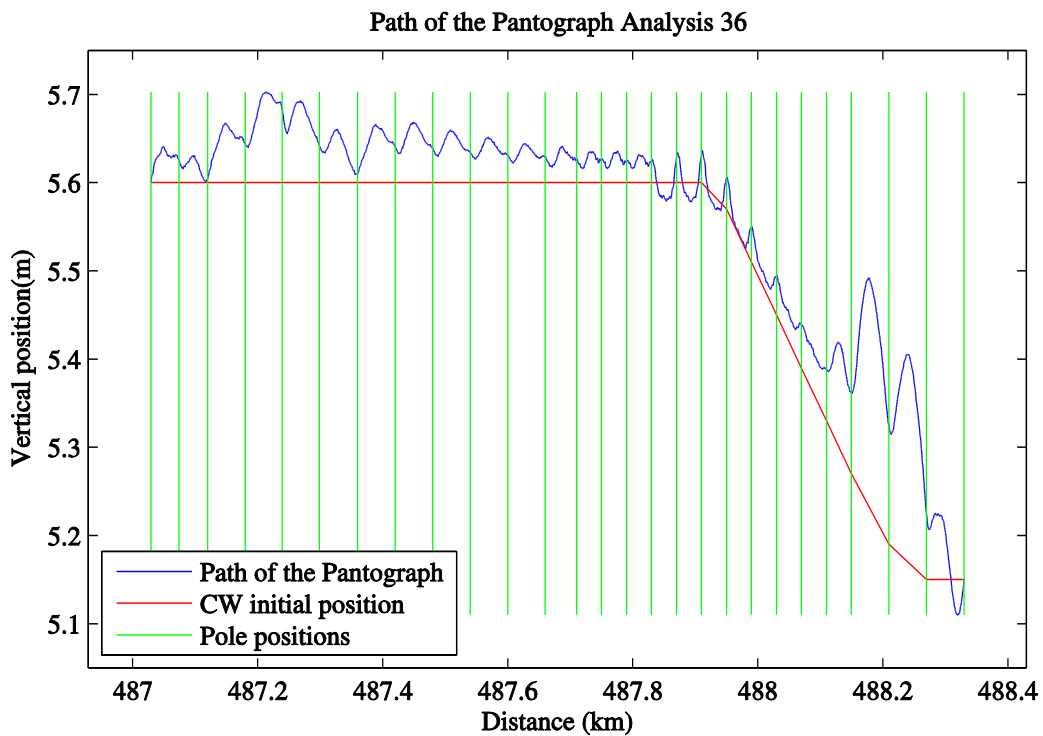


Figure 85 The path of the pantograph in Analysis 36, speed=90 km/h and 20% worn cross section.

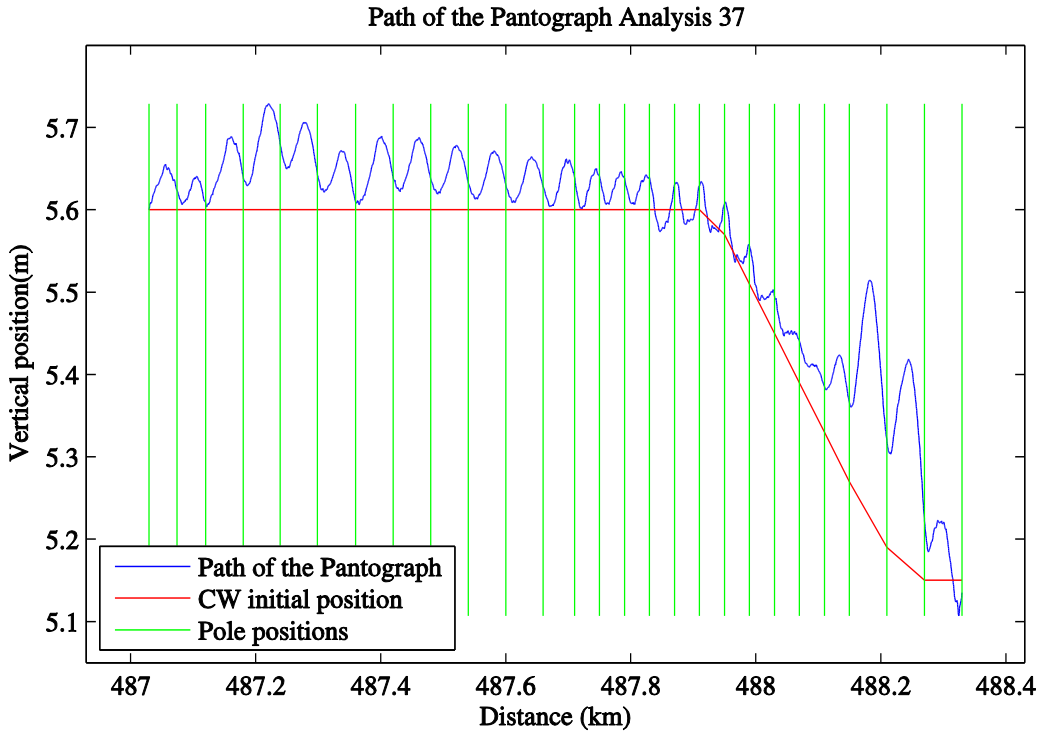


Figure 86 The path of the pantograph in Analysis 37, speed=130 km/h and 20% worn cross section.

In Figure 81, where the situation is quasistatic, the position of the collector is the sum of the pre-sag and the static uplift due to the contact force in that point. As the train speed increases there is also an increase of the displacement component which is due to dynamical effects. Around the train speeds which the section is designed for, the highest position of the collector strip should be at support. In both Analysis 29 and 31, where the train speed is 70 km/h and 90 km/h, the trajectory of the collector strip has the highest vertical position at the supports. This is good because it describes what really happens in the real at the same train speed as the design speed. When the velocity is increased to 130 km/h, which is outside the operating speed range, the highest position is actually at mid span. As the speed is increased to 200 km/h the pantograph pushes the contact wire further up along the whole section, and results in a path which matches the one for 70 km/h, but only lifted up more.

In all the figures of the path of the pantograph one can see that the position is suddenly higher. This is because of the pre-lift discussed earlier, and results in a maximum vertical position in the middle of one span.

There can be seen from most figures that the movement of the pantograph follows a relatively smooth path. This is very good because it matches the actual movement of a running pantograph also at higher train velocities.

6 Conclusion and future directions

In this work a numerical model which successfully describes the train running along a straight catenary section in three dimensions has been made. In addition, a model which describes the train running along a catenary section with curvature in three dimensions has been developed.

Several static and implicit dynamic analyses have been performed on the numerical model to validate it. The obtained results can be summarized as follows:

- (i) The contact force between the pantograph and the contact wire is described accurately in the dynamic analyses. But there are still some errors due to a numerical problem in the contact interaction formulation.
- (ii) The uplift of the contact wire is of the correct magnitude during both elasticity analyses and dynamic analyses.
- (iii) The model has shown to be able to include vertical displacements due to both the transversal and longitudinal impulses.
- (iv) The frequency range of the uppermost importance is found to be between 0.87 Hz and 6 Hz. This is as expected from the literature.
- (v) The pre-sag is found to be too large in the numerical model compared to the measurement; this should therefore be investigated more thoroughly.
- (vi) Analyses done with higher train speeds than the normal speed have shown that the speed limit of the section is of the correct magnitude.

The challenge for future work will be to discover the problems outlined in the following points:

- The interaction between the contact wire and the pantograph should be improved
 - Including friction
 - Including stiffness between wire and collector strip
 - Using the wire as master surface, and the pan head as slave surface
- Change how the pre-tensioning is introduced
- Do frequency analyses of the vertical displacement in selected points; at support and in the middle of the span
- Modal parameter identification should be done to find the damping ratio of the existing system
- Non-linear damping dependent on train velocity should be looked into
- More analyses between 90 km/h and 130 km/h should be performed to find a speed limit of the section
- Consider using Graphics Processing Unit(GPU) to reduce the duration of the analyses

Bibliography

- [1] Y. H. Cho, "Numerical simulation of the dynamic responses of railway overhead contact lines to a moving pantograph, considering a nonlinear dropper," *Journal of Sound and Vibration*, vol. 315, pp. 433-454, 8/19/ 2008.
- [2] B. Simeon and M. Arnold, "Coupling DAEs and PDEs for Simulating the Interaction of Pantograph and Catenary," *Mathematical and Computer Modelling of Dynamical Systems*, vol. 6, pp. 129-144, 2000/06/01 2000.
- [3] F. Kiessling, *Contact lines for electric railways : planning, design, implementation, maintenance*. Munich: Publicis, 2009.
- [4] (19.04.13). *Dovrebanen*. Available: <http://no.wikipedia.org/wiki/Dovrebanen>
- [5] "Overhead Line (Catenary)," <http://www.railway-technical.com/ohl001.gif>, Ed., ed. <http://www.railway-technical.com/etracp.shtml>, 2013.
- [6] Jernbaneverket. (02.06.13). *Mekanisk systembeskrivelse av kontaktledningsanlegg*. Available: http://www.jernbanekompetanse.no/wiki/Mekanisk_systembeskrivelse_av_kontaktledningsanlegg#Ledningsf.C3.B8ring
- [7] Jernbaneverket. JD540 Teknisk regelverk, Kontaktledning/Prosjektering [Online]. Available: <https://trv.jbv.no/PDF/Kontaktledning/542/vedlegg/T4205h00.pdf>
- [8] D. r. f. T. N. N. R. Administration, "Information about "Wire 152", " T. E. Thoresen, Ed., ed, 2013.
- [9] (05.06.13). *Map of Norway from Google Maps*. Available: <https://maps.google.com/>
- [10] (05.06.13). *Norge i Bilder*. Available: <http://ut.no/kart>
- [11] Jernbaneverket. Teknisk regelverk, Kontaktledningsanlegg, Regler for vedlikehold, Kontakttrådslitasje, Kontaktledning [Online]. Available: <https://trv.jbv.no/PDF/Kontaktledning/542/vedlegg/T4205h00.pdf>
- [12] J. M. Sølberg, "Matematisk modellering av strømvogter og kontaktledning," Master, Department of Physics, University of Oslo, 2008.
- [13] NEK, "NEK EN 50119:2009 Railway applications - Fixed installations - Electric traction overhead contact lines," ed, 2009, p. 92.
- [14] NEK, "NEK EN 50119:2001 Railway applications - Fixed installations - Electric traction overhead contact lines," ed, 2001, p. 52.
- [15] C. Yong Hyeon, L. Kiwon, P. Young, K. Bubyong, and K. Ki-nam, "Influence of contact wire pre-sag on the dynamics of pantograph-railway catenary," *International Journal of Mechanical Sciences*, vol. 52, 2010.
- [16] (2000). *Single Arm Pantograph Model: WBL 85 - Balfour Beatty Permaquip, SRS, Description, Maintenance- and Operating Manual*.
- [17] "Information about WBL 88," S. Nordiska, Ed., ed, 2013.
- [18] Jernbaneverket. Teknisk regelverk, Kontaktledning/Vedlikehold/Kontaktledning/Vedlegg/Krav til krefter mellom strømvogter og kontakttråd [Online]. Available: <https://trv.jbv.no/PDF/Kontaktledning/542/vedlegg/T4205h00.pdf>
- [19] J. L. Humar, *Dynamics of structures*. Boca Raton: CRC Press, 2012.
- [20] R. W. Clough and J. Penzien, "Dynamics of structures," 1975.
- [21] M. Iutterer and U. Starossek, "Dynamic cable stiffness and dynamic interaction between cable and beam," 1992.
- [22] S. Sabin, "Understanding and using dynamic stiffness-A Tutorial," *Orbit. Second Quarter*, vol. 2, pp. 44-54, 2000.
- [23] T. X. Wu and M. J. Brennan, "DYNAMIC STIFFNESS OF A RAILWAY OVERHEAD WIRE SYSTEM AND ITS EFFECT ON PANTOGRAPH-CATENARY SYSTEM DYNAMICS," *Journal of Sound and Vibration*, vol. 219, pp. 483-502, 1/21/ 1999.
- [24] Jernbaneverket. (02.06.13). *Dynamisk systembeskrivelse av kontaktledningsanlegg*. Available: http://www.jernbanekompetanse.no/wiki/Dynamisk_systembeskrivelse_av_kontaktledningsanlegg

-
- [25] NEK, "NEK EN 50318:2002 Railway applications - Current collection systems - Validation of simulation of the dynamic interaction between pantograph and overhead contact line," ed, 2002, p. 20.
- [26] J. P. J. Ambrósio, M. Pereira, P. Antunes, A. Mósca, "Recent Developments in Pantograph-Catenary Interaction Modelling and Analysis," *International Journal of Railway Technology*, vol. 1(1), pp. 249-278, 2012.
- [27] B. Stefano, B. Giuseppe, C. Andrea, and F. Alan, "Numerical and Hardware-In-the-Loop Tools for the Design of Very High Speed Pantograph-Catenary Systems," *Journal of Computational and Nonlinear Dynamics*, vol. 7, 2012.
- [28] A. K. Chopra, *Dynamics of structures : theory and applications to earthquake engineering*. Upper Saddle River, N.J.: Pearson Prentice Hall, 2007.
- [29] G. Poetsch, J. Evans, R. Meisinger, W. Kortüm, W. Baldauf, A. Veitl, *et al.*, "Pantograph/Catenary Dynamics and Control," *Vehicle System Dynamics*, vol. 28, pp. 159-195, 1997/08/01 1997.
- [30] M. Aboshi, I. Nakai, and H. Kinoshita, "Current collection characteristics and improvement methods of high-tension overhead catenary systems," *Electrical Engineering in Japan*, vol. 123, pp. 67-76, 1998.
- [31] R. D. Cook, *Concepts and applications of finite element analysis*. New York: Wiley, 2002.
- [32] J. Pombo and J. Ambrósio, "Influence of pantograph suspension characteristics on the contact quality with the catenary for high speed trains," *Computers & Structures*, vol. 110-111, 2012.
- [33] *ABAQUS 6.12 Theory Manual*: Dassault Systèmes, 2012.
- [34] J. Pombo, J. Ambrósio, M. Pereira, F. Rauter, A. Collina, and A. Facchinetti, "Influence of the aerodynamic forces on the pantograph–catenary system for high-speed trains," *Vehicle System Dynamics*, vol. 47, pp. 1327-1347, 2009/11/01 2009.
- [35] M. Bociolone, F. Resta, D. Rocchi, A. Tosi, and A. Collina, "Pantograph aerodynamic effects on the pantograph–catenary interaction," *Vehicle System Dynamics*, vol. 44, pp. 560-570, 2006/01/01 2006.
- [36] A. Alberto, Jes\, #250, s. Benet, E. Arias, D. Cebrian, *et al.*, "A high performance tool for the simulation of the dynamic pantograph-catenary interaction," *Math. Comput. Simul.*, vol. 79, pp. 652-667, 2008.
- [37] J. Benet, A. Alberto, E. Arias, and T. Rojo, "A Mathematical Model of the Pantograph-Catenary Dynamic Interaction with Several Contact Wires," *International Journal of Applied ...*, 2007.
- [38] J. Seo, I. Jung, T. Park, and J. Chai, "Dynamic analysis of a multibody system including a very flexible beam element," *JSME International Journal Series C*, 2005.
- [39] A. Facchinetti and S. Bruni, "Hardware-in-the-loop hybrid simulation of pantograph–catenary interaction," *Journal of Sound and Vibration*, vol. 331, 2012.
- [40] J. Ambr, #243, J. sio, #227, and M. P. o Pombo, "Optimization of high-speed railway pantographs for improving pantograph-catenary contact," *Theor. Appl. Mech. Lett.*, vol. 3, pp. 9-013006, 2013-01-10 2013.
- [41] S. Jong-Hwi, K. Seok-Won, J. Il-Ho, P. Tae-Won, M. Jin-Yong, K. Young-Guk, *et al.*, "Dynamic analysis of a pantograph–catenary system using absolute nodal coordinates," *Vehicle System Dynamics*, vol. 44, 2006.
- [42] A. Facchinetti, L. Gasparetto, and S. Bruni, "Real-time catenary models for the hardware-in-the-loop simulation of the pantograph–catenary interaction," *Vehicle System Dynamics*, vol. 51, 2013.
- [43] W. Zhang, Y. Liu, and G. Mei, "Evaluation of the coupled dynamical response of a pantograph—catenary system: contact force and stresses," *Vehicle System Dynamics*, vol. 44, pp. 645-658, 2006/08/01 2006.
- [44] J. Sung Pil, K. Young Guk, P. Jin Sung, and P. Tae Won, "Estimation of Dynamic Contact Force Between a Pantograph and Catenary Using the Finite Element Method," *Journal of Computational and Nonlinear Dynamics*, vol. 7, 2012.
- [45] G. Y.H and L. I. M. T.C, "COMMENTS ON “THE STABILITY ANALYSIS OF PANTOGRAPH-CATENARY SYSTEM DYNAMICS”," *Journal of Sound and Vibration*, vol. 247, 2001.

-
- [46] J. M. L. Yong Hyeon Cho, Sung Yong Park, Eung Shin Lee, "Robust Measurement of Damping Ratios of a Railway Contact Wire Using Wavelet Transforms," *Key Engineering Materials*, vol. 321-323, pp. 1629-1635, 2006.
- [47] T. Ding, G. X. Chen, J. Bu, and W. H. Zhang, "Effect of temperature and arc discharge on friction and wear behaviours of carbon strip/copper contact wire in pantograph–catenary systems," *Wear*, vol. 271, pp. 1629-1636, 7/29/ 2011.
- [48] (01.06.2013). *Datasheet: Cable / Wire Tension Sensor CableBull*. Available: <http://www.honigmann.com/i437&lang=2>
- [49] Pesola. (20.05.2013). *Item no. PHS040 – Digital Hanging Scale 40 kg / 88 Lb*. Available: http://www.pesola.com/cgi-bin/shop?r0=user&r1=show&r2=item&itemId=360&lang=en_US
- [50] (20.05). *Datasheet: 8208 - Modal sledge hammer, 3 lb. head, cable included*. Available: <http://www.bksv.com/Products/transducers/vibration/impact-hammers/8208.aspx?tab=overview>
- [51] (2008, 20.05). *Datasheet: Ceramic/Quartz Impedance Head for Modal Analysis Type 8770A..* Available: <http://www.kistler.com/no/en/product/acceleration/8770A50>
- [52] N. Labonnote, "Modal Hammer for Dummies," ed, 2012, p. 37.
- [53] (2010, 20.05). *Datasheet: NI cDAQ-9174 NI CompactDAQ 4-Slot USB Chassis*. Available: <http://www.kistler.com/no/en/product/acceleration/8770A50>
- [54] F. Irgens, *Continuum mechanics*: Springer, 2008.

Appendix

Appendix A Wear of the contact wire[8]

Jernbaneverket
Infrastruktur

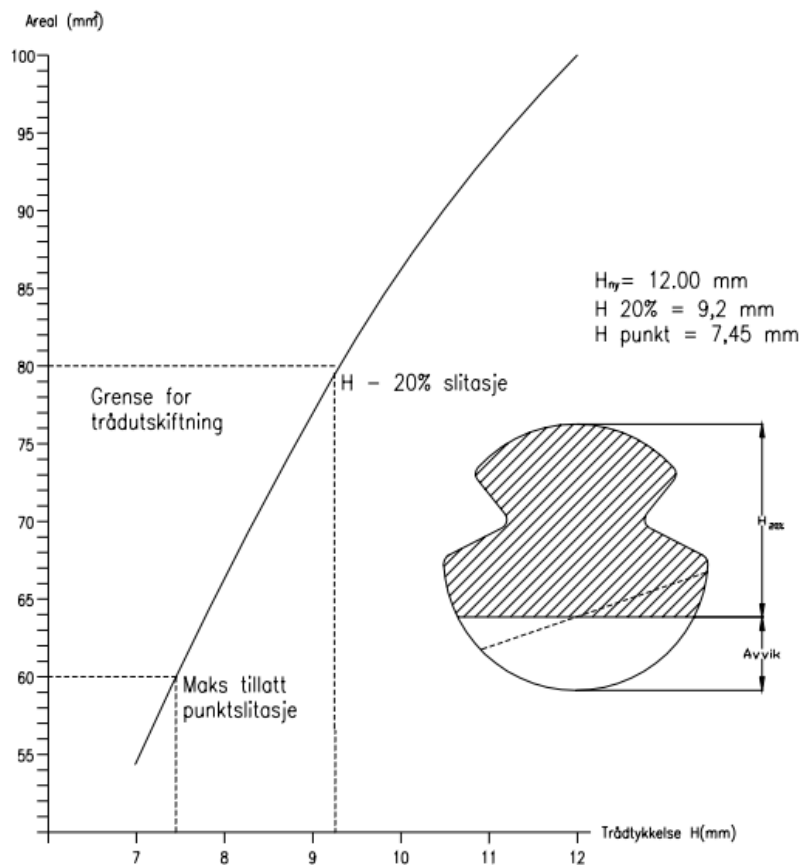
KONTAKTLEDNINGSANLEGG
Regler for vedlikehold
Kontakttrådslitasje
Kontaktledning

Kap.: 5.h
Utgitt: 01.01.04
Rev.: 0
Side: 4 av 9

KONTAKTTRÅDSLITASJE

100 mm² Cu FRHC

Minimum strekkfasthet = 360 N/mm² etter EN 50149
Maksimal strekkbelastning etter EN 50119



Dok.nr.: JD 542

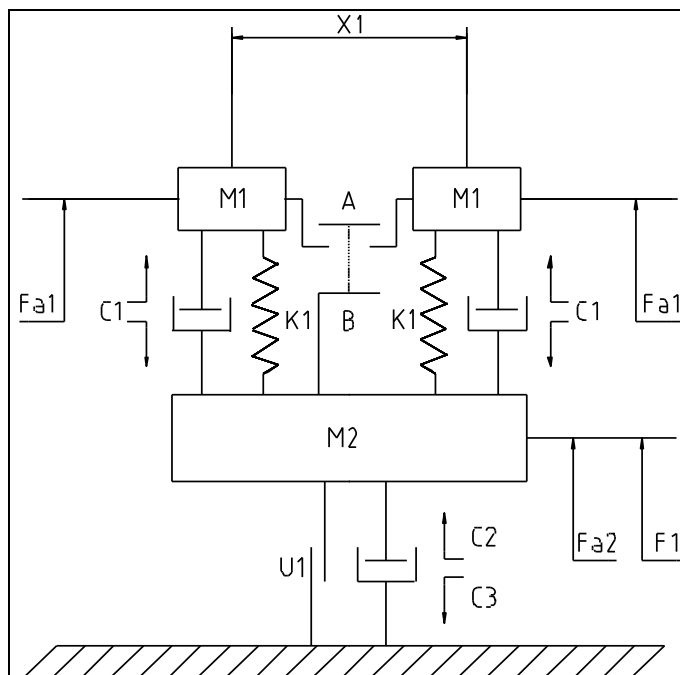
Utgitt av: ITP

Godkjent av: IT

Appendix B The pantograph model from Schunk Nordiska[17]

1.1 Tekniska data för simulering WBL 88 AT ,Flygtoget BM73

Benämning	Del	Data	Enhet	Anmärkning
Toppygel massa	M_1	2x2,3	Kg	primär massa
Avstånd mellan kolslitskenor	X_1	595	mm	
Effektiv dynamisk sax massa	M_2	16.5	Kg	sekundär massa
Toppygelns dämpnings konstant	C_1	10	Ns/m	primär
Saxens dämpnings konstant	C_2	0	Ns/m	sekundär
Saxens dämpnings konstant	C_3	63,5	Ns/m	sekundär
Saxens fiktion	U_1	17	N	
Fjäderkonstant för topppygel	K_1	3100	N/m	
Statiskt upptryck	F_1	60	N	
Fjädväg från A till B	-	35	mm	för primär massan
Fjädväg vid statiskt upptryck (F1)	-	12	mm	
Max höjd	-	2,0	m	maximal höjd för strömvtagaren(från viloläge)
Toppygelbredd		1.8	m	
Längd kolslitskena	-	1,03	m	
Höjd kolslitskena	-	0,039	m	i mitten av kolslitskenan i förhållande till dess ä
Aerodynamisk uppkraft på topppygel	F_{a1}	0	N	vindstilla vid 100 km/h
Aerodynamisk uppkraft på saxen	F_{a2}	5	N	vindstilla vid 100 km/h



Appendix C-1 Overview of the properties of sections in the area of interest[8]

Beskrivelse	Navn/Nr	Fra	Til	Sportype	Spornummer	Ledningsnr	Fra mast (nr)	Mastnr for fix
Kontaktledning, Ledning 145, Gari stasjon	Ledning 145	479.113	480.639	Hovedspor	2	145	47904	1103
Kontaktledning, Ledning 146, Gari - Soknedal	Ledning 146	480.464	481.859	Hovedspor	1	146	1114	1128
Kontaktledning, Ledning 147, Gari - Soknedal	Ledning 147	481.724	482.444	Hovedspor	1	147	1140	
Kontaktledning, Ledning 148, Gari - Soknedal	Ledning 148	482.319	483.029	Hovedspor	1	148	1155	
Kontaktledning, Ledning 149, Gari - Soknedal	Ledning 149	482.889	484.379	Hovedspor	1	149	1171	1188
Kontaktledning, Ledning 150, Gari - Soknedal	Ledning 150	484.199	485.46	Hovedspor	1	150	1200	1211
Kontaktledning, Ledning 151, Soknedal stasjon	Ledning 151	485.28	485.99	Hovedspor	1	151	1218	
Kontaktledning, Ledning 1, Soknedal stasjon	Ledning 1	485.82	487.074	Hovedspor	1	1	1228	1241
Kontaktledning, Ledning 2, Soknedal stasjon	Ledning 2	486.158	486.84	Togspor	2	2	1235	
Kontaktledning, Ledning 152, Soknedal stasjon	Ledning 152	486.939	488.39	Hovedspor	1	152	1259	1272
Kontaktledning, Ledning 153, Soknedal - Støren	Ledning 153	488.21	489.78	Hovedspor	1	153	1285	1300
Kontaktledning, Ledning 154, Soknedal - Støren	Ledning 154	489.65	491.261	Hovedspor	1	154	1315	1334
Kontaktledning, Ledning 155, Soknedal - Støren	Ledning 155	491.082	492.682	Hovedspor	1	155	1346	1361
Kontaktledning, Ledning 156, Soknedal - Støren	Ledning 156	492.542	494.152	Hovedspor	1	156	1374	1394
Kontaktledning, Ledning 157, Soknedal - Støren	Ledning 157	493.972	495.613	Hovedspor	1	157	1402	1418
Kontaktledning, Ledning 158, Soknedal - Støren	Ledning 158	495.473	497.053	Hovedspor	1	158	1435	1460
Kontaktledning, Ledning 159, Soknedal - Støren	Ledning 159	496.894	498.313	Hovedspor	1	159	1473	1489
Kontaktledning, Ledning 160, Soknedal - Støren	Ledning 160	498.163	499.528	Hovedspor	1	160	1500	1512
Kontaktledning, Ledning 161, Soknedal - Støren	Ledning 161	499.408	500.163	Hovedspor	1	161	1525	
Kontaktledning, Ledning 162, Soknedal - Støren	Ledning 162	499.983	500.694	Hovedspor	1	162	1537	
Kontaktledning, Ledning 7a/ RB, Støren stasjon	Ledning 7a/ RB	500.284	500.704	Togspor	111	7a	1561	
Kontaktledning, Ledning 7b/ RB, Støren stasjon	Ledning 7b/ RB	500.524	501.16	Togspor	111	7b	1565	
Kontaktledning, Ledning 1/Støren st, Soknedal - Støren	Ledning 1/Støren st	500.542	502.273	Hovedspor	1	1	1551	1598
Kontaktledning, Ledning 2/sløyfe S, Støren stasjon	Ledning 2/sløyfe S	500.874	501.591	Øvrige spor	5	2	1558	
Kontaktledning, Ledning 4, Støren stasjon	Ledning 4	500.974	501.839	Togspor	2	4	1575	

Til mast (nr)	Spomr.	System	Kontakttråd tverrsnitt	Strekk kontakttråd (kg)	Kontakttrådmateriale	Bæreline tverrsnitt	Strekk bæreline (kg)	Bæreline materiale	Tillatt hastighet på kontakt	Y-Line	Avspenning (fra km) type	Avspenning (til km) type
1117		System 35 MS	100 Rund	720	Kobber	50	720	Kobber	130	Ja	Lodd	Lodd
1143		System 35 MS	100 Rund	720	Kobber	50	720	Kobber	130	Nei	Lodd	Lodd
1159		System 35 MS	100 Rund	720	Kobber	50	720	Kobber	130	Nei	Lodd	Fast
1174		System 35 MS	100 Rund	720	Kobber	50	720	Kobber	130	Nei	Fast	Lodd
1203		System 35 MS	100 Rund	720	Kobber	50	720	Kobber	130	Nei	Lodd	Lodd
1222		System 35 MS	100 Rund	720	Kobber	50	720	Kobber	130	Ja	Lodd	Lodd
1232		System 35 MS	100 Rund	720	Kobber	50	720	Kobber	130	Ja	Lodd	Fast
1262		System 35 MS	100 Rund	720	Kobber	50	720	Kobber	130	Nei	Lodd	Lodd
1258		Tabell 54	100 Rund	720	Kobber	50	720	Kobber	130	Nei	Fast	Lodd
1289		Tabell 54	100 Rund	1000	Kobber	50	500	Kobber	130	Nei	Lodd	Lodd
1319		Tabell 54	100 Rund	1000	Kobber	50	500	Kobber	130	Nei	Lodd	Lodd
1350		Tabell 54	100 Rund	1000	Kobber	50	500	Kobber	130	Nei	Lodd	Lodd
1378		Tabell 54	100 Rund	1000	Kobber	50	500	Kobber	130	Nei	Lodd	Lodd
1406		Tabell 54	100 Rund	1000	Kobber	50	500	Kobber	130	Nei	Lodd	Lodd
1439		Tabell 54	100 Rund	1000	Kobber	50	500	Kobber	130	Nei	Lodd	Lodd
1477		Tabell 54	100 Rund	1000	Kobber	50	500	Kobber	130	Nei	Lodd	Lodd
1503		Tabell 54	100 Rund	1000	Kobber	50	500	Kobber	130	Nei	Lodd	Lodd
1529		Tabell 54	100 Rund	1000	Kobber	50	500	Kobber	130	Nei	Lodd	Lodd
1541		Tabell 54	100 Rund	1000	Kobber	50	500	Kobber	130	Nei	Lodd	Fast
1555		Tabell 54	100 Rund	1000	Kobber	50	500	Kobber	130	Nei	Fast	Lodd
1568	1111	Tabell 54			Cu					Nei	Fast	Lodd
1584	1111	Tabell 54			Cu					Nei	Lodd	Fast
1658		Tabell 54	100 Rund	1000	Cu	50	500	Kobber	130	Nei	Lodd	Lodd
1607		Tabell 54	100 Rund	1000	Cu	50	500	Kobber		Nei	Lodd	Fast
1619		Tabell 54	100 Rund	1000	Cu	50	500	Kobber		Nei	Lodd	Fast

Appendix C-2 Table of poles for the section "Wire 152" from pole 1261 to 1288[8]

Beskrivelse	Navn/Nr	Fra	Til	Sportype	Spør num mer	Side	Avst. spormidtd	Mastetype	Maste høyde (m)	Spennlengde til neste påfølg	Ledningsnr.	Avspenning	Kurvebardun
Mast, 1261, Soknedal stasjon	1261	487.029	487.029	Hovedspor	1	Venstre	3.20	T	10.5	45			ba
Mast, 1262, Soknedal stasjon	1262	487.074	487.074	Hovedspor	1	Venstre	3.10	T	10	46		L - ledn 1	2ba
Mast, 1263, Soknedal stasjon	1263	487.12	487.12	Hovedspor	1	Venstre	3.20	T	10	60			ba
Mast, 1264, Soknedal stasjon	1264	487.18	487.18	Hovedspor	1	Venstre	2.90	T	10.5	59			ba
Mast, 1265, Soknedal stasjon	1265	487.239	487.239	Hovedspor	1	Venstre	2.75	T	10	60			ba
Mast, 1266, Soknedal stasjon	1266	487.299	487.299	Hovedspor	1	Venstre	2.90	T	10.5	61			ba
Mast, 1267, Soknedal stasjon	1267	487.36	487.36	Hovedspor	1	Venstre	2.85	T	10	60			ba
Mast, 1268, Soknedal stasjon	1268	487.42	487.42	Hovedspor	1	Høyre	2.95	T	10.5	60			ba
Mast, 1269, Soknedal stasjon	1269	487.48	487.48	Hovedspor	1	Høyre	2.95	T	10.5	60			ba
Mast, 1270, Soknedal stasjon	1270	487.54	487.54	Hovedspor	1	Høyre	2.90	T	10	60			ba
Mast, 1271, Soknedal - Støren	1271	487.6	487.6	Hovedspor	1	Høyre	2.90	T	10	60		fix-avsp.	ba
Mast, 1272, Soknedal - Støren	1272	487.66	487.66	Hovedspor	1	Høyre	2.95	T	10	50		FIX-pkt.	ba
Mast, 1273, Soknedal - Støren	1273	487.71	487.71	Hovedspor	1	Høyre	3.00	T	10	40		fix-avsp.	ba
Mast, 1274, Soknedal - Støren	1274	487.75	487.75	Hovedspor	1	Høyre	2.90	T	10	40			ba
Mast, 1275, Soknedal - Støren	1275	487.79	487.79	Hovedspor	1	Venstre	3.15	T	10.5	40			ba
Mast, 1276, Soknedal - Støren	1276	487.83	487.83	Hovedspor	1	Venstre	3.10	T	10.5	40			ba
Mast, 1277, Soknedal - Støren	1277	487.87	487.87	Hovedspor	1	Venstre	3.05	T	10	40			ba
Mast, 1278, Soknedal - Støren	1278	487.91	487.91	Hovedspor	1	Venstre	3.00	T	10	40			ba
Mast, 1279, Soknedal - Støren	1279	487.95	487.95	Hovedspor	1	Venstre	3.05	T	10	40			ba
Mast, 1280, Soknedal - Støren	1280	487.99	487.99	Hovedspor	1	Venstre	3.10	T	10	40			ba
Mast, 1281, Soknedal - Støren	1281	488.03	488.03	Hovedspor	1	Venstre	3.35	T	10	40			ba
Mast, 1282, Soknedal - Støren	1282	488.07	488.07	Hovedspor	1	Venstre	3.00	T	10	40			ba
Mast, 1283, Soknedal - Støren	1283	488.11	488.11	Hovedspor	1	Venstre	2.85	T	10	40			ba
Mast, 1284, Soknedal - Støren	1284	488.15	488.15	Hovedspor	1	Venstre	2.70	T	10	60			bbs
Mast, 1285, Soknedal - Støren	1285	488.21	488.21	Hovedspor	1	Høyre	3.10	T	10	60		L - ledn 153	2ba
Mast, 1286, Soknedal - Støren	1286	488.27	488.27	Hovedspor	1	Høyre	3.20	T	10	29			ba
Mast, 1287a, Soknedal - Støren	1287a	488.299	488.299	Hovedspor	1	Høyre	3.25	T		2			
Mast, 1287b, Soknedal - Støren	1287b	488.301	488.301	Hovedspor	1	Høyre	3.25	T		29			
Mast, 1288, Soknedal - Støren	1288	488.33	488.33	Hovedspor	1	Høyre	2.95	T	10	60			ba

Appendix C-3 Geometrical design of the droppers in section "Wire 152" [8]

Ledning nr 152

Soknedal - støren

1259 / 1259A		1	40	Avsp. hengetr. tilp.							
1259A / 1261		1	50	164 8,2	148 16,3	123 24,5	117 32,7	129 40,8	153 49,-		
1261 / 1263		2	45	148 1,9	123 8,8	109 15,6	104 22,5	109 29,4	123 36,2	148 43,1	
1263 / 1272		9	60	135 3,-	88 12,-	60 21,-	51 30,-	60 39,-	88 48,-	135 57,-	
1. 2 / 1273		1	50	144 2,3	113 9,9	95 17,3	88 25,-	95 32,6	113 40,1	144 47,7	Bunten deles her
1273 / 1276		3	40	148 2,1	129 9,3	118 16,4	118 23,6	129 30,7	148 37,9		
1276 / 1283		7	40	148 2,1	136 9,3	129 16,4	129 23,6	136 30,7	148 37,9		
1283 / 1284		1	40	148 2,1	129 9,3	118 16,4	118 23,6	129 30,7	148 37,9		
1284 / 1286		2	60	135 3,-	88 12,-	60 21,-	51 30,-	60 39,-	88 48,-	135 57,-	
1286 / 1288		1	60	152 1,-	108 10,8	86 20,7	86 30,5	113 40,3	142 50,2		
1. 3 / 1289		1	60	Avsp. hengetr. tilp.							

Ledning nr 153






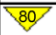
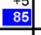





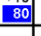
Soknedal - Støren

1285 / 1286		1	60	Avsp. hengetr. tilp.							
1286 / 1288		1	60	142 9,8	113 19,7	86 29,5	86 39,3	108 49,2	152 59,-		
1288 / 1297		9	60	135 3,-	88 12,-	60 21,-	51 30,-	60 39,-	88 48,-	135 57,-	
1297 / 1301		4	50	144 2,3	113 9,9	95 17,3	88 25,-	95 32,6	113 40,1	144 47,7	
1. 1 / 1302		1	60	135 3,-	88 12,-	60 21,-	51 30,-	60 39,-	88 48,-	135 57,-	
1302 / 1303		1	50	144 2,3	113 9,9	95 17,3	88 25,-	95 32,6	113 40,1	144 47,7	Bunten deles her forts.

Ek. 100863 - 000

Appendix C-4 Geometrical design of the track[8]

Løfteskjema

Banestrekning: 1111 (Oppdal) - Støren										Dato:15.04.13		Side 1 av 1		
Sportype: Hovedspor										Spornr.:				
Symbolforklaring:Tunnel begynner/ender:  Bru begynner/ender:  Planovergang:  Kjedebrudd:  Sporveksel: 														
STEDREFERANSE		VUL-DATA		TRASEDATA										
Faste pkt. eller Vul-nr.	Km	Avst. mrk.-skinne		Horisontalkurvatur					Vertikalkurvatur			Hastighets/tvangspkt.		
		Hor.	Vert.	R	h	L	V	Krumming	H	Høyde	Radius/Stigning	Tgl	I Km-retning	Mot Km-retning
OE	486,0100			1190	70	40								
OE	1150			1190	70	45								
Hastsign.	1310												+5	
Hastsign.	1500													
OB	1600			0	0									
OB	2080			0	0									
OE	2380			-3846	25	30								
OE	2950			-3846	25	28								
OB	3230			0	0									
Hastsign.	8370												85	+5
OB	8390			0	0									
OE	8850			1250	30	46								
OE	487,3530			1250	30	69								
FOB	4220			0	0									
OE	5020			-1190	30	80								
OE	6930			-1190	30	57								
M.merke 486.1310	7280													
Hastsign.	7470													
FOB	7500			0	0									
OE	8230			323	105	73								
OE	488,1220			323	105	57								
FOB	1790			0	0									
OE	2400			-1111	30	61								
OE	4640			-1111	30	90								
OB	5540			0	0									
OB	5930			0	0									
OE	6450			2174	15	52								
OE	8200			2174	15	58								
Hastsign.	8670												+10	
FOB	8780			0	0									
OE	9510			-532	60	73								

Appendix D Matlab code for writing the input file for pre-scribed displacements and the .csv-file for the track geometry

```
clear                                     all
close                                     all
clc

format                                     longe
filename='C:\Users\Mastermind3\Dropbox\Sko1e\Masteroppgave\Infoommaterialg
eometri osv\GeometriLedning152SoknedalStasjon.xlsx';
sheet='TilAbaqusSpor';
xlRange1='B1:GP1';
xlRange2='B3:GP3';

valuesU1=xlsread(filename,sheet,xlRange1);
b=0;
c=0;
for i=1:length(valuesU1)
    c=c+1;
    a=isnan(valuesU1(c));
    if a==0
        b=b+1;
        U1(b)=valuesU1(c);
    else
    end
end

valuesU3=xlsread(filename,sheet,xlRange2);
b=0;
c=0;
for i=1:length(valuesU3)
    c=c+1;
    a=isnan(valuesU3(c));
    if a==0
        b=b+1;
        U3(b)=valuesU3(c);
    else
    end
end

%Speed
prompt = 'what is the train speed in km/h? ';
speedkmh = input(prompt)

%%SPLINE%%
u1u1=0:1:1200;
u3u3=spline(U1,U3,u1u1);
```

```

figure(7)
plot(U1,U3,'o',u1u1,u3u3)

e=length(u1u1);
torg(1)=0;
speed=speedkmh/3.6;
for i=1:e-1
    ds(i)=sqrt((u1u1(i+1)-u1u1(i))^2+(u3u3(i+1)-u3u3(i))^2); %arc-length
for each new step
    torg(i+1)=torg(i)+ds(i)/speed; %when the train are at each point, in
seconds from start
end

%%%%RESAMPLE%%%%
figure(4)
subplot(1,2,1),plot(torg,u1u1),grid, xlim([min(torg) max(torg)])
TS = timeseries(u1u1,torg);
t = min(torg):0.02:max(torg);
RETS = resample(TS,t);
tid=RETS.time;
u1=squeeze(RETS.data);
subplot(1,2,2),plot(tid,u1),grid, xlim([min(t) max(t)])
%%save SFT.txt y -ascii

%New spline
u1u1=u1;
u3u3=spline(U1,U3,u1);
figure(8)
plot(U1,U3,'o',u1u1,u3u3)

%%%%Include rotations
d=1;
f=length(u1u1);
ur2=zeros(1,f);
for i=1:(f-2)
    d=d+1;
    ur2(d)=-atan((u3u3(d+1)-u3u3(d))/(u1u1(d+1)-u1u1(d)));
end
ur2(f)=ur2(f-1);
U=[tid u1u1 u3u3 ur2'];
%
%%TIL ABAQUS%%%%
filename=sprintf('SpanMast1261to1288SoknedalStasjonAmpInp%dkmt.inp',speedk
mh);
fid = fopen(filename,'w');
for j=1:3

```

```

if j==1
    fprintf(fid,'*Amplitude, name=U1\n');
elseif j==2
    fprintf(fid,'\n*Amplitude, name=U3\n');
else
    fprintf(fid,'\n*Amplitude, name=UR2\n');
end
u=1;
N=length(tid);
Nstart=1;

for t=Nstart:N
    Amp=round(U(t,j+1)*100000)/100000;
    if u==1
        fprintf(fid,'%g, %g',tid(t-Nstart+1),Amp);
    elseif u>1 && u<4
        fprintf(fid,', %g, %g',tid(t-Nstart+1),Amp);
    else
        fprintf(fid,', %g, %g\n',tid(t-Nstart+1),Amp);
        u=0;
    end
    u=u+1;
end
end

fprintf(fid,'\n** Name: U1 Type: Displacement/Rotation');
fprintf(fid,'\n*Boundary, op=NEW, amplitude=U1');
fprintf(fid,'\nTrain, 1, 1, 1. ');
fprintf(fid,'\n** Name: U3 Type: Displacement/Rotation');
fprintf(fid,'\n*Boundary, op=NEW, amplitude=U3');
fprintf(fid,'\nTrain, 3, 3, 1. ');
fprintf(fid,'\n** Name: UR2 Type: Displacement/Rotation');
fprintf(fid,'\n*Boundary, op=NEW, amplitude=UR2');
fprintf(fid,'\nTrain, 5, 5, 1. ');

fclose(fid);
disp('klart - PUH')

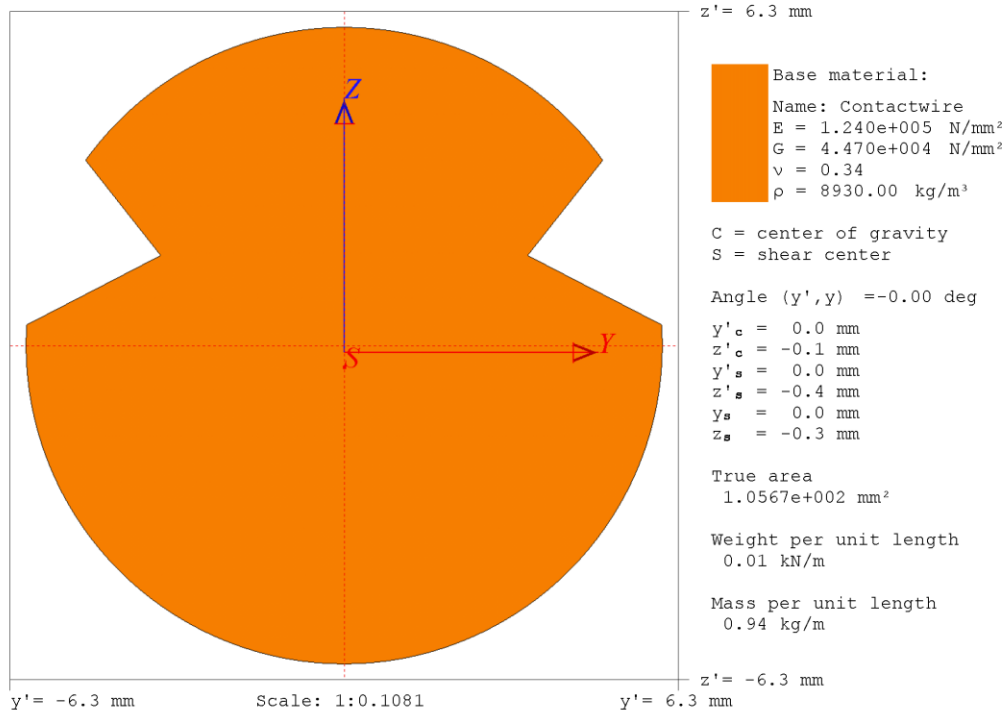
% %%
% %Trackgeometry
%
% fid = fopen('SpanMast1261to1288SoknedalStasjonTrackgeometry.csv','w');
%
% for t=1:length(u1u1)-1
%     x1=round(u1u1(t)*100000)/100000;
%     Y1=0;

```

```
%           z1=round(u3u3(t)*100000)/100000;
%           x2=round(u1u1(t+1)*100000)/100000;
%           y2=0;
%           z2=round(u3u3(t+1)*100000)/100000;
%           fprintf(fid,'%g, %g, %g, %g, %g, %g\n',x1,y1,z1,x2,y2,z2);
%           end
%
%
%           fclose(fid);
% disp('klart - Track - PUH')
```

[Published with MATLAB® R2013a](#)

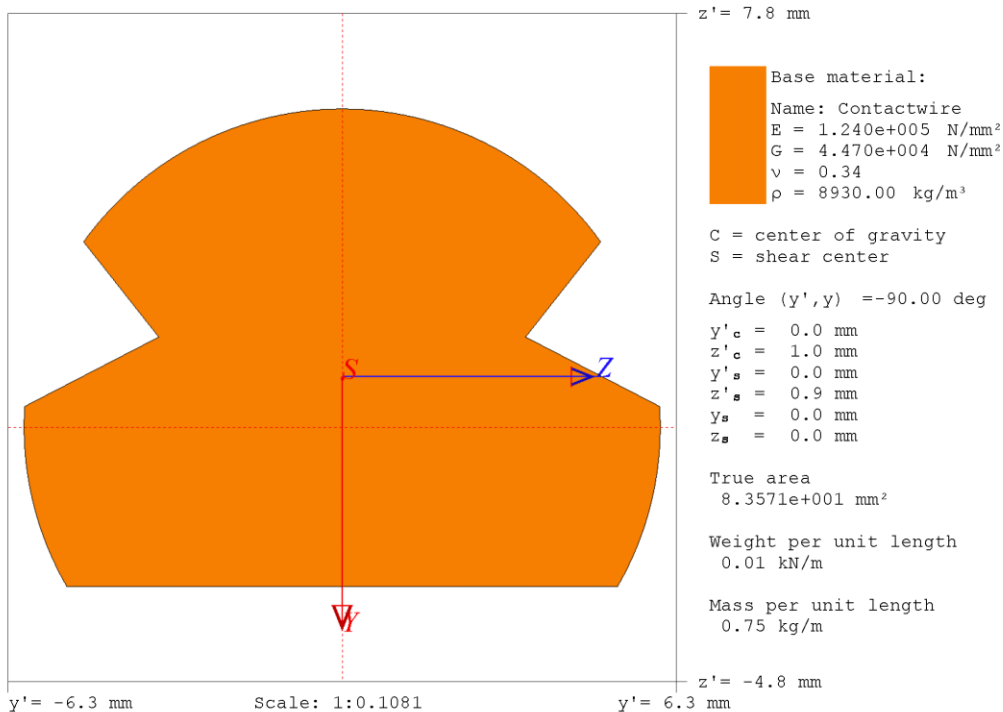
Appendix E-1 The cross sectional properties for the contact wire obtained from CrossX



PARAMETER*	VALUE	STIFFNESS	VALUE
A	1.0567e+002 mm ²	EA	1.3104e+004 kN
I _y	9.8650e+002 mm ⁴	EI _y	1.2233e-001 kN·m ²
I _z	8.3921e+002 mm ⁴	EI _z	1.0406e-001 kN·m ²
I _t	1.5115e+003 mm ⁴	GI _t	6.7562e-002 kN·m ²
S _y	1.6089e+002 mm ³	GA _{sy}	4.1545e+003 kN
S _z	1.3987e+002 mm ³	GA _{sz}	3.7353e+003 kN
r _y	3.0554e+000 mm	GA	4.7237e+003 kN
r _z	2.8181e+000 mm		
K _y	1.13699	EI _{y'}	1.2233e-001 kN·m ²
K _z	1.26461	EI _{z'}	1.0406e-001 kN·m ²
I _{y'} (y' at C)	9.8650e+002 mm ⁴	EI _{y'z'}	5.7744e-018 kN·m ²
I _{z'} (z' at C)	8.3921e+002 mm ⁴		
I _{y'z'} (at C)	0.0000e+000 mm ⁴		

* Apply to an equivalent cross section of base material

Appendix E-2 The cross sectional properties for the worn contact wire obtained from CrossX



PARAMETER*	VALUE	STIFFNESS	VALUE
A	8.3571e+001 mm ²	EA	1.0363e+004 kN
I _y	7.1043e+002 mm ⁴	EI _y	8.8094e-002 kN·m ²
I _z	5.0325e+002 mm ⁴	EI _z	6.2402e-002 kN·m ²
I _t	8.3527e+002 mm ⁴	GI _t	3.7336e-002 kN·m ²
S _y	1.1841e+002 mm ³	GA _{sy}	2.6307e+003 kN
S _z	9.9701e+001 mm ³	GA _{sz}	3.1490e+003 kN
r _y	2.9156e+000 mm	GA	3.7356e+003 kN
r _z	2.4539e+000 mm		
K _y	1.42000	EI _{y'}	6.2402e-002 kN·m ²
K _z	1.18629	EI _{z'}	8.8094e-002 kN·m ²
I _{y'} (y' at C)	5.0325e+002 mm ⁴	EI _{y'z'}	6.0217e-016 kN·m ²
I _{z'} (z' at C)	7.1043e+002 mm ⁴		
I _{y'z'} (at C)	0.0000e+000 mm ⁴		

* Apply to an equivalent cross section of base material

Appendix F Zip-file contents

1. SpanMast1261to1288SoknedalStasjonrightgeometry.cae
 - a. This is the numerical model of “Wire 152” in Abaqus
2. SpanMast1261to1288SoknedalStasjonrightgeometry.jnl
3. Analysis31Contact.mov
 - a. Displays an animation of the train running along the contact wire, with the contact forces which occur displayed in black text. Only look at the number at the top for the sum of forces acting between the collector strip and the contact wire.
 - b. One can also see how the train follows a curved path.
 - c. The speed was 90 km/h.
4. Analysis31Dynamics.mov
 - a. Displays an animation of the dynamics which occurs when the train runs under the contact wire. The y-axis is scaled with a factor of five, and the deformations are scaled with a factor of ten. Thus the deformations in the y-axis are scaled with a factor of fifty.
 - b. One can also see how the train follows a curved path.
 - c. The speed was 90 km/h.
5. GeometriLedning152SoknedalStasjon.xlsx
 - a. This file displays the geometry of “Wire 152”